Physical Layer Impairment-Aware Resource Allocation in Multiband and Multicore Elastic Optical Networks

---

A

Ph.D. Dissertation

Presented to

the faculty of the School of Engineering and Applied Science

University of Virginia

---

in partial fulfillment

of the requirements for the degree of

Doctor of Philosophy

by

Jaya Lakshmi Ravipudi

May 2024

APPROVAL SHEET

This

dissertation

is submitted in partial fulfillment of the requirements
for the degree of

Doctor of Philosophy

Author: Jaya Lakshmi Ravipudi

R. Jaya Lakshmi

Advisor: Dr. Maïté Brandt-Pearce

Advisor:

Committee Member: Dr. Nikolaos D. Sidiropoulos

Committee Member: Dr. Suresh Subramaniam

Committee Member: Dr. Yixin Sun

Committee Member: Dr. Haifeng Xu

Committee Member:

Committee Member:

Accepted for the School of Engineering and Applied Science:

Jennifer L. West, School of Engineering and Applied Science

Copyright

Abstract

Elastic optical network (EON)s offer flexible spectrum allocation, allowing for the accommodation of varying bandwidth traffic. Multiband and multicore fiber (MCF) EONs that extend the capacity in spectral and spatial dimensions have been proposed to meet future communication demands. Planning the resource usage of these networks has been the subject of extensive research. Careful design of routing, spectrum, core (if MCF), and modulation assignment algorithms enable efficient use of network resources in the wake of an increasing number of network users. In addition, consideration of physical layer impairments in EONs is important in the network planning stage for long-haul systems, especially when dealing with large dynamic traffic.

This dissertation investigates the resource provisioning problem for multiband and multicore fiber EONs using heuristic and machine learning approaches. The contributions of the dissertation work are mainly divided into four parts: (1) a Q-learning (reinforcement learning) based routing selection for C+L band multiband network is proposed considering dynamic network status; (2) the impact of different impairments in a dynamic multicore fiber provisioning scheme is analyzed that highlights the importance of inclusion of non-XT impairments; (3) a multi-attribute decision-making based route and core selection method and a new spectrum assignment scheme is proposed for multicore networks while considering network fragmentation and energy efficiency; and (4) machine learning (ML) is introduced to capture the hidden relationships in the network to judge the suitability of candidate resources and to estimate the links noises, thereby speeding the quality of transmission constraint verification in comparison to the analytic Gaussian Noise model.

For each part of the dissertation, the performance of the proposed algorithms is evaluated and compared with standard and published algorithms as benchmarks. Results show that both multiband and multicore are potential candidates for handling increasing network traffic. Although each of them comes with new

associated impairments, it is found that multiband can handle the demand increase only to a certain level, and multicore can considerably multiply the capacity, also providing greater flexibility in the impairment-aware design. Heuristic solutions enable the design of resource allocation so that the individual network aspects can be tackled by designing the rules for the selection and utilization of network resources in a unique manner while also being straightforward and easy to design and implement. On the other hand, the ML based solutions, especially the supervised approaches, enable learning unknown relationships of the network, allowing for different insights to help design the allocation solutions. The incorporation of ML can also help reduce the computation time for tasks that can become time-consuming when considering dynamic resource allocation for large loads and traffic. However, ML usage also comes with the need for a careful design and expertise with the problem domain. Hence, depending on the problem's goal and the long-term network requirements, either heuristic, ML based, or a combination of their approaches can be chosen. The proposed algorithms are simple, practical, and can be used easily by the network operators.

Acknowledgements

First, I would like to express my gratitude and thankfulness to my advisor, Prof. Maïté Brandt-Pearce, for her guidance and patience. Her continuous enthusiasm, encouragement, and knowledge helped me greatly during my graduate studies at the University of Virginia. Her meticulous and dedicated attitude has inspired me and is the guidance for my future career.

Secondly, I would like to thank my parents for their constant support, love, and belief in me. I am forever grateful to my loving parents, who have always encouraged me for higher pursuits.

Third, I'd also thank my fellow colleagues and friends for their advice and friendship throughout the time of my graduate studies.

I gratefully acknowledge my defense committee, Professor Nicholas D. Sidiropoulos, Professor Suresh Subramaniam, Dr. Yixin Sun, Dr. Haifeng Xu, and Professor Maïté Brandt-Pearce for their direction and insights.

I also acknowledge the Research Computing at the University of Virginia for providing computational resources and technical support that have contributed to the results of this dissertation.

Lastly, I would like to thank the National Science Foundation (NSF) for the financial support of my studies.

To my beloved parents.

Contents

List of Tables

List of Figures

Acronyms

AHP analytic hierarchy process 73, 74, 76–78, 80

ASE amplified stimulated emission 31, 34, 36, 38, 50, 56–64, 67–70, 91, 99, 114, 116, 118, 123

AST average setup time 101, 114, 120, 121

AUC ROC area under the curve of the receiver operating characteristic 100, 102, 104, 108, 111–113

BBP bandwidth blocking probability 27, 50, 101, 114, 118, 120

BCE binary cross entropy 107, 108

BER bit error rate 35, 95, 96, 98

BP blocking probability 27, 50, 58, 101, 114–118, 121

BVT bandwidth variable transponders 18, 21, 24, 65

BW Bandwidth 90, 91

DGCNN deep graph convolutional neural networks 98

DNN deep neural network 35, 36, 94, 97–102, 104, 106–118, 120, 121, 124

DRL deep reinforcement learning 35, 36, 97

DSP digital signal processing 31

DWDM dense wavelength division multiplexing 18, 22, 24

EDFA erbium-doped fiber amplifiers 31, 33, 34, 36–38, 65

EF exact fit 27, 28, 34, 42, 83

EON elastic optical network 2, 18, 20–24, 28, 29, 34–37, 42, 43, 55–57, 65, 97, 98, 102, 109, 111, 115, 118, 122, 123

EONs elastic optical networks 26, 33

FC first core 28, 102, 114

FF first fit 27, 28, 34, 42, 83, 84, 86, 88–91, 102, 114, 115, 120

FWM four wave mixing 30–32

GN Gaussian noise 20, 97, 102, 114, 115, 117, 118, 120, 124

GVD group velocity dispersion 30

ILP integer linear programming 20, 58

ISRS inter-channel stimulated Raman scattering 34, 36–39, 50, 56

ITU-T International Telecommunication Union Telecommunication Standardization Sector 18, 22

KSP K-shortest paths 27, 34, 67, 84–86, 88–91, 97, 102, 114–121

LF last fit 27, 28, 34, 42, 83

MADM multi-attribute decision making 64–67, 73, 74, 78, 84–86, 88–91, 93, 124

MCF multicore fiber 2, 19, 23, 28, 32, 57–59, 61–63, 65, 66, 69–71, 79, 83, 84, 90, 91, 93, 97, 98, 102, 114–117, 123, 124

MF modulation format 98, 99

MILP mixed integer linear programming 21, 34, 35, 66, 67

ML machine learning 2, 3, 20, 35, 36, 94–98, 100–102, 104, 114, 121, 124

MODM multi-objective decision making 73

NLI nonlinear interference 30, 35, 38, 39, 57, 59–62, 64, 68, 70, 97, 114, 116, 118, 123

NN neural network 36, 98

OFDM orthogonal frequency-division multiplexing 35

OSNR optical signal-to-noise ratio 34, 38, 40, 41, 44, 46, 47, 50, 52

OXC bandwidth variable optical cross-connects 65

PLI physical layer impairments 19–21, 28, 31, 34–37, 50, 56–58, 66–69, 94, 97, 116, 119, 123

PMD polarization mode dispersion 30

PROMETHEE preference ranking organization method for enrichment evaluations 73, 74, 76–78, 80, 88

PSD power spectral density 38

QoT quality of transmission 19, 20, 31, 34, 36, 50, 51, 57–60, 65, 95–100, 102, 109, 110, 112, 114, 115, 117, 118, 120, 121, 124

RF Random Forest 94, 99–102, 105, 106, 109, 111, 113–115, 117, 118, 120, 121

RFE recursive feature elimination 102, 113

RL reinforcement learning 35, 36, 41–43, 55, 97

RMSA routing, modulation and spectrum assignment 21, 28, 33–37, 44, 46, 48, 50, 52, 54, 56, 97

RMSCA routing, modulation, spectrum and core assignment 21, 25, 28, 58–60, 63–68, 71, 73, 76, 84, 88, 91, 94–96, 100–102, 108–112, 121, 124

RMSE root mean square error 101, 102, 106

ROADM reconfigurable optical add-drop multiplexers 19, 24–26, 37, 65

RSA routing and spectrum assignment 19, 21, 26–28, 34, 35, 96

RSCA routing, spectrum, and core assignment 19

RWA routing and wavelength assignment 20, 26

SA spectrum assignment 27, 28

SDM space division multiplexing 19, 23–26, 35, 65, 97, 98, 118, 122

SDM-EON space division multiplexing based elastic optical networks 19, 23, 66, 70, 86, 91, 93, 94, 98, 99, 102, 121

SDN software defined networks 23, 36

SF score fit 83–86, 88–91

SNR signal to noise ratio 70, 97

SPM self-phase modulation 30, 31, 34, 38, 57, 58, 63, 67, 68, 84, 85, 91, 99

SRS stimulated Raman scattering 31

TL transfer learning 97

TR transmission reach 20

WDM wavelength division multiplexing 20, 26, 33, 35, 97

WSS wavelength selective switches 24, 25

XPM cross-phase modulation 30–32, 34, 38, 57, 58, 62, 63, 67, 68, 99

XT crosstalk 32, 57–68, 71, 82, 86, 90, 91, 97–100, 114, 116–118, 123

Chapter 1

Introduction

This chapter presents a motivation for the dissertation and outlines the organization and contributions of the work.

1.1 Research Motivation and Background

The proliferation of electronic devices, social media platforms, video streaming services, and machine-to-machine communications underscores the critical importance of optimizing communication networks [1]. Projections indicate a substantial rise in the global number of internet-connected devices, with estimates suggesting a staggering 22 billion devices by 2025. Moreover, there is a corresponding surge in data consumption per smartphone, expected to escalate from 21 GB in 2023 to 56 GB in 2029, driven by the growing popularity of gaming, extended reality experiences, and video-centric applications [2]. The capacity demand will also be fueled by cyber-physical systems, fiber for 6G and future generation networks, data center switching speeds, etc. This exponential growth places considerable strain on the optical backbone networks, which have served as a vital component of telecommunications infrastructure, facilitating long-distance data transmission across continents since the 1970s. Given this dynamic landscape, it is now crucial that the optical networks are utilized efficiently and new techniques for capacity increase are researched and utilized.

Optical networks comprise fiber links and network nodes (data switch exchanges) and are designed to transport large volumes of data over long distances efficiently. Each traffic demand is modulated and transmitted as a light signal from its source node, along fiber links through several intermediate nodes, to its destination node. The light is transmitted inside the fiber core and amplified

by optical amplifiers at the end of each fiber span. The path from the source to the destination node is called the lightpath. Each data signal is transmitted at a specific wavelength range. Selecting network resources such as a lightpath and wavelength band for each traffic request is referred to as resource allocation. This dissertation is a comprehensive study of resource allocation algorithms that utilize heuristic and machine learning techniques for multi-band and multicore fiber networks.

Current optical networks use dense wavelength division multiplexing (DWDM) based on a fixed-width wavelength grid to transmit the traffic demands over C-band. The C-band wavelengths are conventionally used for data transmission to enable long-distance data transmission because of the low attenuation of the signal in the fiber and high bandwidth range. Following the industry standard International Telecommunication Union Telecommunication Standardization Sector (ITU-T) G.694.1, 88 channels, each spaced 50 GHz apart, are supported by DWDM networks. However, because of the fixed 50 GHz grid, data beyond 100 Gbps using standard modulation cannot be accommodated in this scheme [3]. Therefore, DWDM networks find it difficult to satisfy the growing demands for communications. To address this issue, elastic optical networks (EONs) with a flexible spectrum structure have been developed that can switch broader spectrum channels to support high bit rate (such as 400 Gbps or 1 Tbps) demands [4, 5].

Unlike conventional DWDM networks, EONs use bandwidth variable transponders (BVT), making them suitable to serve heterogeneous traffic demands. Ideally, EONs finely segment the optical spectrum into infinitely many frequency slots with arbitrarily small granularity, making the network bandwidth appear elastic and continuous. However, due to hardware limitations, full elasticity, i.e., arbitrarily small spectrum granularity, is challenging to achieve. As a more achievable approach, we focus on flexible grid networks that partition the spectrum into a fine grid of frequency slots (12.5 GHz or 6.25 GHz) and where demands can occupy one or more slots [3, 6, 7].

There is no doubt that EON technology has dramatically influenced optical networking and considerable research has been done both in the fiber aspects and in the networking part. However, the current single-core fiber technologies are nearly exhausted and won't be able to handle the explosive data growth effectively. Therefore, it is imperative to look for ways to utilize the existing resources efficiently and explore new structures to address the problem of capacity

crunch. There is a need to find potential cost-effective solutions to scale the existing link capacity in the next five to ten years.

The data transported in an optical fiber via light is over a certain spectrum range. The spectrum is a limited network resource, and the conventionally used single-core C-band can be extended to include L and S bands. In this dissertation, we explore the effective use of L-band to increase the network capacity. Other solutions to augment capacity include using multiple fibers, hollow-core fibers, open reconfigurable optical add-drop multiplexers (ROADM), increasing symbol rates, etc. Alternatively, space division multiplexing (SDM) exploits the space dimension to accommodate more data in the same fiber. The spatial aspect can be incorporated into the optical fiber using cores or modes. A MCF has multiple cores in the fiber, with each core having its own individual spectrum range. This multiplies the available transmission capacity. In contrast, multi-mode fibers allow multiple orthogonal transverse fiber modes in a single fiber core and are typically used for short-range links. A variant of multi-mode fibers using a lower number of modes (3-15) is the few-mode fiber and is relatively more common than the multi-mode type in SDM research. However, MCF is the most common one among these because of its practicality and is expected to be deployed within this decade. MCF are the focus of this dissertation, and space division multiplexing based elastic optical networks (SDM-EON)s is the expression used to refer to MCF-based fiber networks in this dissertation.

Efficient planning of the use of network resources (spectrum, switches, optical amplifiers, etc.), whether new or existing technologies, is a must from the cost, time, and energy points of view. The planning scope is broadened depending on the objectives to achieve and the resources that are at the focus of the optimized planning. Planning the resource usage in EON, the so-called routing and spectrum assignment (RSA) problem, is an essential networking problem and has been the subject of extensive research [8, 9]. The spectrum is a scarce resource due to the limited low-loss available bandwidth in standard fibers versus the rapid increase of data traffic. In addition, spectrum usage is related to optical switches, amplifiers, and filters. In SDM-EON network planning, the RSA becomes routing, spectrum, and core assignment (RSCA) as there is the choice of which core to use as well.

The performance of optical networks is limited by physical layer impairments (PLI)s, such as fiber loss, dispersion, and nonlinearities, which can impair quality of transmission (QoT) of the signals in long-haul networks. When the QoT

is unsatisfied due to PLIs, signal regeneration is needed to recover the lost/degraded transmitted data and fully negate the effects of the accumulated PLIs. Different modulation formats offer different levels of sensitivity to the PLIs. How to estimate the PLIs has been studied for several years since the estimated disturbances can help the network provisioning. The most common model is the transmission reach (TR) model, which, as the name suggests, estimates the maximum distance a signal can travel without regeneration amidst the noises while still maintaining an acceptable QoT level. However, this model provides worst-case estimates and lacks accuracy and flexibility. A more accurate PLI estimate accounting for real-time network state is the so-called Gaussian noise (GN) model [10]. Resource allocation techniques that account for the PLIs are referred to as impairment-aware.

The EON resource assignment problem is an NP-Hard problem where finding an exact optimal solution is computationally intractable. Hence, heuristic approaches have often been employed, and they generally provide rule-based strategies aiming to find suitable solutions in a reasonable amount of time, though sub-optimal ones. Many impairment-aware resource allocation algorithms in the literature use heuristic and ML approaches to model the PLIs, with the former dominating the literature [9, 11]. In recent years, ML techniques are finding a place in resource allocation tasks [9, 12], comparatively more on the single-core side. ML is generally known to capture hidden relationships in the considered problem domain, in our case the resource allocation. However, as fancy as ML may sound, a wealth of heuristic solutions developed over the years tackling multiple network aspects cannot simply be sidelined by throwing in ML. Hence, cautious use of the latter is necessary while assessing the need for ML and the advantages gained with its incorporation.

The literature relevant to the contributions of the dissertation is comprehensively discussed in the respective chapters. However, a succinct overview of some of the important works is presented here. The initial resource provisioning problem in transparent wavelength division multiplexing (WDM) networks called the routing and wavelength assignment (RWA) problem was published in 1995 by Ramaswami et al. [13], and integer linear programming (ILP) was used to model the problem. In [14], a RWA in translucent (network has regeneration nodes) optical WDM networks was presented. The allocation of regeneration nodes was optimized using new heuristic algorithms. This work initiated subsequent studies on translucent optical networks. The work presented in [5] in 2012 paved the

way for the next generation of optical networks by presenting the idea of EONs. The paper described the structure, advantages, and associated challenges of using EONs. Accordingly, resource provisioning now means flexible spectrum allocation. Subsequently, in [15], the heuristic method was proposed to solve a static RSA problem in EONs. Although a basic RSA without PLIs was considered, it greatly influenced future studies based on mixed integer linear programming (MILP) solutions. The research on PLI modeling in [10, 16, 17, 18, 19] further fueled network state-dependent PLI-aware resource allocation research. Adaptive modulation schemes enabled by BVT in the EON structure increased the degree of freedom in the assignment and pushed the research towards routing, modulation and spectrum assignment (RMSA) designs [12, 20, 21, 22].

While the research on finding improved allocation algorithms using heuristic and machine learning methods [4, 23, 24, 25, 26] continued, the optical networking community also started focusing more on networking solutions with additional resources using multi-band and multicore EONs [21, 27, 28, 29, 30]. This dissertation focuses on these multi-band and multicore networks.

1.2 Dissertation Outline

The dissertation is organized as follows. Chapter 2 elaborates on EONs, single-core multi-band networks, and multicore single-band fiber networks, including their hardware equipment and infrastructures. This chapter also describes physical layer impairments in detail and defines the resource allocation problem necessary to understand the allocation schemes presented in the subsequent chapters. The first contribution of the thesis is given in Chapter 3, where a reinforcement learning based resource provisioning scheme for single core C+L multi-band networks is presented. In Chapter 4, the impacts of impairments in the multicore fiber networks are analyzed under the realm of dynamic resource provisioning, necessary for understanding the importance of PLI aware multicore provisioning; it is the second contribution of the dissertation. Chapter 5 presents the third contribution of the dissertation, a dynamic routing, modulation, spectrum and core assignment (RMSCA) heuristic algorithm for multicore fiber optical networks. In Chapter 6, machine learning is utilized and a dynamic RMSCA algorithm is proposed, which is the fourth contribution of the dissertation. Finally, the conclusions of the dissertation work and future scope are provided.

Chapter 2

EON Description and Problem Formulation

This chapter presents the fundamental concepts of elastic optical networks, multi-core fiber-enabled optical architecture, and the physical layer impairments needed to understand the problem addressed in this dissertation. This is followed by describing the impairment-aware resource provisioning problem and the associated constraints.

2.1 Elastic Optical Networks (EONs)

Until 2012, the ITU-T recommendation for DWDM networks included only the 1530–1565 nm C-band spectrum divided into fixed 50 GHz frequency slots [3]. This division limits the transmission to 50 GHz, meaning that higher bandwidth signals have to be divided into multiple fixed slots, requiring additional signal processing and often leaving a spectrum gap in the last block. This also results in spectrum wastage for bandwidth demands less than 50 GHz. This problem is illustrated in Fig. 2.1.

With this in mind, EONs have been proposed to support long-haul transmission beyond 100 Gbps and to better adapt to heterogeneous traffic [5]. Hence, in 2012, in order to support the adaptive spectrum allocation concept of EON, the ITU-T updated its G. 694.1 recommendation to include the flexible grid option based on the new frequency slot concept. A frequency slot is defined as the frequency range that an optical channel is allowed to occupy. The allowed frequency slots have a nominal central frequency and a slot width defined by an integer multiple of 6.25 GHz. Some characteristics of EONs include improved effi-

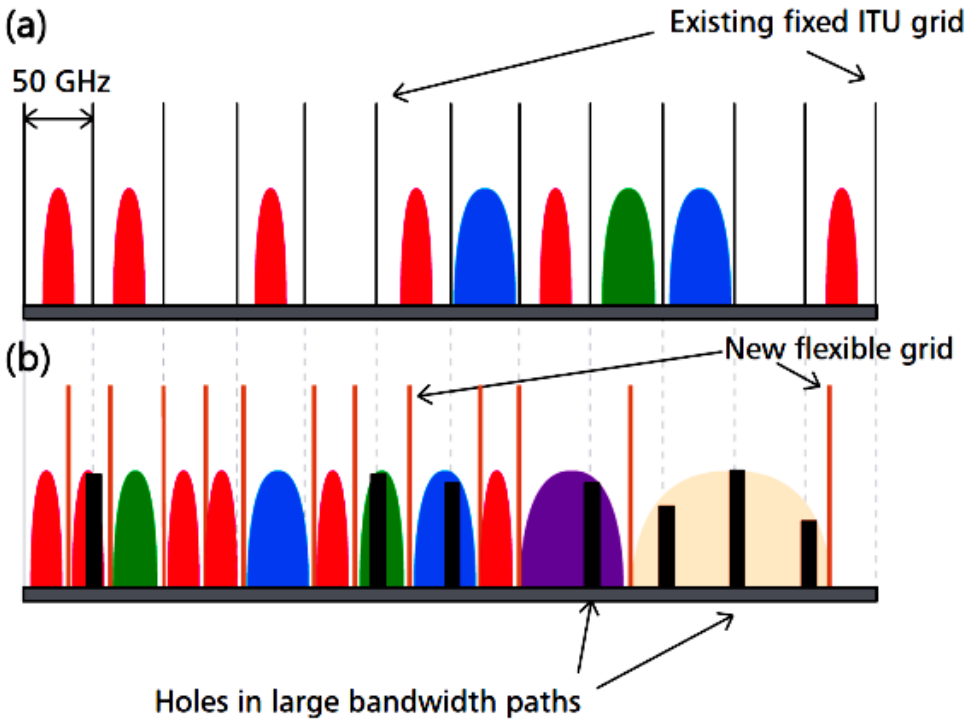

Figure 2.1: Spectrum in (a) conventional DWDM networks and (b) EON [5] ©[2012] IEEE

ciency, simultaneous support to low and high data rate traffic via super-channels, adaptive modulation format selection enabling optimization of spectrum usage, and cost- and energy-efficient traffic grooming. In addition, EONs can be operated together with the idea of software defined networks (SDN)s. Realizing these benefits of the EONs, they have been widely researched over the last few years.

However, despite the added capabilities of the EON structure, the currently deployed single-core fiber capacity is nearly exhausted. Possible solutions to this problem include using extended frequency bands [21, 29], multi-fiber links [31], and multi-core fiber links [7]. Frequency band extension includes using L- and S-bands with original C-band or hybrid links utilizing a combination of C and frequency-extended links [32]. The extension can increase the network capacity by a small factor and with an additional need for new transponders and multiplexers compared with exploiting MCFs. Hence, the network will eventually need to rely on more transmission dimensions as available in SDM-EON. Examples of SDM fibers are bundles of single-core single-mode fibers, MCFs, few-mode fibers, and few-mode MCFs where *spatial* can refer to fiber, core, mode or group of modes [33].

2.2 Enabling Technologies for Space Division Multiplexed EONs

There are two significant hardware-enabling technologies needed for EONs: flexible wavelength selective switches (WSS)s and bandwidth variable transponders (BVTs). Fig. 2.2 shows a node architecture utilizing these two components. BVTs can send and receive optical signals with any bandwidth and datarate. A BVT may adapt to numerous modulation formats to preserve spectrum while maintaining the necessary transmission quality, in contrast to conventional DWDM transponders that support only one particular datarate and modulation. Hence, the BVTs need more sophisticated filtering, sampling, synchronization, and other techniques. The WSSs are used to add or drop optical signals at specific source or destination nodes, respectively. The channels of EONs occupy various spectrum widths, and the arbitrary bandwidth connections are switched from any input port to the desired output port using WSS to achieve spectrally efficient routing and grooming. Bandwidth variable WSSs supporting the 12.5 GHz granularity are currently commercially available.

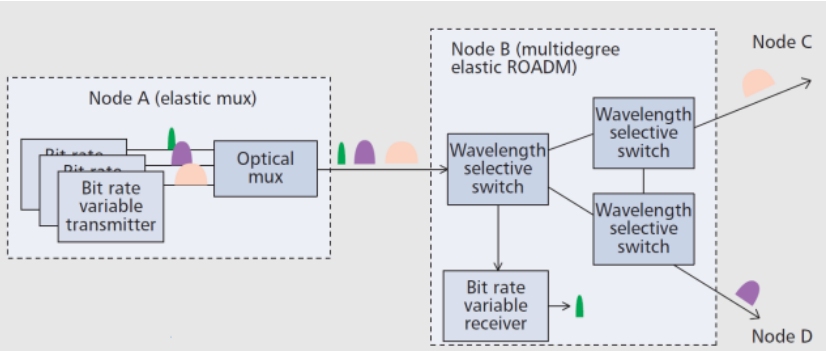

Figure 2.2: A node architecture using BVTs and WSSs [5]©[2012] IEEE

In a transparent optical network, signals traverse from their source to their destination solely within the optical domain, avoiding any conversion to the electrical domain. A ROADM is a crucial networking device that has access to all wavelengths on a fiber and allows for specific wavelengths to be dropped or added at a location while also allowing other wavelengths to optically pass through the site without requiring termination. The 'reconfigurable' capability allows adaptation to varying traffic volume and patterns and enables remote (re)configuration of lightpaths. In the realm of SDM enabled networks, the granularity of spatial switching plays a pivotal role in shaping the architecture of ROADM in all-optical

switching scenarios. Opting for a finer switching granularity offers greater routing flexibility at the network layer, albeit at the expense of requiring more WSSs within the ROADM infrastructure. Conversely, adopting a coarser switching granularity reduces the ROADM deployment costs but concurrently diminishes routing flexibility. This arises from the need to treat optical carriers within a core and spectrum block as unified entities, necessitating their collective switching during routing operations. Thus, the employed core and spectrum scheme depends on the design of the ROADM architecture. Additionally, the number of add/drop ports supported by a ROADM significantly impacts its architecture. A higher number of add/drop ports enhances network layer performance but with increased device costs and power consumption associated with the ROADM infrastructure.

To improve the flexibility in fiber core usage, a spatial lane change (SLC) technology was proposed to alleviate the impact of spectral continuity constraints. SLC allows traffic connections to use different spatial dimension indices on each link along the lightpath while still using the same spectral range [34]. Thus, the routing flexibility can be further improved by deploying ROADMs with SLC support at intermediate nodes. However, the architecture of such a ROADM is considerably more complex than that of a ROADM without SLC support because WSSs with higher port-count are required. Hence, a no SLC assumption is quite common in many contemporary RMSCA studies [35, 36, 37].

Three switching paradigms are available for SDM based optical networks: independent, fractional, and joint, with the spatial dimension possibly corresponding to either a mode or a core. In the independent switching paradigm, each spatial dimension can be independently switched to output ports sharing the same spatial index or ports of any index if SLC is supported. While this approach offers superior routing flexibility, it necessitates the most significant number of WSSs. Conversely, joint switching treats all spatial dimensions as a unified entity, regardless of SLC support, making it a cost-effective option for implementing SDM optical networks but at the expense of reduced routing flexibility. The third paradigm, fractional switching, strikes a balance between cost and flexibility. Here, spatial dimensions are grouped, with each group requiring joint switching. This architecture can also be implemented with or without SLC support. Fig. 2.3 illustrates these three switching schemes under no SLC assumption for spatial switching granularities of 1,4, and 2, where the WSSs are depicted by trapezoids.

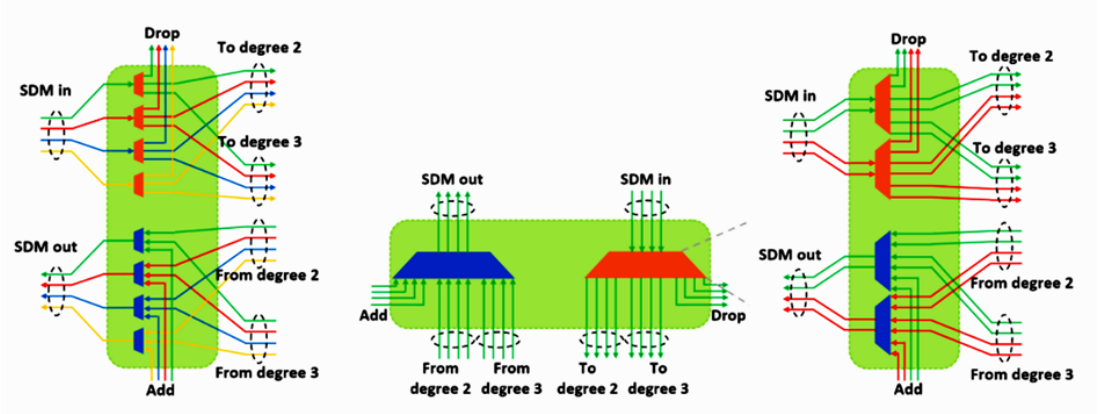

Figure 2.3: Illustration of three switching paradigms for different spatial switching granularities [38] ©[2019] IEEE

Hence, all SDM transmission technologies are closely associated with one another, and each of them has a great influence on the architectures of the corresponding physical devices (i.e., SDM transceivers and ROADMs). Therefore, the choice of architecture affects the design of new SDM optical networking algorithms. In this dissertation, a joint switching paradigm is assumed in all networking scenarios, as is common in current literature [37, 39, 40, 41].

2.3 Resource Provisioning Problem

The task of selecting network resources to enable the transmission of the signal of a given traffic demand from source to destination is known as a resource provisioning/assignment/allocation problem. In elastic optical networks (EONs), the RSA problem is the equivalent of the RWA problem in WDM networks. However, in transparent EONs, as assumed here, RSA comes with the additional constraints of spectrum contiguity, spectrum continuity, and non-overlapping of frequency slots, as depicted in Fig. 2.4(a). The spectrum contiguity constraint requires the assigned frequency slots on the network link to be adjacent, maintaining the same spectrum range across all selected links in the chosen optical path (spectrum continuity). The non-overlapping spectrum constraint indicates that the frequency ranges assigned to multiple requests at any time in the network must be distinct. Consider a request that needs links 1 through 4 and three spectrum slots as shown in Fig. 2.4(a); the selected slots fulfill the adjacency requirement and are the same frequencies on all the links.

The traffic demand may be static (i.e., a fixed or offline traffic matrix) or

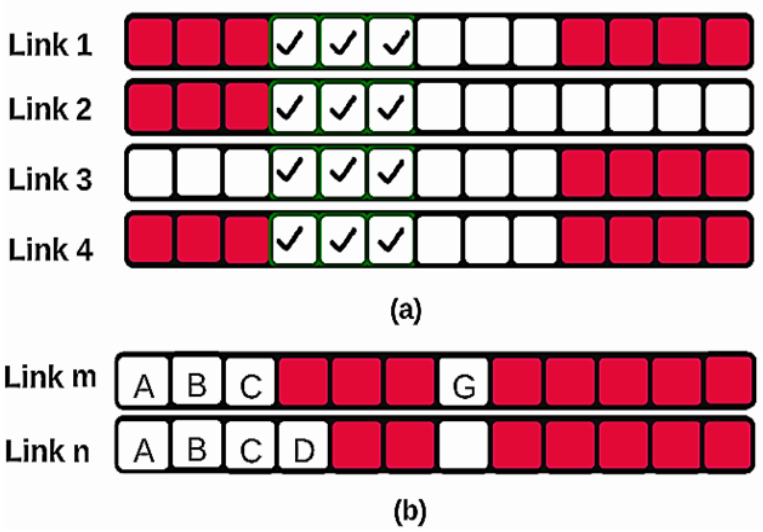

Figure 2.4: Example showing the (a) contiguity and continuity constraints and (b) fragmentation in EONs

dynamic (i.e., time-varying traffic); our work focused on the latter since, in a real network, there is a lack of information on the upcoming user traffic, but the network has to be able to accommodate it. With dynamic traffic, the performance of an RSA algorithm is often measured by the blocking probability (BP), which is the proportion of traffic demands that are not successfully provisioned. The input traffic load is measured in Erlangs. The BP and bandwidth blocking probability bandwidth blocking probability (BBP) are calculated as:

$$\text{BP} = \frac{\text{Number of blocked requests}}{\text{Total number of requests}} \tag{2.1}$$

$$\text{BBP} = \frac{\text{Amount of blocked bandwidth}}{\text{Total amount of requested bandwidth}} \tag{2.2}$$

In dynamic RSA, dynamically setting up and tearing down connections can lead to bandwidth fragmentation, resulting in inefficient spectrum use. Fig. 2.4(b) shows this phenomenon for a demand seeking four slots. They are available on both links but cannot be assigned due to non-contiguity, thus leading to unnecessary blocking.

The conventionally used routing algorithm is the K-shortest paths (KSP) algorithm, which is based on distance, although sometimes hop count may be used as the definition of shortest. For the spectrum assignment (SA), three common approaches exist, first fit (FF), last fit (LF), and exact fit (EF) [4]. In FF, the

first available frequency slot is selected, i.e., starting from the lowest frequency. In the LF, the free slots are checked from the other end of the spectrum, i.e., higher frequencies. Finally, in EF SA, a search for the exact number of required slots is performed; if it is not found, the first-fit criterion is used.

When adaptive modulation is considered, the RSA problem becomes the RMSA problem. Adaptive modulation helps in spectrum savings as it enables the selection of higher-order modulation formats having higher spectral efficiency. The state-of-the-art digital coherent technology makes it possible to generate and detect optical signals with a wide variety of modulation formats with a single type of transceiver [3]. However, as the modulation order increases, the sensitivity to impairments increases and is mostly suitable for shorter distances. This influences the acceptance of the present request as well as future requests, particularly when evaluating the impact of noise on existing lightpaths in service. For a given demand, the modulation format selection, the required number of slots, and the PLI sensitivity are interrelated. Hence, the selection of a modulation format offers cautious flexibility when designing a resource assignment algorithm. The number of frequency slots of width δf needed for a demand requesting a certain data rate when using a modulation spectral efficiency η_M denoted as S_{req}, is calculated using

$$S_{\text{req}} = \left\lceil \frac{\text{data rate}}{2 * \delta f * \eta_M} \right\rceil + 1. \tag{2.3}$$

One slot is used as a guard band.

In MCF networks, the choice of the core is another degree of freedom for allocation, and the assignment is termed as RMSCA. The design of the core selection strategy is affected by the switching paradigm and the number of neighbor cores due to crosstalk effects that may deteriorate the due-to-be-provisioned request and future ones. Also, the minimization of crosstalk effects requires the signal to be spaced out, whereas this spreading can introduce spectrum gaps, leading to spectral fragmentation. Hence, core selection plays an important role in the RMSCA design. In this work, core continuity is assumed to be similar to spectrum continuity. Similar to the FF spectrum scheme, the commonly used core allocation method is the first core (FC) that allocates the first available core depending on the considered constraints. Fig. 2.5 illustrates the route, core, and spectrum selection process in a MCF network for a request traveling from node 1 to node 5 using core 1 and occupying frequency slots f_4 to f_6 that obey the three EON constraints.

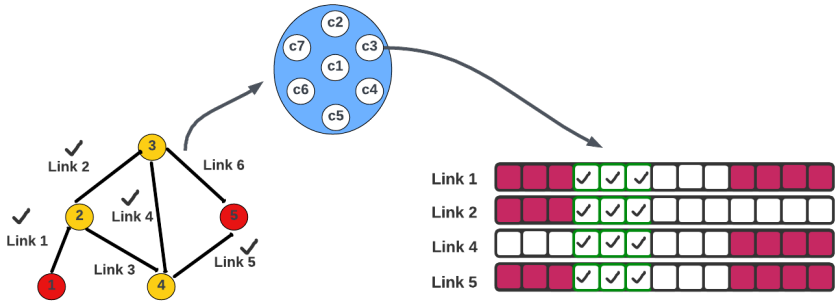

Figure 2.5: Illustration of resource provisioning in multicore fiber EON (adapted from [9])

2.4 Algorithm Performance Validation Approach

The performance of resource allocation algorithms is usually tested on large-scale network topologies. In this dissertation, the various networks used are the single and multicore 11-node COST-239, 14-node NSFNET, and 24-node USNET. All these topologies have varying connectivity, i.e., nodal degrees, and have a wide diversity of link distances (200 km - 2400 km), which is essential while considering the inclusion of PLI. Fig. 2.6(a) shows the 14-node NSFNET with 21 optical fiber links, the European 11-node COST-239 network with 52 optical fiber links is shown in Fig. 2.6(b), and the 24-node USNET with 43 links in Fig. 2.7.

The traffic requests demand connection provisioning on these networks and arrive in a Poisson manner with an exponential holding time. A request is composed of a source node, destination node, and data rate. The EON in this dissertation is represented by a graph $G(V, E)$ where V is the set of nodes and E is the set of links/edges. This work considers transparent EONs, i.e., the data transmission is entirely in the optical domain, and there is no optical-electrical-optical conversion in the nodes. This dissertation assumes the modulation format continuity along the entire route, unlike the case of translucent EONs, where regenerators can be equipped with a modulation conversion facility.

2.5 Physical Layer Impairments

This section gives an overview of the significant physical layer impairments affecting the optical network performance.

Many losses and impairments, such as dispersion, fiber losses, and nonlinear impairments, limit the performance of optical systems. The dispersion effects

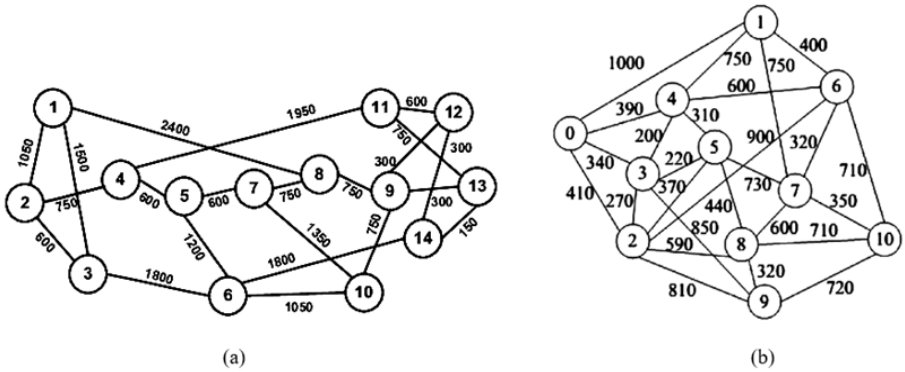

Figure 2.6: (a) 14-node NSFNET (b) 11-node COST-239 network [24] ©[2019] IEEE

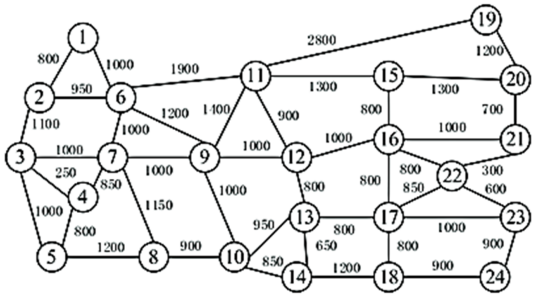

Figure 2.7: 24-node USNET topology [42]

include group velocity dispersion (GVD), material dispersion, waveguide dispersion, and polarization mode dispersion (PMD). The fiber losses, called attenuation, result from material absorption, Rayleigh scattering, coupling losses, and waveguide imperfections (bending losses). The nonlinear interference (NLI) effects include stimulated light scattering such as Brillouin and Raman scattering and phase modulation such as self-phase modulation (SPM), cross-phase modulation (XPM), and four wave mixing (FWM).

Dispersion affects all kinds of fibers. In single-mode fibers, chromatic dispersion causes the group velocity of the fundamental frequency mode to be frequency-dependent, known as GVD. This effect causes spectrum pulse broadening during propagation, causing different signal components to travel at different velocities and arrive at the output non-simultaneously. Material dispersion is caused by irregularities in the refractive index of silica, fabrication materials, and characteristic resonant frequencies that cause radiation absorption. Waveguide dispersion is caused by a dependence of the operating wavelength of the signal on the core radius and the differences in the core and cladding of the fiber waveguides. The

dispersion can be managed by using dispersion compensating fibers, fiber Bragg gratings for long-haul systems and dispersion equalizing filters. As the bit rates increase, tunable dispersion compensators and electronic dispersion compensation can be used. The use of digital signal processing (DSP) in the electronic method has greatly improved the reverting of dispersion effects. In this dissertation, dispersion is assumed to be electronically compensated while considering the PLIs.

Fiber losses limit the transmission distance of the signals. Amplifiers are required to boost the signal for fiber lengths over 100 km [43]. During the 1990s, all-optical amplifiers began to supersede the intricate and costly optoelectronic repeaters, eliminating the necessity of converting signals into electrical form at the receiver before regeneration. There are two main approaches to all-optical amplifiers: lumped and distributed. In lumped amplifiers, pumped erbium-doped fibers are used to compensate for the accumulated losses over a span of 60 to 80 km. In the distributed method, the fiber itself is used for the loss compensation by controlled use of the nonlinear stimulated Raman scattering (SRS) effect, and pump lasers are periodically placed to pump optical powers at suitable wavelengths. In this dissertation, erbium-doped fiber amplifiers (EDFA) are assumed for the signal amplification. However, amplifier noise in itself is a signal QoT-degrading source and is an ultimate limiting factor. The spontaneous emission during the amplification process adds noise to the signal, termed as amplified stimulated emission (ASE) noise. Its spectral density is assumed to be constant i.e., white noise assumption. Despite the low noise levels of EDFAs, the performance of long-haul optical fiber communication systems employing multiple EDFAs is often limited by the ASE noise [43]. Hence, this dissertation considers the ASE impairment for QoT-aware networking algorithm design.

Using optical amplifiers and dispersion management together can extend the length of an optical system to several thousand kilometers. However, in an all-optical domain amplifier-cascaded long-haul system, the other factors limiting the performance are the nonlinear effects: SPM, XPM, FWM, and Raman-induced nonlinearities, especially the SPM and XPM. The origin of these nonlinearities is the nonlinear relation between the refractive indices of the core-cladding medium and the light signal intensity, called the Kerr nonlinearity effect for optical fibers. In the SPM effect, this nonlinearity results in a varying refractive index profile for the medium producing frequency chirping and phase shifts in the propagating optical pulses. Whereas in XPM, a similar effect is produced when two or more

optical signals are transmitted at different wavelengths, and one affects the other by changing the refractive index of the propagation medium. In FWM, three optical carriers produce a fourth optical field with frequency as a sum or difference combinations of the three frequencies. Unlike XPM, FWM causes energy transfer in the pulses, thus creating new ghost bits, leading to bit errors in the system.

These effects pertain to each core in the fiber link. In MCF links, another noise to consider is the inter-core crosstalk (XT). As the name suggests, inter-core XT is the leakage of signal power from one core to another, thus causing disturbances to each other. Different methods are employed to minimize the XT effects, such as trench-assisted core design, increasing distance between the cores, and switching off a few cores during operation.

In conclusion, considering the impairments is crucial in the network design and planning stage. Hence, in this dissertation, the proposed networking algorithms consider a cross-layer (physical and network) design of the optical network.

Chapter 3

Multi-Band Resource Allocation Algorithm

The chapter presents a routing, modulation, and spectrum allocation algorithm for C+L band elastic optical networks considering fiber impairments such as cross-phase modulation, self-phase modulation, amplified spontaneous emission, and inter-channel stimulated Raman scattering. A reinforcement learning-based dynamic routing algorithm is proposed using Q-learning. The effect of fragmentation is considered in the Q-learning process in addition to considering constraints related to spectrum continuity, contiguity, and non-overlapping. The proposed RMSA approach is evaluated on two network topologies, NSFNET and COST-239 and is shown to have a lower blocking probability compared with using K-shortest path routing combined with the three classical spectrum allocation strategies: first-fit, last-fit, and exact-fit. This work has been published in [29].

3.1 Introduction

Although EONs offer better spectrum utilization than WDM networks, it is still essential for network operators to find ways to utilize the existing resources efficiently and explore new technologies to increase the networks' capacity. Starting from a single core fiber network, a cost-effective solution is extending the operational range of frequencies by targeting the already existing spectrum resource of a fiber network. At present, the C-band is majorly used by all optical systems. Adding the next band, i.e., the L band, to this existing C-band would increase the system's capacity to 10 THz. This is possible due to the negligible attenuation coefficient variation in C+L bands and the possibility of using the same EDFA

for the L-band. However, this also introduces inter-channel stimulated Raman scattering (ISRS), resulting in a power transfer from high-frequency components to lower ones and making the optical signal-to-noise ratio (OSNR) frequency-dependent [44]. Hence, when dealing with the C+L band, it is vital to consider the ISRS nonlinear effects in addition to the usual Kerr nonlinear effects such as the XPM and SPM, as well as the EDFA's ASE noise.

The KSP algorithm is a state-independent routing scheme that selects the same path for a pair of nodes for the entire lifetime of the network operation. This chapter presents a state-dependent dynamic routing scheme using a reinforcement learning technique called Q-learning. The fiber impairments of C+L band EONs such as XPM, SPM, ASE, and ISRS are considered. The effect of fragmentation is considered in the Q-learning process in addition to considering constraints related to spectrum continuity, contiguity, and non-overlapping. Three classical spectrum allocation strategies, FF, LF, and EF are used after the Q-learning routing algorithm.

The rest of this chapter is organized as follows. Section 3.1.1 summarizes the current literature in this area and highlights the novel contributions. Section 3.2 provides the C+L band model and the QoT estimation process. Section 3.3 briefs about Q-learning and provides a detailed pseudocode of the proposed algorithm. An example demonstration is also given. Section 3.4 discusses the time and space complexity of the algorithm. Section 3.5.2 details the simulation and discusses the obtained RMSA results, followed by a chapter summary in Section 3.6.

3.1.1 Related Works

Several research works can be found in the literature on solving the RSA problem in EONs. Xu et al. [45] proposed an online-offline algorithm for spectrum assignment of demands with varying bandwidths. To accommodate the randomness of bandwidth demands, the authors proposed a probabilistic PLI model. In another work, Xu et al. [46] proposed a Gaussian noise-based PLI model and a MILP design using a heuristic approach, resulting in resource savings and comparatively higher speeds. Yan et al. [47] investigated the regenerator allocation problem in flex-grid optical networks to deal with PLI and included time as an extra optimization dimension to address time-varying traffic. Wang et al. [20] studied the impacts of using multiple-modulations, regeneration, modulation conversion, and wavelength conversion techniques in EONs using a recursive

MILP approach. Chatterjee et al. [8] compared different routing and spectrum allocation approaches and summarized recent works on RSA related issues such as modulation, fragmentation, traffic grooming, survivability, QoT, energy saving, and networking cost. Adhikari et al. [6] presented a bit error rate (BER) and fragmentation-aware RSA algorithm; their simulation results showed that BER-awareness increases the blocking probability, which can be addressed by increasing the transmit power but at the cost of increased NLI noise. Abkenar and Rahbar [12] reviewed existing RSA and RMSA algorithms and compared them in terms of their computational complexity and quality of performance in resource management. Li and Li [48] presented an RMSA algorithm with a trade-off between minimizing the interval between spectrum blocks and the consumed resources. Choudhury et al. [49] described the performances of different routing and spectrum allocation approaches for multi-cast traffic in EONs.

A few techniques using machine intelligence have been proposed to optimize network routing, as described in recent survey papers. Zhang et al. [9] presented an overview on routing and resource allocation based on machine learning in different optical networks such as WDM, orthogonal frequency-division multiplexing (OFDM)-based EON, and SDM-EON. Dai et al. [50] investigated state-of-the-art techniques in machine intelligence-enabled network routing and discussed development trends. Amirabadi [51] reviewed ML applications in optical communications, providing a comprehensive view of ML techniques applicable in this field. Amin et al. [52] surveyed applications of machine learning techniques for routing optimization based on unsupervised learning, supervised learning, and reinforcement learning in software-defined networking. Mammeri [53] provided a comprehensive review of literature on reinforcement learning (RL) applications for optimal route selection in different types of communication networks under various user quality-of-service requirements.

The following works are the closest to the contribution in this chapter. Yu et al. [26] proposed a deep learning-based RSA strategy and reported that the neural network model had reduced spectrum fragmentation and blocking probability. Shimoda and Tanaka [54] proposed a deep reinforcement learning (DRL)-based RSA algorithm enhanced with domain-specific knowledge. Chen et al. [24] proposed DeepRMSA, a deep reinforcement learning-based neural network for addressing the RMSA problem. The DeepRMSA learned the correct online RMSA policies by parameterizing the policies with deep neural network (DNN)s to sense complex EON states; PLIs were considered but limited to modulation format se-

lection based on distance. The same authors [55] extended the Deep RMSA to multi-domain EONs and presented a new architecture for network management using multi-agent RL showing better performance than a heuristic-based design. Further, Chen et al. [56] proposed a transfer learning-based DeepRMSA that can transfer knowledge of different DRL agents depending on the network tasks. However, efficient network feature extraction remains a challenge, and graph neural networks (GNNs) were cited as a potential solution. Lia and Zhu [57] used GNNs for resource orchestration in elastic optical data center interconnections.

Mitra et al. [27] studied the effect of reduced link margins on C+L band EONs and reported that significant gains in capacity can be achieved by operating at low margins across the networks. Jana et al. [58] proposed a signal-quality-aware proactive defragmentation scheme for C+L band systems using deep neural networks; minimizing the fragmentation index and QoT maintenance was prioritized for both nonlinear-impairment-aware and unaware defragmentation.

3.1.2 Chapter Contribution

Based on the literature review, only a few researchers have considered ML approaches such as RL, neural network (NN)s DNNs, DRL, with or without consideration of different impairments. The PLIs considered in previous works do not simultaneously include linear and nonlinear impairments. Furthermore, the NN, DNN, and DRL models presented in the current literature are knowledge-intensive, and most of them consider only the C-band.

The novelty of the work in this chapter lies in attempting to adopt a simple model-free Q-learning algorithm, which belongs to the family of RL algorithms, to solve the RMSA problem in single-core EONs using C+L band. From our literature survey, Q-learning has not been applied to the optical network routing problem; Q-learning does not require pre-collected training data, can be used by the SDN network controller, and is simple to implement. In addition, the present work considers the ISRS, Kerr nonlinear impairments (SPM, XPM), and the EDFA ASE noise encountered by the signal along the chosen network path. These impairments have rarely been jointly considered [58] for resource provisioning in C+L band operation. The effect of fragmentation of the network is also considered in the Q-learning process.

The significance of the work lies in proposing a state-dependent routing scheme using Q-learning and crafting local and global custom reward functions for the Q-

learning algorithm while simultaneously considering PLIs, fragmentation, and the constraints of spectrum continuity, contiguity, and non-overlapping to perform online RMSA for C+L band EONs. The algorithm's performance is evaluated against a standard K-shortest path algorithm, commonly used as a benchmark. Employing the Q-learning routing algorithm yielded lower blocking probabilities across all spectrum algorithms, network loads, and topologies examined.

3.2 C+L Band Lightpath Model and OSNR Estimation

The considered C+L band EON consists of 10 THz bandwidth links, each divided into spans. A typical network lightpath connection in such a network is shown in Fig. 3.1. The signal is launched with power P_{ch} and travels through a series of intermediate ROADMs placed at the end of each link. At the end of each span, two Erbium-doped fiber amplifiers amplify the signals, one for the C-band and one for the L-band. The EDFAs are capable of compensating for the ISRS power transfer variations across all the active channels in the C+L band by bringing the power back to P_{ch} and thereby restoring the originally transmitted power spectrum.

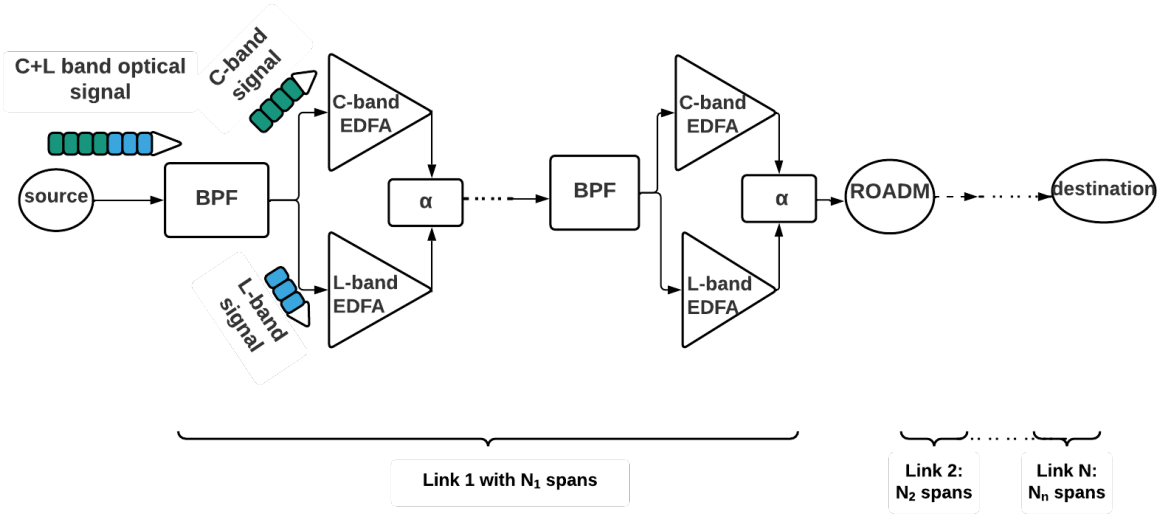

Figure 3.1: Lightpath example with multiple hops. The symbol α represents the fiber attenuation.

The Gaussian noise model used to estimate the PLI levels accounts well for

the Kerr nonlinearity effects, but it cannot be directly applied to the C+L band scenario due to the additional ISRS effect in this extended bandwidth. ISRS can be either accounted for by using an extra exponential power decay term or by numerically solving the ISRS differential equations. The first approach is suitable for approximating weak ISRS regimes, and the second approach can approximate any level of ISRS but has a higher computational complexity. The latter necessitates a closed-form model, and one such model was used in [27]. The ISRS gain is modeled using a linear approximation up to 15 THz by using the slope of the normalized Raman gain spectrum. Hence, this can also be applied to the considered 10 THz C+L band scenario. The current work adopts the OSNR estimation model of [27].

The OSNR of a light path Υ traversing N_Υ set of links is calculated as [Eq.(1), [27]],

$$\frac{1}{OSNR(f)} = \sum_{e=0}^{N_\Upsilon - 1} \left(\frac{P_{ASE}^{(e)}(f) + P_{NLI}^{(e)}(f)}{P_z} \right). \tag{3.1}$$

$P_{ASE}^{(e)}(f)$ is the ASE noise due to the EDFA present on the e^{th} link of Υ, $P_{NLI}^{(e)}(f)$ is the NLI power due to SPM and XPM, and P_z is the power of channel of interest, z. The signal power spectral density (PSD) is assumed to be rectangular, and so, the NLI power is calculated for the center frequency f of the signal. In the current work, f refers to the center frequency of the channel z that the spectral assignment algorithm proposes to assign to the request.

The total ASE noise power on link e with $N_s^{(e)}$ spans having symmetrically spaced EDFA modules is given by

$$P_{\text{ASE}}^{(e)}(f) \approx 2N_s^{(e)} \eta_{sp} g(f) h\nu B_{ref}, \tag{3.2}$$

where η_{sp} is the noise figure of the EDFA and h is the Planck's constant. ν is the optical light frequency and B_{ref} is the reference bandwidth of the operating ASE noise power measurement. The gain $g(f)$ needs to account for both the power loss due to attenuation in the fiber span and the power transfer due to ISRS i.e. the frequency-dependent ISRS gain profile across the C+L band. Hence the overall gain $G(f)$[dB] (linear $g(f)$) for the EDFA module that affects the ASE generation in Eq. (3.2) is given by

$$G(f) = \begin{cases} \alpha L_{\text{span}} - \rho^{\text{span}}(f) & \text{positive ISRS Gain at f} \\ \alpha L_{\text{span}} & \text{no ISRS gain at f f} \\ \alpha L_{\text{span}} + \rho^{\text{span}}(f) & \text{negative ISRS Gain at f} \end{cases} . \tag{3.3}$$

where L_{span} is the span length, α is the fiber loss, and $\rho^{\text{span}}(f)$ is the ISRS gain at frequency f approximated as

$$\rho_f^{\text{span}} = \ln \left[\frac{P_z(L_{\text{span}})}{P_z(0) \exp(-\alpha L_{\text{span}})} \right]. \tag{3.4}$$

where P_z is the launch power of channel z. The total NLI power experienced by z with center of frequency f_z in the e^{th} optical link with $N_s^{(e)}$ spans is given by

$$P_{NLI}^{(e)}(f) = P_z^3 N_s^{(e)} \left(\eta_{XPM}(f_z) + \eta_{SPM}(f_z) \right). \tag{3.5}$$

The NLI coefficients, $\eta_{XPM}(f_z)$ and $\eta_{SPM}(f_z)$ are computed as below [27, Eqs. (7)-(11)].

$$\begin{aligned} \eta_{\text{SPM}}(f_z) \approx & \frac{4}{9} \frac{\gamma^2 \pi}{B_z^2 \phi_z \bar{\alpha}(2\alpha + \bar{\alpha})} \\ & \cdot \left[\frac{T_z - \alpha^2}{\alpha} \operatorname{asinh}\left(\frac{\phi_z B_z^2}{\alpha \pi} \right) + \frac{A^2 - T_z}{A} \operatorname{asinh}\left(\frac{\phi_i B_z^2}{\pi A} \right) \right] \end{aligned} \tag{3.6}$$

$$\begin{aligned} \eta_{\text{XPM}}(f_z) \approx & \frac{32}{27} \sum_{k=1, k \neq z}^{D_{\text{act}}} \frac{\gamma^2}{B_k \phi_{z,k} \bar{\alpha}(2\alpha + \bar{\alpha})} \\ & \cdot \left[\frac{T_k - \alpha^2}{\alpha} \operatorname{atan}\left(\frac{\phi_{z,k} B_z}{\alpha} \right) + \frac{A^2 - T_k}{A} \operatorname{atan}\left(\frac{\phi_{z,k} B_z}{A} \right) \right] \end{aligned} \tag{3.7}$$

where $\phi_z = \frac{3}{2}\pi^2 (\beta_2 + 2\pi\beta_3 f_z)$, $\phi_{z,k} = 2\pi^2 (f_k - f_z) [\beta_2 + \pi\beta_3 (f_z + f_k)]$, $A = \alpha + \bar{\alpha}$, $T_z = (A - P_{tot} C_r f_z)^2$, $T_k = (A - P_{tot} C_r f_k)^2$, B_z and B_z are the bandwidths of channels z and k.

Fully filled channels were considered in [59] to show the effectiveness of these closed-form expressions. For the scenario in this work, D_{act} is the total number of demands active on the particular link that can vary as requests arrive and depart. This model can be utilized as the closed-form of the GN-model under both the C-band and C+L band scenarios. This aspect was mutually acknowledged by the authors of both models in [60, 61, 21]. The parameter description is as follows

and Table 3.1 presents their typical values used in the current work [59]:

- f_k: frequency of channel k
- γ: fiber nonlinearity coefficient
- B_k: bandwidth of channel k
- α: attenuation coefficient in C-band
- $\bar{\alpha}$: attenuation coefficient in L-band. The attenuation coefficient variation over the considered C+L band is assumed to be negligent in this work, hence $\alpha = \bar{\alpha}$.
- β_2: group velocity dispersion
- β_3: linear slope of β_2
- P_{tot}: Total launch power
- C_r: Raman gain slope

Table 3.1: System and Fiber Parameters Used for multi-band EON

Parameters	Values
Fiber attenuation α, dB/km	0.2
Group velocity dispersion β_2, ps/nm/km	17
Dispersion slope β_3, ps/nm^2/km	0.067
Nonlinear coefficient γ, 1/W/km	1.2
Raman gain slope C_r, 1/W/km/THz	0.028
Raman gain $C_r \cdot 14$ THz, 1/W/km	0.4
Channel launch power P_{ch}, dBm	0
Number of channels	Variable
Optical bandwidth, THz	10
Slot bandwidth, GHz	12.5

The OSNR that the current request would experience if it were to be assigned the particular tentative route is calculated using the models above and compared with the OSNR threshold. Also, alongside satisfying its OSNR constraint, the new and

about-to-be provisioned request should not degrade different existing requests along with various links of the tentative route. Hence, the OSNR constraint also includes checking their corresponding OSNR threshold requirements.

Another term that requires defining is fragmentation since it is used as a part of the proposed algorithm. To compute the fragmentation on a particular link of a lightpath, an entropy-based fragmentation metric is used, [62]

$$F^{(e)} = \sum_{\gamma_e \in \Gamma_e} \frac{|\gamma_e|}{S} \cdot \ln \frac{S}{|\gamma_e|}, \tag{3.8}$$

where Γ_e is the set of fragments on link $e \in E$, $|\gamma_e|$ is the size of fragment γ_e, and S is the total number of frequency slots on e. This fragmentation metric is based on the entropy concept and better captures the difference in fragment sizes, i.e., better distinguishes differently fragmented links compared to the commonly-used external fragmentation formula [62] [33].

3.3 Q-learning-based EON Routing Algorithm

Reinforcement learning (RL) stands out as a powerful methodology for attaining optimal behavior within complex systems through the mechanism of reward-based interactions between an agent and its environment [63]. These positive or negative rewards reflect the efficacy of the agent's decisions in achieving desired objectives. Hence, in the long run, the agent tries to maximize the cumulative rewards by taking favorable actions to get the desired output. RL has found application in areas such as robotics, gaming, networks, telecommunications, and building autonomous systems. RL is commonly considered suitable for solving optimization problems related to distributed systems in general and for network routing in particular. Fig. 3.2 shows the general scheme of reinforcement learning.

Table 3.2: Q-table Used in Q-learning

States	Action 1	Action 2	Action N
State 1	$Q(s_1,a_1)$	—	$Q(s_1,a_N)$
State 2	$Q(s_2,\ a_1)$	—	$Q(s_2,\ a_N)$
State M	$Q(s_M,a_1)$	—	$Q(s_M,a_N)$

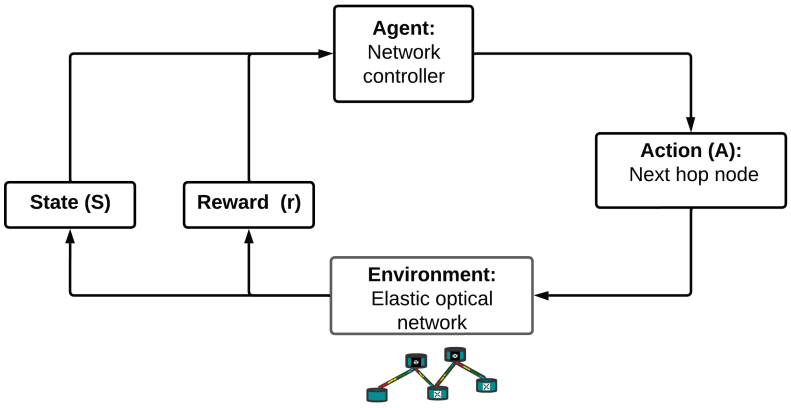

Figure 3.2: General scheme of reinforcement learning

Q-learning is one of the widely known RL algorithms [63]. Q-learning algorithms use a state-action table consisting of Q-values that indicate the quality of the action at each state, as shown in Table 3.2. Each Q-value is denoted by $Q(s, a)$, representing the expected reinforcement of taking action a in state s. The action space contains the actions that the agent can perform, while the state space represents possible system conditions.

The entries in the Q-table are updated using the Bellman equation after an action is taken, and the update model is,

$$Q_{\text{new}}(s, a) = (1 - \xi)Q(s, a) + \xi \left(rew_{t+1} + d \max_{a' \in actions}, Q\left(s', a'\right) \right), \tag{3.9}$$

where $Q_{\text{new}}(s, a)$ is the updated value denoting the quality of action a taken, $Q(s, a)$ is the old value, and rew_{t+1} is the reward obtained for taking action a; ξ is the learning rate parameter, and d is the discount factor that determines the importance given to the anticipated future rewards; s' is the state attained after taking action a; a' is the particular action that has the maximum Q-value among all the possible actions from the given state s'.

This work uses the Q-learning algorithm to perform dynamic routing in C+L EONs. After the routes are decided by the Q-learning algorithm, the modulation assignment is done based on the length of the chosen tentative route. The spectrum allocation (SA) for each route is then assumed to use one of three well-known algorithms: first-fit (FF), last-fit (LF), and exact-fit (EF), as described in Chapter 2. In the EON scenario of this chapter, the network nodes, $s \in V$, are considered as the states, and their respective Q-values are affected

by the estimated PLI, fragmentation, and link availability as seen by the adjacent nodes. The action is a decision on what the next hop should be, given the desired destination, and thus the action space is represented as the pair (network node, destination) $\in (V, V)$. The proposed routing algorithm includes the effect of fragmentation, link availability, and physical layer impairments in the Q-learning process through local (fragmentation-based and link availability-based) and global (PLI-based) rewards. The proposed approach is modeled on recent literature defining the state and/or action spaces similar to this current work [Table 2 and 3, [53]], [64, 65, 66, 67]. However, these prior studies have targeted different applications than what is considered in this work: here, the Q-learning method is adopted to perform routing in EONs by including EON-specific system parameters and performance metrics, which has not been reported in the literature.

In RL, an episode is defined as a sequence of states that ends at a terminal state. To adapt the Q-learning algorithm to the proposed resource allocation scenario, an episode is defined as one lightpath selection made by the central network controller, starting from the requested source node and reaching the destination node. Consequently, the proposed approach emulates hop-by-hop routing without the network actually making the node-level decisions. This is possible due to the automated EON data plane control by the network controller.

The algorithm collects current network information in a Q-table as a result of rewards acquired both during the provisioning of other requests and during the current request's episodic runs. It uses a randomizing parameter ϵ that controls whether to explore different paths or exploit the gained knowledge in the Q-table. This ϵ decays over the episodes to make the system take exploratory decisions initially; as the ϵ decays over the episodes, the algorithm tends to take more exploitative actions through the knowledge already acquired.

Table 3.3 shows $K = 3$ routes obtained using our Q-routing algorithm for the NSFNET, shown in Fig. 2.6(a), for two repeated requests tracked for demonstration purpose. Requests for routes with (source, destination) $= (13, 5)$ result in different candidate lightpaths since the Q-table values vary based on the different reward values. This is not the case for KSP routes. Similarly, when requests for transmission between nodes $(4, 14)$ occur, different routes become candidate choices at different request arrival times. Note that some repetition in the candidates' route list is normal since the K routes cannot all be unique to each arrival time; they all belong to the same subset of all possible paths.

Table 3.3: $K = 3$ Routes Obtained by the Q-routing Algorithm for a Given (source, destination) Pair Connection Request

(Src,Dest)	**Routing**	**Route 1**	**Route 2**	**Route 3**
(13,5)	KSP	[13,9,8,7,5]	[13,14,1,9,8,7,5]	[13,14,6,5]
	Q-routing	[13,9,8,7,5]	[13,14,6,5]	[13,9,10,6,5]
	Q-routing	[13,14,6,5]	[13,11,4,5]	[13,9,10,6,5]
(4,14)	KSP	[4,11,13,14]	[4,11,12,14]	[4,5,7,8,9,13,14]
	Q-routing	[4,11,13,14]	[4,5,6,14]	[4,2,3,6,14]
	Q-routing	[4,2,3,6,14]	[4,11,12,9,13,14]	[4,11,13,14]
	Q-routing	[4,2,3,6,14]	[4,5,6,14]	[4,5,7,8,9,12,14]

Algorithm 3.1 gives a pseudo-code of the proposed Q-learning algorithm for EON routing. Consider a particular network provisioning demand where X is the current node, Z is the destination node, and Y is the next-hop node for X. Then, $Q(X,(Y,Z))$ represent the Q-value for X to reach Z via Y It is important for the Q-value to be a function of the destination node so that the node-by-node learning accounts for how beneficial it is to traverse through a particular Y to reach Z.

Rewards play a major role in steering the decisions of the Q-learning agent, and this work uses rewards to avoid routing loops, invalid actions, and proper node selections, all enabling destination-reaching capability. The actions of non-connected nodes and already visited nodes are penalized, and additionally, each episode restricts the search to a maximum number of steps to curb routing loops. Positive rewards are given upon reaching Z based on computed fragmentation, link availability, and PLI satisfaction for all remaining action scenarios.

Algorithm 3.2 shows the PLI-aware RMSA algorithm that uses the output routes of Algorithm 3.1. The algorithm computes the required frequency slots based on the chosen modulation format and checks for continuity and contiguity of the frequency slots. It then checks if the route satisfies the OSNR threshold constraint and accepts it if all constraints are satisfied. If K candidate paths are assumed ($K = 3$ in the present work), then the above procedure is repeated for those K paths until a proper route is found, or else the request is blocked.

Algorithm 3.1 Q-learning-based EON routing algorithm

```
1: procedure ROUTING(source = X, destination = Z, Q-table (initialized to 0))
2:     while Maximum number of episodes is not reached do
3:         Set Visited nodes = [ ]
4:         Set Current node = X
5:         Set Candidate_route = [ ]
6:         while Current node is ≠ Z (i.e. terminal state) do
7:             Obtain Q(possible_actions) where possible_actions ∈ (|V|, Z)
8:             if exploitation is True then
9:                 action = argmax_(|V|,Z) {Q(possible_actions)}
10:            else exploration is True
11:                action = random number ∈ |V|
12:            end if
13:            Get neighbors of Current node
14:            if action ∈ neighbors then
15:                Append action to final_route
16:                Get reward for (Current node, action)
17:                Update Visited nodes
18:                Perform Bellman Q-value update (Eq. (3.9))
19:                Do Current node = action
20:            else
21:                Get a negative reward
22:                Perform Bellman Q-value update (Eq. (3.9))
23:            end if
24:        end while
25:        Store the route of current episode if it is a feasible path
26:    end while
27:    Extract K-1 more paths from stored set of feasible path from over the episodes
28:    return K valid routes from X to Z
29: end procedure
```

Algorithm 3.2 PLI aware RMSA scheme based on proposed routing algorithm

procedure RMSA(source = X, destination = Z, requested bandwidth)
    Obtain K paths from Algorithm 3.1
    Set route counter $k = 0$
    while a valid route satisfying all constraints is not found or $k \neq K$ **do**
        Obtain modulation format, number of frequency slots (Eq. (2.3)), and OSNR_threshold
        Find feasible spectrum slots using First Fit/Last Fit/Exact Fit
        if spectrum constraints are satisfied **then**
            Compute OSNR (Eq. (3.1))
            if OSNR_computed $\geq$ OSNR_threshold **then**
                Assign the light path (LP) resources
                Compute the local reward for each node of the LP: fragmentation (Eq. (3.8)) and available spectral slots on the corresponding link
                Compute a positive global reward if PLI constraint satisfied, else a negative global reward
                Add the global to reward to each local reward
                Perform Bellman update similar to Algorithm 3.1
            else
                Check on next feasible spectrum block
            end if
        else
            Check on next feasible spectrum block
        end if
        Set k=k+1
    end while
    return a valid RMSA solution
end procedure

3.3.1 Example Scenario

The algorithm's application is explained with an example scenario. Consider a traffic demand from source X to destination Z with a data rate of 200 Gbps. K routes are found for this source-to-destination pair using Algorithm 3.1; $K = 3$ in the presented results. The number of frequency slots, S_{req}, is computed using Eq. (2.3). Then, the spectrum allocation part of the algorithm begins. A set of frequency slots is found using either the first fit, last fit, or exact fit SA. The contiguity constraint (the S_{req} are adjacent on the link), continuity constraint (the S_{req} are at the same spectral positions on each link of the route), and frequency non-overlapping constraint are checked on the selected route. If all constraints are satisfied, the OSNR satisfaction constraint is checked.

The $OSNR$ is obtained from Eq. (3.1); the $OSNR_{\text{threshold}}$ is based on the chosen modulation format. If any of the three constraints were not satisfied or the OSNR condition failed for the selected frequency slots, then the next frequency is selected and again checked. If all the frequencies are exhausted, then the next route in the already-found routes from Algorithm 3.1 is picked, and the conditions are checked. If no suitable route is found even after three paths, the request is blocked. The blocking can be either frequency blocking or PLI blocking.

Whether a route acceptance or rejection happens, rewards are assigned to all the nodes of the route that led to success or failure. If it is a success, the local reward is calculated based on the fragmentation occurring on each of the chosen links (Eq. (3.8)) and the links' availability, i.e., number of unoccupied frequency slots. These two are considered in the reward calculation since high fragmentation and low link availability can lead to higher blocking. If the chosen route has three nodes, then the local reward will be a vector of three elements. Including this information is a way of praising or criticizing the action taken to choose that particular node's link for any next request to the same destination. The fragmentation reward is negative since the Q-learning algorithm tries to maximize the reward, and fragmentation values are desired to be low. In the proposed Q-learning routing algorithm, the global reward is related to OSNR satisfaction. A global reward of +1 or -1 is added to the above-decided local reward for each node on the route depending on whether the OSNR constraint is satisfied or not. The total rewards (sum of the local and global rewards) are then used to update the Bellman equation, Eq. (3.9), for each node of the considered route. It is these same node values that the Q-learning EON routing later uses to tentatively choose a path at each node, thus emulating hop-by-hop routing for

upcoming requests.

As a side note, this approach could be extended to EON using multimode or multicore fibers, where the fragmentation computation is different than for the single-core single-mode RMSA case [68, 69]. Perhaps more carefully crafted reward functions can then be used in order to capture the fragmentation differences in the spatial modes/cores rather than considering a single value in the reward.

3.4 Time and Space Complexity

The worst case time complexity of Algorithm 3.1 can be deduced as follows. The Q-table is stored in the form of a dictionary that is implemented as a hash table to make it less time-consuming to find the desired Q-value using the state as the key. The time complexity to search for one value in a dictionary is O(1). Hence, the worst-case scenario for a given destination is when all the states in the state and action space are visited, and the complexity would then be $O\left(|V|^2\right)$.

The size of the Q-table in the proposed algorithm is $|V| \times |V| \times |V|$ because for each of $|V|$ state node, there are $|V|$ potential next hops on the way to $|V|$ potential destinations. This size is reasonable for Q-learning provided all the entries are visited and updated [63]. This condition is fulfilled in the considered network scenario since, as part of the training and during provisioning, the source/destination pairs are randomly generated for thousands of requests, and node-by-node tabular updates are performed for both success and failure scenarios.

3.5 Results and Analysis

3.5.1 Training Setup

As mentioned in Section 3.3, a Q-table is maintained by the centralized controller. Multiple episodes are run in order for the Q-table to converge, even though a route may be found before all episodes are considered. This also helps to finalize a better route than one found along the episode iterations. Figs. 3.3 and 3.4 show the mean rewards obtained for two example source/destination pairs, where the data has been downsampled for plotting purposes. For any given source and destination, convergence was always reached before 10,000 episodes. Note that the overall trend of the rewards is increasing; reward values are more often positive than negative.

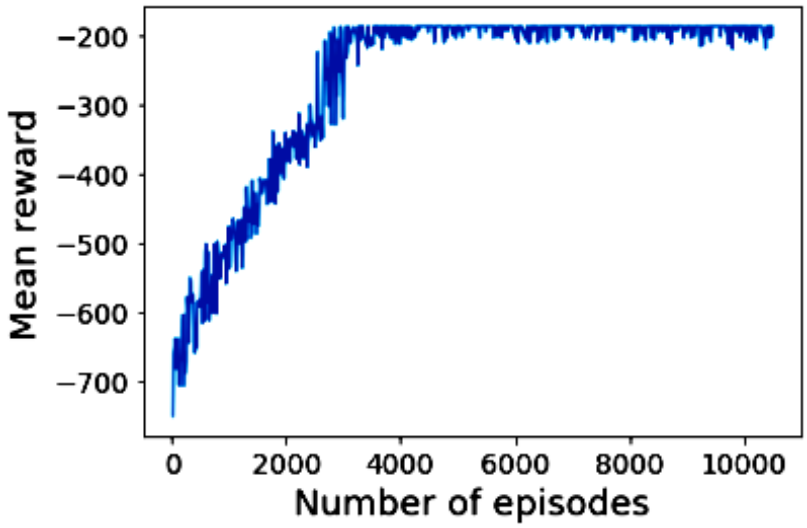

Figure 3.3: Obtained mean reward over the number of episodes for one (source, destination) pair

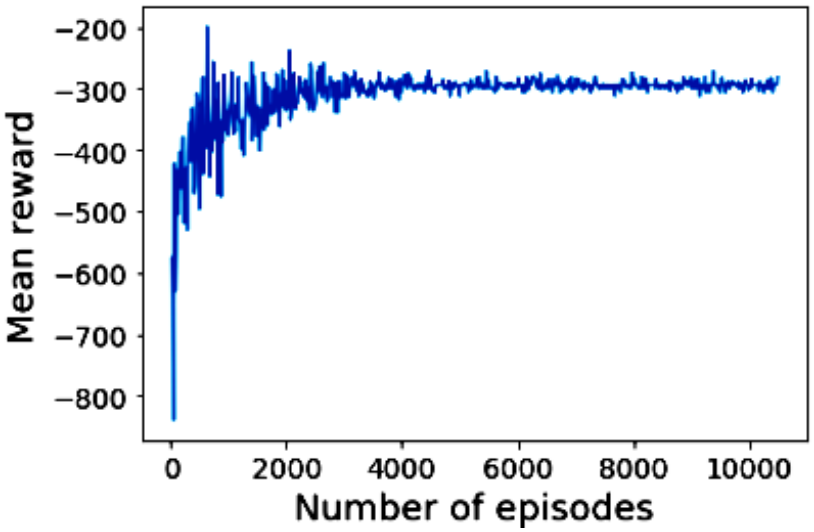

Figure 3.4: Obtained mean reward over the number of episodes for another (source, destination) pair

3.5.2 Network Results

The 14-node NSFNET and 11-node COST-239 networks described in Chapter 2 are used to test the performance of the proposed Q-learning algorithm for routing combined with the three classical spectrum allocation strategies.

Data rates considered are between 50 Gbps to 300 Gbps. Modulation formats considered are BPSK, QPSK, 8QAM, 16-QAM and 32-QAM; the threshold OSNRs are 9 dB, 12 dB, 16 dB, 18.6 dB, and 21.6 dB, respectively [70].

The algorithm's effectiveness is measured by calculating the BP, BBP, and network fragmentation (F_{NET}). For each trial, 300,000 requests are considered to determine these network metrics. The BP and BBP are computed using [Eqns. (2.1)-(2.2)]. The network-wide fragmentation F_{NET} for a network with $|E|$ number of edges can be computed as in [33],

$$F_{NET} = \frac{\sum_{e \in E} F^{(e)}}{|E|}, \tag{3.10}$$

In optical networks, PLIs are typically addressed either through a PLI-aware algorithm, as described above, or using an algorithm that ignores the PLI and then performs a final quality PLI-check just before provisioning; the proposed approach is compared to KSP under each assumption. The PLI effects considered are the fiber Kerr nonlinearity (SPM and XPM) and ASE noise, including the ISRS effect. In the PLI-check approach, the OSNR constraint is checked after the algorithm finds a route and a spectrum allocation. If the constraint is satisfied, the request is provisioned, but no attempt is made to find another route if the condition fails. This process is like the basic RMSA problem but with the additional OSNR constraint. This checking increases the blocking when compared to basic RMSA algorithms, but in a practical network, there is no use in provisioning a request just based on the availability of resources without considering physical layer aspects. Conversely, in the PLI-aware type RMSA, OSNR constraints are checked as a part of the RMSA problem, and re-attempts are made to find another route and/or spectrum allocation (still among the K paths) if the OSNR constraint fails.

Simulation results of blocking probabilities with KSP and Q-learning PLI-check routing using first and exact fit allocation in the NSFNET topology are given in Figs. 3.5 and 3.6. The last fit performance is almost identical to the first fit and, hence, not shown here. As the load increases, a higher resource blocking or QoT blocking is inevitable, irrespective of the chosen routing or spectrum

strategy. For all three SA algorithms tested, the Q-learning routing performed better than the traditional KSP routing.

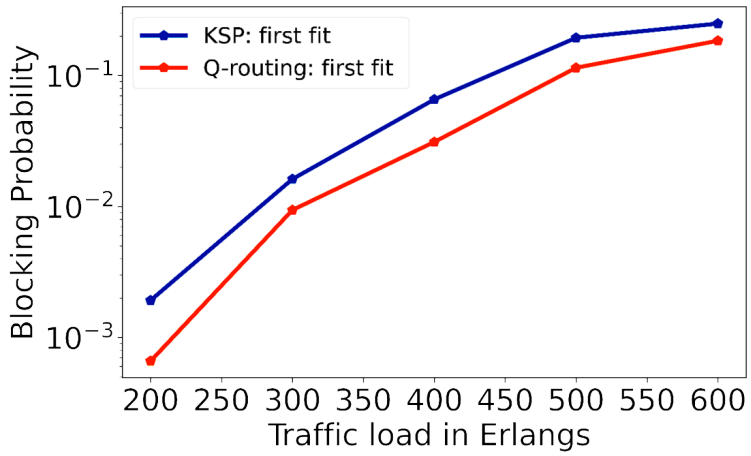

Figure 3.5: Blocking probabilities in NSFNET for PLI-check type RMSA considering KSP routing and Q-learning EON routing using first fit for spectrum allocation.

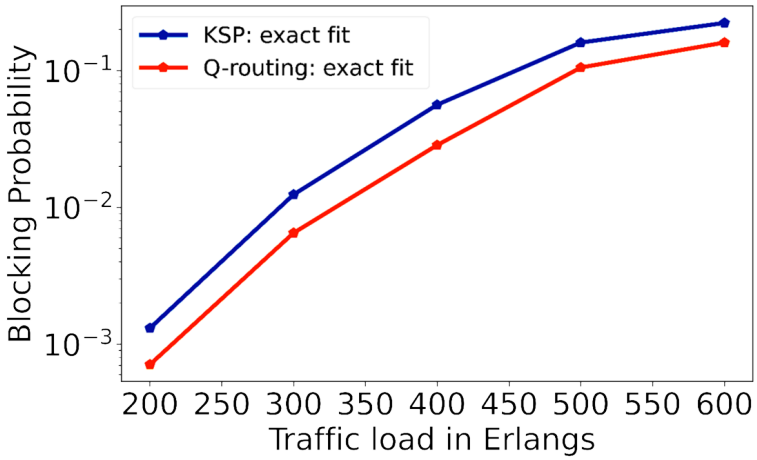

Figure 3.6: Blocking probabilities in NSFNET for PLI-check type RMSA considering KSP routing and Q-learning EON routing using exact fit for spectrum allocation.

When requests arrive repeatedly with sources and destinations whose routes include many common crowded links, shortest path routing leads to repeated blocking due to unavailability of frequency slots or QoT degradation to existing requests on these links. Hence, always following the shortest path rule is not wise in high-usage network operations. Conversely, in the proposed Q-learning routing for C+L band EON, the decision of how to hop from one node to the next is

optimized, thus finding the best Q-valued routes. Unlike the KSP PLI-check case, the likelihood of failure is reflected in the Q-values of the nodes of a failed route. This leads to the selection of different routes over time since the network state changes and gets reflected in the Q-values through the rewards. Consequently, the agent chooses the path that is in the best interest of the current request being considered and also for better service provisioning in long-term operation.This is supported by the simulation results shown in Figs. 3.5 and 3.6.

Figs. 3.7, 3.8 and 3.9 show the blocking probabilities obtained using KSP and Q-learning routing in the NSFNET for the PLI-aware RMSA scenario. The results are plotted with 95% confidence intervals, confirming the stability of the measurements.

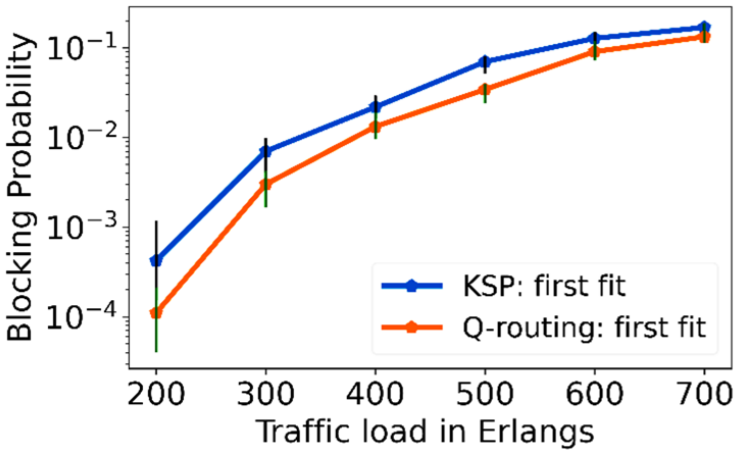

Figure 3.7: Blocking probabilities for PLI-aware RMSA with first fit for spectrum allocation in NSFNET.

The blocking probabilities for these algorithms are lower than for the PLI-check versions, as expected because there is a re-attempt to find another route (among the K routes) and/or frequency spectrum if the OSNR constraint is violated. Q-learning routing continues to perform better than conventional KSP routing, even at high loads. The proposed algorithm achieves 1% blocking at loads greater than around 120 Erlangs than the benchmark. Even with the inclusion of PLI constraints, the Q-learning EON routing can adapt well in the long run. This behavior is explained as follows. For the KSP algorithm, routing decisions affect the blocking probability but are unaffected by spectrum decisions since routing decisions are solely based on distance. On the other hand, for the Q-learning routing, the spectrum affects the routing because the provisioning success or failure is included in the Q-learning process through local (fragmentation, link

availability-based) and global (PLI-based) rewards, affecting the routing of future requests.

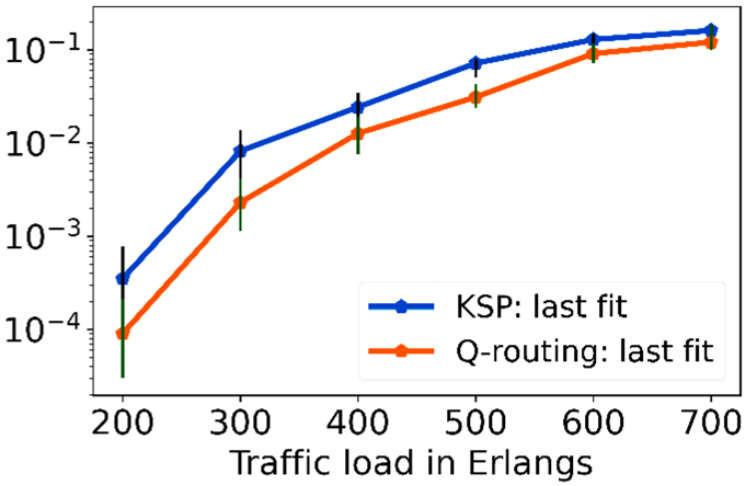

Figure 3.8: Blocking probabilities for PLI-aware RMSA with last fit for spectrum allocation in NSFNET.

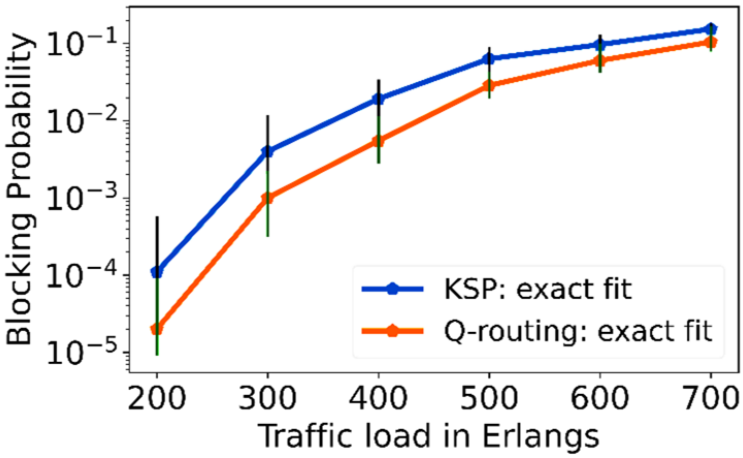

Figure 3.9: Blocking probabilities for PLI-aware RMSA with exact fit for spectrum allocation in NSFNET.

Fig. 3.10 depicts the bandwidth blocking probability for the PLI-aware NSFNET scenario. The Q-learning based routing results in lower BBP when compared to the KSP for all loads tested. The improvement is smaller at higher loads because the fragmentation and PLI effects are higher, and link availability is lower.

Fig. 3.11 shows the F_{NET} for the PLI-aware algorithm on the NSFNET network. At each load, the F_{NET} for every 10,000 requests were collected and then averaged to obtain each of the points on the graph. The proposed Q-learning

based RMSA algorithm is able to maintain lower fragmentation levels because rewards are calculated based on the fragmentation that occurs after provisioning. Note that the considered metric, Eq. (3.8) is a relative measure and not bounded between 0 to 1.

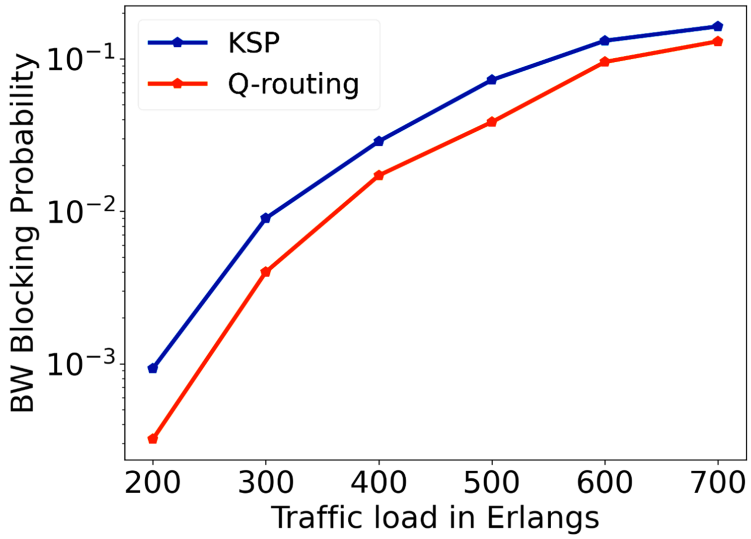

Figure 3.10: Bandwidth blocking probabilities for PLI-aware RMSA in the NSFNET network.

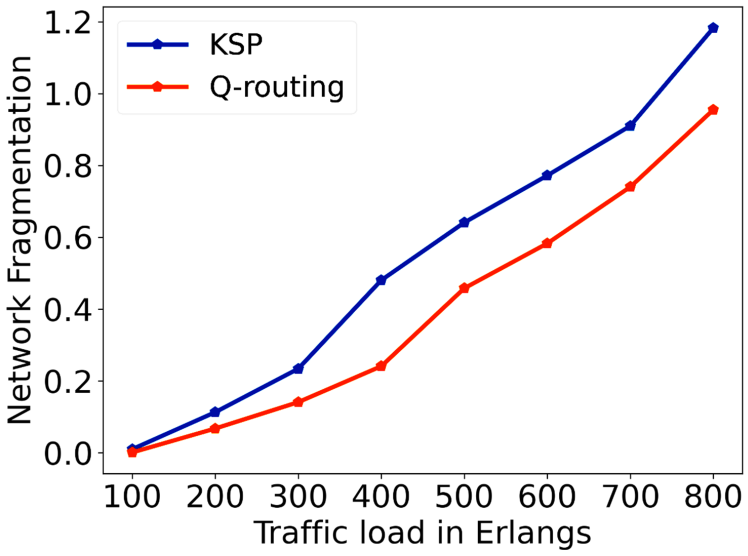

Figure 3.11: Network fragmentation for PLI-aware RMSA in the NSFNET network.

To verify that the proposed Q-learning RMSA algorithm performs well in different network topologies, a similar traffic pattern, as used on the NSFNET

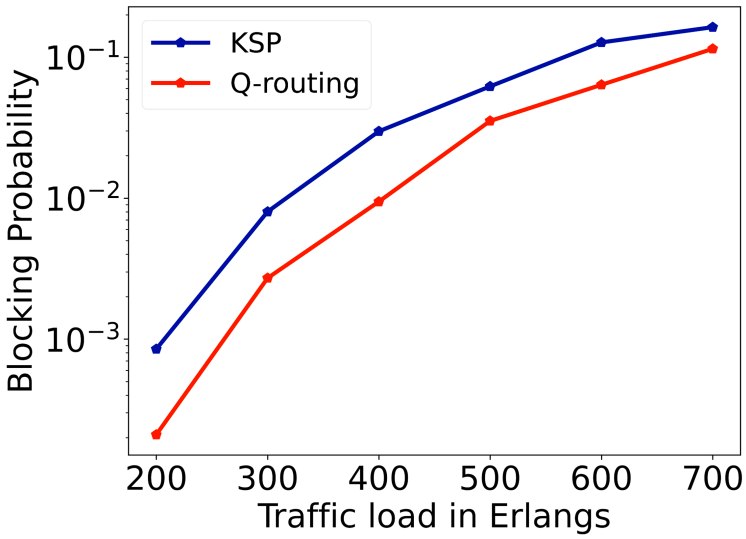

Figure 3.12: Blocking probabilities for PLI-aware COST-239 network with exact fit SA.

topology, is given as input to the European COST-239 network. Fig. 3.12 shows the blocking probabilities obtained using KSP and Q-learning for PLI-aware routing for this topology. Similar conclusions as the PLI-check scenario of NSFNET topology are applicable here as well; hence, only exact fit results are shown. In this network topology as well, the Q-learning routing algorithm is more robust than KSP routing and maintains lower blocking probabilities. Note that the blocking is minutely higher in the COST-239 network when compared to the NSFNET network. In both cases, the proposed algorithm outperforms the traditional KSP algorithm.

The better performance of the proposed algorithm in both continental-sized networks indicates that Q-learning routing can perform better than widely-used KSP routing. As the primary intention of moving towards C+L band EON operation is to support higher capacity traffic, the results showing improved performance at high loads with the inclusion of realistic PLI provides a notable contribution towards the realization of this emerging technology.

3.6 Chapter Summary

Using Q-learning for routing combined with classical spectrum allocation strategies of first-fit, last-fit, and exact-fit is investigated for C+L band EONs. The Q-learning algorithm belongs to the family of RL techniques. The present work

has considered the ISRS effect, Kerr nonlinear impairments such as SPM and XPM, and also the ASE noise encountered by the signal along the chosen network path. The effect of fragmentation and link availability of the network is also considered through the reward-based interactions of Q-learning. To our knowledge, this is the first application of the Q-learning algorithm for routing considering the PLIs, fragmentation, and the constraints of spectrum continuity, contiguity, and non-overlapping to perform online RMSA for C+L band EONs. The simulations are performed on two topographically diverse topologies, NSFNET and COST-239, and the results are analyzed. In general, Q-learning routing performed better than the K-shortest path algorithm. The proposed Q-learning for routing is simple and can be used easily by operators in real situations.

Chapter 4

Important Impairments for QoT-Aware Provisioning in Multicore Fiber Networks

This chapter presents a brief quantitative overview of the effect of various impairments that are significant in MCF EONs when operating with dynamic traffic having varying requirements. This work has been accepted for the *IEEE 2024 Conference on Optical Network Design and Modeling*.

4.1 Introduction

High-capacity optical networks and their management are crucial to support the increasingly connected world. Hence, the next portion of the thesis focuses on multicore single-band networks, that is, the exploitation of spatial diversity instead of spectrum diversity for a multifold increase in capacity. The signals in MCF EONs are also plagued by PLIs that degrade the QoT and limit the transmission reach in continental-scale networks. As mentioned in Chapter 2, linear PLI effects include amplified spontaneous emission (ASE) and crosstalk (XT), and nonlinear impairments (NLI) include self-phase modulation (SPM) and cross-phase modulation (XPM). The XT is an additional impairment in MCF-EONs compared to the single core EONs. Hence, impairment effects are inevitable, and the networking algorithms need to be all-impairment-aware. However, before delving into the design of novel algorithms in the next chapters, we first discuss the state-of-the-art followed by a brief quantitative discussion on the importance

of the PLIs and impact on resource provisioning in MCFs.

4.1.1 Literature Review

Many impairment-aware algorithms in the realm of MCF networking consider only the XT impairment. The ASE, XPM, and SPM effects that have dominated the QoT-aware single core literature are ignored. In [71], the focus was on inter-mode and inter-core XT and to reduce the BP. A bi-partitioning method wass proposed to maximize the number of non-adjacent cores and modes in each partition of the bipartite graph, essentially using two distinct sets of cores and modes in a counter-propagation manner for lightpath establishment. In [72], two heuristic algorithms were proposed for multi-cast traffic using a rating method for the links. A strict strategy of avoiding XT was employed to reduce the amount of calculations, which can lead to a decrease in spectral efficiency due to the unnecessary spreading of signals. In [73], the authors solved an RSCA problem that simultaneously finds the route, core, and spectrum for each request. The advantage is the reduction in provisioning time, which can be useful for provisioning in large-scale networks. However, a static traffic scenario was considered, and since the complexity of the problem increases in a dynamic scenario, it would be interesting to extend the proposed approaches. Moreover, a worst-case XT was assumed, leading to conservative over-provisioning of the network.

In [39], an ILP-based attack aware RMSCA was solved by considering all impairments, whose levels were computed using extensive analytical models [74]. However, extending this work to a dynamic scenario would be interesting since jamming signals are unpredictable, and real-time accurate impairment computation is a challenge. In [75], the authors presented a new approach to RMSCA using the bit-loading concept to independently modulate each frequency slot according to the experienced interference level. A congestion-based ordering strategy is proposed to reduce the fragmentation. However, a static traffic matrix was used, and an extension to dynamic traffic may be needed since the variation in fragmentation levels is large due to the dynamic arrival and departure of demands. Most RMSCA studies ignore the impact of the current candidate traffic request on existing signals that share the same lightpath on the network [71, 72, 76, 77, 75, 78].

It is clear that there is a gap in the impairment-aware RMSCA literature on the importance of considering the effects of different noise sources, especially

in dynamic scenarios where impairments must be calculated in real time. The non-XT linear and nonlinear impairments are either ignored or considered in the worst-case scenario and under static traffic conditions, where traffic demands are pre-defined. Hence, in this chapter, we focus on dynamic provisioning and answer whether including only XT in provisioning is enough to predict and optimize the performance of impairment-aware RMSCA algorithms accurately. The contribution of different factors on the blocking probability in analyzed at different loads and channel launch powers for realistic dynamic impairment-aware networking algorithms.

4.2 Test and Analysis

The MCF-EON analysis is performed on two different network topologies, the USNET (24-node, 43-link) and COST-239 (11-node, 52-link) network, with $|C| = 7$ core MCF per link. Each core has 320 frequency slots, each supporting 12.5 GHz transmission. A Poisson traffic distribution model generates $R = 100,000$ requests with data rates uniformly distributed in $[50, 600]$ Gbps at 200 to 600 Erlangs traffic loads. Spectrally efficient modulation formats (PM-BPSK, PM-QPSK, PM-8QAM, and PM-16QAM) are selected to satisfy the QoT threshold as per dynamically calculated XT, ASE, and NLI levels [76].

Figs. 4.1 and 4.2 show the contribution of different factors when a failure to accommodate traffic requests occurs in the MCF-enabled USNET and COST-239 topologies at 300 and 600 Erlangs for two input launch powers: 0 dBm and 2 dBm. For $R = 100,000$ requests, there are $[RKC, RKC \times N_B] = [2100000, 2100000 \times N_B]$ total candidate RMSCA solutions, where $K = 3$ shortest paths, $|C| = 7$ cores, and N_B is the number of spectral blocks obeying the continuity and contiguity EON constraints. Hence, considering the extensive range of values, we show the percentage contribution of different factors counted when a candidate solution fails, for an easier comparison. The columns labeled 'NLI', 'XT', and 'ASE' refer to cases where each impairment is high enough to cause a provisioning failure on its own. 'PLI combinations' account for situations where only a sum of these noises causes enough degradation to the QoT to block the request. The 'Spectrum' failures include insufficient spectrum to accommodate demands, spectral contiguity, and continuity constraint failures.

Figs. 4.1 and 4.2 consider the reason for the failure when the current request is blocked, including when it negatively impacts in-service lightpaths. However,

much of the RMSCA literature only considers the former [71, 72, 76, 77, 75, 78], even when the work includes all impairments. From the same figures, note that, at both power levels and for both networks, NLI plays a pivotal role in deciding the request's QoT failure when compared to XT. With the increase in launch power, the NLI influence on provisioning failures rises, and the ASE influence decreases, as expected. ASE plays an essential role compared to XT and cannot be ignored, as assumed in some networking studies on RMSCA [39, 71, 72, 73, 79, 75]. ASE contributes less to failures in USNET than in COST-239, which is because COST-239 is a more highly connected network (density of 5.7) than USNET (density of 1.7), and hence, it is easier to find shorter paths. As the load doubles from 300 to 600 Erlang, XT has a stronger influence on a request's failure. At the higher load, NLI and ASE still play a significant role, with NLI contributing $\sim 58\%$ compared to XT contributing $\sim 21\%$ to failures. PLI combinations also play an essential role in QoT failure, with spectrum continuity, contiguity, and spectrum unavailability failures increasing with increasing load.

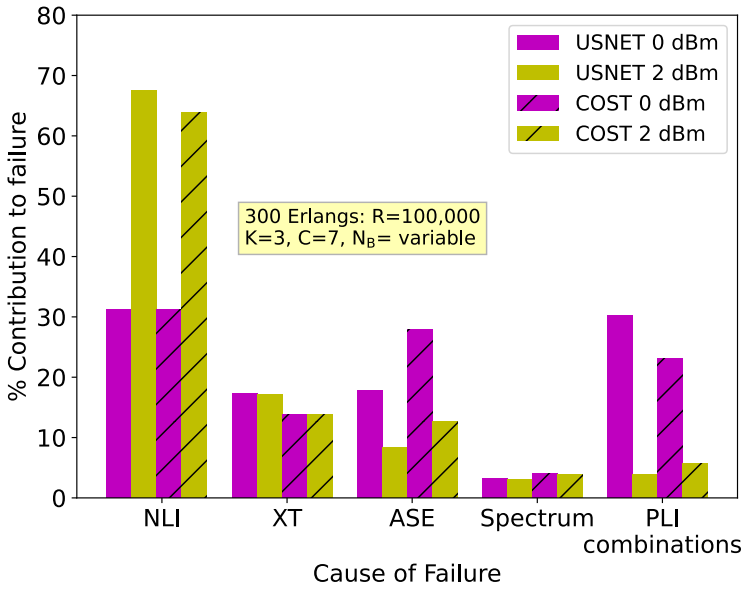

Figure 4.1: Contribution of different factors to a request's failure computed in USNET and COST-239 at 300 Erlangs

Figs. 4.3 and 4.4 show a comparison of the various noise powers on different network links of the USNET and COST-239 topologies at 300 and 600 Erlangs. The noise power values used for the comparison are an average over multiple time instants (every 1000 requests) of network provisioning, as the 100,000 requests are dynamically allocated. Whenever the noise experienced by a request is

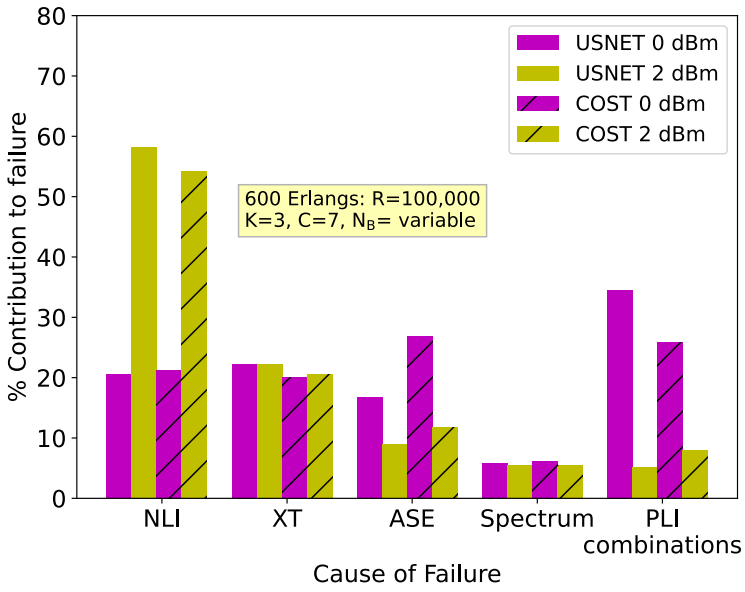

Figure 4.2: Contribution of different factors to a request's failure computed in USNET and COST-239 at 600 Erlangs

computed, the corresponding ASE, NLI, and XT powers are captured for the candidate route/core/spectrum. The results estimate how a new request perceives the different noise sources in the MCF-EON.

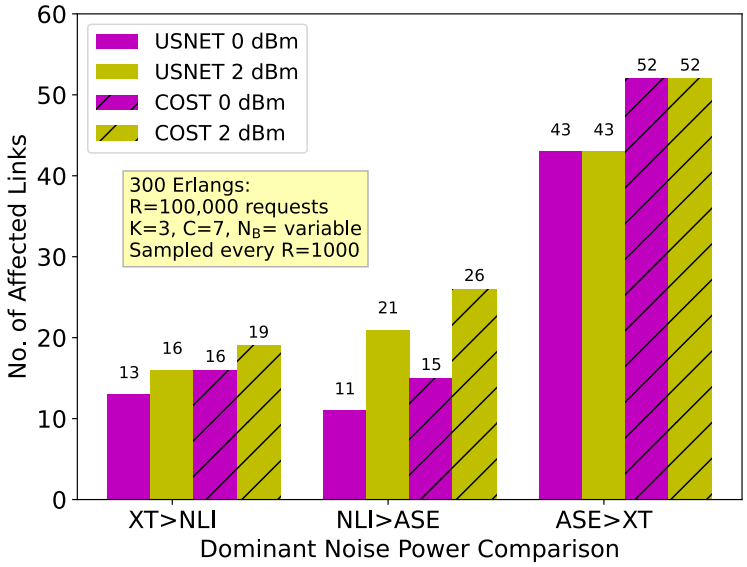

Figure 4.3: Noise power comparison in USNET and COST-239 at 300 Erlangs

The large majority of the 43 links of the USNET and 52 links of the COST-239 network are more affected by ASE noise than XT. At a low load of 300 Erlangs in both networks and at both launch powers, XT is stronger than NLI on only ∼1/3

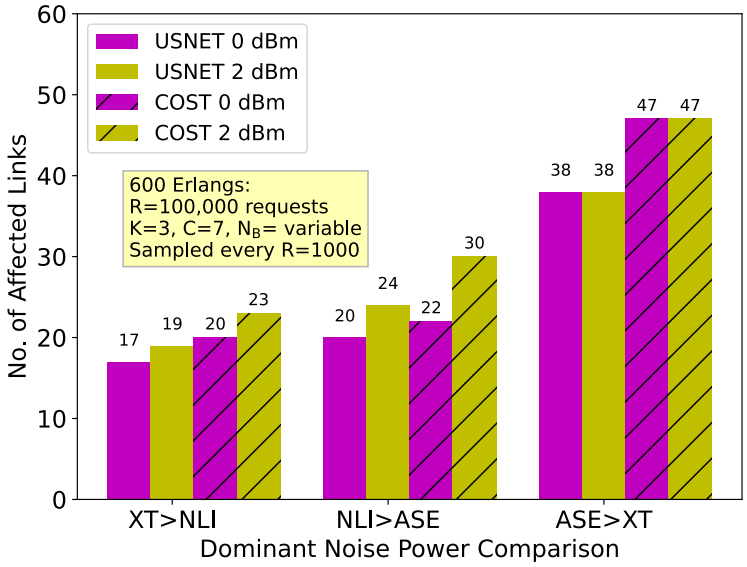

Figure 4.4: Noise power comparison in USNET and COST-239 at 600 Erlangs

of the links. As the load increases to 600 Erlangs, XT exceeds NLI on ∼1/2 of the links. Moreover, unlike the 300 Erlangs case, XT starts to dominate the ASE on a few links. Also, as expected, the number of NLI-affected links increases in both networks as the channel launch power increases and becomes dominant on par with the ASE-affected links. Similarly, the XT noise power effects increase slightly with the input channel power. Note that Figs. 4.3 and 4.4 show only the noise distribution on different links over different points of network operation, and hence, the NLI contribution to failure is observed to be stronger in Figs. 4.1 and 4.2 as they also account for blocking due to degradations on the in-service lightpaths. XT is an additional noise contribution for MCF compared to single-core fibers and is often considered the dominant source of impairment in these systems. However, Figs. 4.1 and 4.2 show that a large proportion of MCF links are more affected by ASE, SPM, and XPM effects at different loads. These can cause signal degradation that can go unnoticed if the resource allocation schemes only consider XT.

To further validate the noise analysis conclusions drawn from Figs. 4.1 to 4.4, a blocking probability difference is shown in Fig. 4.5 when considering only XT vs. NLI+ASE vs. all impairments for a 2 dBm launch power. Considering NLI and ASE along with XT clearly increases the number of blocking events that would go unnoticed if the provisioning scheme only considers XT or when the effects on in-service lightpaths are ignored.

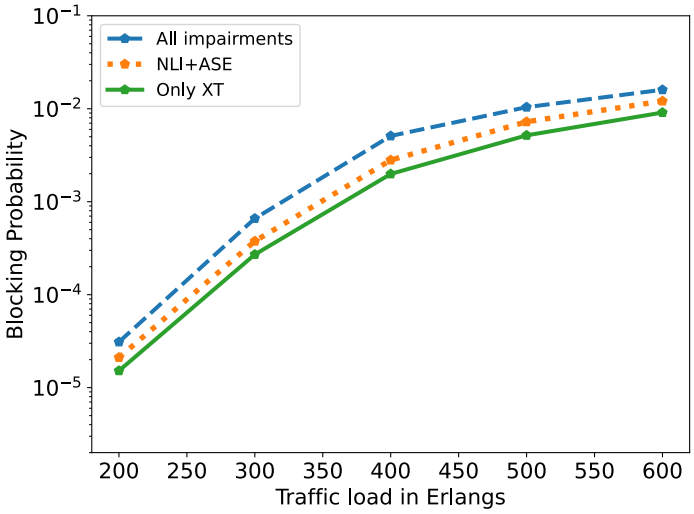

Figure 4.5: Blocking probabilities in MCF-enabled USNET under different impairment settings for $R = 100,000$.

4.3 Chapter Summary

An analysis of MCF networks affected by various impairments, many of which are ignored in the literature, is provided. The impact of XPM, SPM, and ASE noise is shown for dynamic networks with different power levels, where they account for ∼30% to ∼60% of QoT failures compared to ∼20% XT-induced failures. A link noise distribution is also provided that re-iterates the importance of holistic impairment modeling for RMSCA algorithm designs. Ignoring non-XT impairments or effects on in-service demands will result in an underestimation of the blocking probability obtained. The remaining portion of the thesis builds on this conclusion, and the next chapter presents an impairment and fragmentation aware RMSCA algorithm.

Chapter 5

Multicore Resource Allocation: Multi-attribute Decision-Making Approach

This chapter presents a routing, modulation, spectrum, and core allocation algorithm for space-division multiplexing-based elastic optical networks. A network state-dependent route and core selection method using multi-attribute decision-making (MADM) is proposed. This systematic resource allocation allows the network designer to choose which resources are most valuable. It is followed by a novel spectrum allocation algorithm using a weighted score function to rate and select the best spectrum blocks. Physical layer impairments, including inter-core XT, ASE, and Kerr fiber NLIs, are considered alongside fragmentation and power consumption. The proposed RMSCA approach is compared with published benchmarks incorporating QoT constraints and evaluated on two network topologies, NSFNET (7 and 12-core multicore fiber links) and COST. It is shown to be superior in terms of blocking probability, bandwidth blocking probability, network fragmentation, and power consumption compared to standard and published benchmarks. This work has been published in [30].

5.1 Introduction

From the previous chapters, it is clear that, for a truly impairment-aware RMSCA algorithm, XT and non-XT effects should be considered for a proper analysis of the network blocking under a dynamic traffic model. In addition, fragmentation

and power consumption are two network aspects worth considering in the RMSCA algorithm design. The dynamic setting and tearing up of traffic connections increase the random occurrence of scattered and varying-sized spectral gaps, thus making it challenging to allocate contiguous and continuous spectral blocks along an entire route. A spatial continuity constraint is also placed in the RMSCA decision as it is enforced in the majority of proposed SDM-EON architectures, e.g., in the case of independent switching over single-mode MCFs, or for fractional joint switching over few-mode MCFs [33]. This constraint is needed for switching devices with limited flexibility for lane changes such as lower complexity and cost ROADMs. Hence, under these spectral and spatial constraints for spectrum and core allocation, it is important to focus on the impacts of fragmentation in the algorithm design.

As emphasized in Chapter 4, impairments affect the optical planning schemes, and the inter-core XT is an added impairment in the considered MCF network. XT minimization prefers inter-signal spacing in the spectral assignment phase to avoid signal overlap. In contrast, fragmentation mitigation demands compact spectral assignment to avoid unnecessary spectrum gaps and make it easier to satisfy continuity and contiguity constraints. Hence, it becomes important to view the two issues collectively while allocating the spectrum of a MCF link [78].

The power consumption increases with an increase in traffic volume. Hence, SDM-EONs offering higher capacity via multiple cores also increases the power consumption because of more network elements such as BVTs, bandwidth variable optical cross-connects (OXC)s, and EDFAs. It is a common assumption to consider a two-part network power consumption model: a fixed part that is independent of traffic served and a dynamic part that is traffic dependent [80]. The fixed part contributes constant power while the elements are in operation, while the dynamic part represents the variable power consumption that is proportional to the traffic that the network element handles. Keeping the power usage to a minimum while solving the RMSCA problem is another essential aspect to consider [81, 82, 83, 84].

Keeping these aspects in mind, this chapter presents a heuristic dynamic RMSCA algorithm that reduces the probability of a connection request being blocked. It is achieved using a MADM method to choose the core and route and a weighted score function to select the spectral block for transmission. These algorithms are designed to minimize the effects of fiber impairments on the signal QoT while maintaining lower network fragmentation and power consumption

than the baseline approaches.

The rest of this chapter is organized as follows. Section 5.2 summarizes the current literature in this area and highlights our novel contributions. Section 5.3 gives the system description and the evaluation metrics. Section 5.4 elaborates on the MADM technique and its adaptation for routing. Section 5.5 details the proposed RMSCA algorithm. Finally, Section 5.6 gives the performance evaluation of the algorithm, followed by a chapter summary in Section 5.7.

5.2 Literature Review

Several research works can be found in the literature on solving the RMSCA problem in SDM-EONs. Fujuii et al. [82] proposed an RSCA algorithm for power-efficient architecture on-demand modules as these modules provide flexibility of SDM-EON architectures but suffer from high power consumption. Tode and Hirota [85] proposed an RSCMA algorithm ('M' here stands for Mode) where they included both MCF and multi-mode fibers. However, XT was the only impairment considered, and more effects, such as modal dispersion and mode coupling, could be considered. Yang et al. [73] solved a static RCSA problem using MILP models for XT-aware and XT-unaware cases; the dynamic traffic case was not considered. Zhang and Yeung [86] presented an RMSCA scheme to reduce the wasted spectrum and to exploit path diversity, but in this case, the XT was assumed to be negligible. In [87], Zhu et al. proposed an power-efficient RMSCA scheme while considering a multi-path scheme for survivability. XT was the only PLI considered, and the objective was to improve spectral efficiency during fluctuating traffic without regard to fragmentation. The work of [84], which preceded [83] described above, also considered energy efficiency for static traffic scenarios.

Some recent works solve the RMSCA problem differently by considering aspects of network load balancing, different XT representation and traffic, or a combination of network issues. In [88], Zhang et al. examined a new concept of SDM-EONs supporting super-channels that allow the usage of frequency slots on neighboring cores to form contiguous spectrum blocks. The RMSCA used a load-balancing strategy and a metric accounting for spatial and spectral fragmentation to minimize the number of wasted slots; impairments, however, were not considered. In [89], Li et al. devised an effective XT representation model and an RMSCA strategy that minimizes it, but other PLIs were not considered. In [90],

Aretor et al. proposed an RMSCA scheme based on mixed integer linear programming (MILP) and a heuristic approach for delay-sensitive multi-cast traffic; again only XT impairment was considered. In [78], an RMSCA scheme was presented to improve spectrum efficiency while focusing on XT and fragmentation issues. A new modulation format selection method is provided w.r.t. XT-fragmentation reduction. Until that time, this was the only paper (except for own work [91]) that addressed the importance of the combined XT- XT-fragmentation problem. However, other impairments were not included. In [92], a dynamic impairment-aware RMSCA algorithm was proposed considering XT, ASE, and XPM effects, but not the quite important SPM. The work considered other PLIs (except SPM), unlike most other PLI-aware RMSCA studies, and hence, this chapter uses this algorithm for benchmarking purposes. In [93], fragmentation-aware RSCA algorithms were proposed using a core classification method for spectrum assignment and a cost function to increase spectrum efficiency. However, impairments were not considered in the design process.

Most XT-aware networking studies compute the worst-case XT levels, i.e., all neighbor cores are considered active [73, 94, 95, 96]. This approach simplifies the computation but increases the blocking of incoming traffic demands due to conservative XT estimates. On the other hand, computing precise XT levels dynamically, as used in [97, 23], can be time-consuming. A lesser time-consuming version that considers spectral blocks can be found in [77] and is used in this work. However, these researchers did not consider the network fragmentation and power consumption aspects.

Almost all of the RMSCA algorithms in the literature use the K-shortest paths (KSP) method for routing. KSP routing based on distance results in the same paths used for any network source-destination pair, irrespective of the network state. This increases link congestion and blocks future traffic requests. In addition, as distance-based KSP focuses only on the shortest paths, the routing part of the RMSCA design does not consider other network issues, such as PLIs or fragmentation. In [88], a load-balanced routing method that considers fragmentation is proposed. In [98], traffic-aware routing is performed to choose routes based on the incoming traffic demand. [99] suggests a fragmentation and alignment aware routing for 3D elastic optical networking. However, more relevant network metrics could be incorporated into routing decisions. Using MADM approaches to perform routing using multiple metrics in a systematic manner, as proposed in this chapter, has not been previously considered.

Recently, approaches using machine learning (ML) for RMSCA have been explored. In [100], an ML model trained with synthetic traffic estimated a path's acceptability based on crosstalk, fragmentation, and required slots. More features related to impairments and network topology would need to be included to compare their results to the current work. In [101], the authors used a deep reinforcement learning approach to solve the RMSCA task. However, only XT impairment was considered. Using ML for RMSCA is an attractive prospect to consider; however, care should be taken in the design and implementation.

Fiber PLIs, specifically the ASE, SPM and XPM effects, have been widely considered in single-core RMSA algorithms; a search of the relevant literature yielded that there are no published RMSCA algorithms that holistically consider these impairments alongside XT. This chapter's work addresses this gap. There are two reasons it is important to do this. Firstly, these impairments together significantly limit the signal reach, which is a major design aspect of any impairment-aware RMSCA, and hence, as shown in Chapter 2, considering XT alone is not enough. Secondly, a higher utilization in one core increases the NLI effects, whereas spreading the traffic over different cores exacerbates the XT. Hence, these factors affect the routing decisions, the required spectrum range, and, subsequently, the networking costs.

Table 5.1 shows the literature works that considered impairments, fragmentation, and power efficiency aspects. We observed from the literature that no works have covered all impairments while including fragmentation and power consumption issues in performing dynamic resource allocation. Therefore, keeping all the above aspects in mind, the following contributions are made in this chapter:

- A power-efficient PLI- and fragmentation-aware dynamic RMSCA is proposed. The physical layer impairments consider ASE , XPM, and SPM effects in addition to XT.

- The routing is improved by including network-dependent parameters in the decisions and applying a new multi-attribute decision-making approach. The proposed routing method checks the best path and core combinations while considering multiple network features.

- A weighted score function combining XT, fragmentation, and power consumption is proposed to rate and select the best spectral block for spectrum allocation.

- The results of the proposed algorithm are compared with standard and published benchmarks on 7 and 12 core-based NSFNET and COST networks.

Table 5.1: Literature on Dynamic Allocation Considering Impairments, Fragmentation, and power Efficiency

Related works	**Network issues considered**			
	Impairments		**Fragmentation**	**power efficiency**
	XT	**ASE,SPM,XPM**		
Liu [81]	✓	-	-	✓
Fujii [82]	-	-	✓	✓
Tode [85]	-	-	-	-
Yang [73]	✓	-	-	-
Zhang [86]	-	-	✓	-
Zhu [87]	✓	-	-	✓
Zhang [88]	-	-	✓	-
Li [89]	✓	-	✓	-
Samuel[90]	✓	-	-	-
Zhang [78]	✓	-	✓	-
Ravipudi [91]	✓	-	✓	✓
Su [92]	✓	✓(except SPM)	-	-
Pourkarimi [93]	-	-	✓	-
Zhao [95]	✓	-	✓	-
Moghaddam [97]	✓	-	-	-
Tang [23]	✓	-	-	-
Klinkowski [77]	✓	-	-	-
Oliveira [100]	✓	-	✓	-
Pinto [101]	✓	-	-	-
Current chapter	✓	✓	✓	✓

5.3 System Description and Evaluation Metrics

This section describes the PLIs and provides the MCF QoT model used in this work. The network's fragmentation and power consumption aspects are discussed, accompanied by the corresponding evaluation metrics.

5.3.1 Physical Layer Impairments Model

The QoT of optical signals is degraded by phenomena such as Kerr nonlinear impairments and ASE noise occurring during the propagation and detection pro-

cesses. The NLI is caused by the interaction of nonlinearity and dispersion in the fiber and the ASE noise is due to EDFAs. These impairments affect the end-to-end QoT, thus limiting the signal's transmission reach. A well-known and widely used PLI estimation model in long-haul transport networks is the so-called Gaussian noise (GN) model, which is a state-dependent (traffic-dependent) model [45].

The ASE noise power, $P_{ASE}^{(e)}$ is modeled as additive Gaussian noise, and, for a link e with $N_s^{(e)}$ spans, can be computed as

$$P_{ASE}^{(e)} = N_s^{(e)} \left(e^{\alpha L_s} - 1\right) h\nu\eta_{sp}\Delta f, \tag{5.1}$$

where α is the fiber attenuation, L_s is the fiber length per span, i.e., the length of the fiber between amplifiers, h is Planck's constant, ν is the optical light frequency, η_{sp} is the spontaneous emission factor and Δf is the signal bandwidth.

The noise power originating from the nonlinear impairments, SPM, and XPM are computed using Eq. (3.5). The power of XT, the additional impairment in SDM-EON systems, can be estimated using [77]

$$P_{XT}^{(e)} = P_z \cdot XT_{\Upsilon}^{(e)}, \tag{5.2}$$

and

$$XT_{\Upsilon}^{(e)} = A_{max}(L, e) \cdot h \cdot \ell^{(e)}, \tag{5.3}$$

where $\ell^{(e)}$ is the length of the fiber link e, and h is the power-coupling coefficient. $XT_{\Upsilon}^{(e)}$ is the XT of the most affected spectral slice of lightpath Υ on link e, and $A_{max}(\Upsilon, e)$ is the maximum number of currently active adjacent cores surrounding the spectral block of the core under consideration on link e of Υ.

Hence, the signal to noise ratio (SNR) of Υ propagating through N_Υ MCF links is calculated using

$$SNR(f) = \frac{P_z}{\sum_{e \in N_\Upsilon} \left(P_{ASE}^{(e)}(f) + P_{NLI}^{(e)}(f) + P_{XT}^{(e)}\right)}. \tag{5.4}$$

In this work, the SNR that the current request would experience if it were to be assigned a particular tentative route is calculated using Eq. (5.4) and compared with an SNR threshold,

$$SNR(f) > SNR_{\text{th}}, \tag{5.5}$$

where SNR_{th} depends on the modulation format chosen. Also, in addition to satisfying its SNR constraint, the new and about-to-be-provisioned request should not degrade existing requests already provisioned along various links of the tentative route. Hence, the SNR constraint also includes checking their corresponding SNR threshold requirements.

5.3.2 Fragmentation

As considered in Chapter 3, fragmentation is another cause of blocking in RMSCA due to the creation of spectrum fragments that cannot be used by incoming calls and still satisfy continuity and contiguity constraints, leading to spectrum wastage. As explained in Chapter 2, fragmentation and XT effect mitigation desire opposing strategies. Hence, this factor is considered in this chapter. The network-wide fragmentation F_{NET} for a network with $|E|$ number of edges is computed as the average of link fragmentation, $F^{(e)}$ (Eq. (3.10)). However, in the MCF scenario, the $F^{(e)}$ is modified as the average of core fragmentation over all cores computed as

$$F^{(e)} = \frac{1}{|C|} \sum_{c \in C} F_c^{(e)}, \tag{5.6}$$

with

$$F_c^{(e)} = \sum_{\gamma_{ec} \in \Gamma_{ec}} \frac{|\gamma_{ec}|}{S} \cdot \ln \frac{S}{|\gamma_{ec}|} \tag{5.7}$$

C is the set of cores per link, $|C|$ is the number of cores per link, Γ_{ec} is the set of fragments on link e of core c, $|\gamma_{ec}|$ is the size of fragment γ_{ec}, i.e., number of frequency slots in that fragment, and S is the total number of frequency slots in the C-band.

5.3.3 Power Consumption

The BVTs typically consume more power than the other two power-consuming elements, OXCs and EDFAs, while provisioning a traffic request [87]. The power consumption of a BVT depends on the number of frequency slots used by the request and hence, depends on the resource allocation decisions. Longer paths demand more spectral resources and are influenced by chosen modulation formats [Table 1, [87]]. The power consumption model given by [Eqs.(5.8)-(5.13)] is adapted from [87].

The power consumed by the BVTs to provision a lightpath Υ traveling N_Υ set of links is given by

$$E_{BVT}^{\Upsilon} = \sum_{e \in N_\Upsilon} S_{(\Upsilon,m)}^{(e)} \cdot E_{BVT}(m), \tag{5.8}$$

where $S_{(\Upsilon,m)}^{(e)}$ is the total number of the spectrum slots allocated to Υ using modulation m on link e. $E_{BVT}(m)$ is the power consumed by the BVT per spectral slot when using a given modulation format m, which depends on $T(m)$, the data rate supported by a frequency slot using modulation format m, and can be estimated as

$$E_{BVT}(m) = 1.683 \cdot T(m) + 91.333 \tag{5.9}$$

The power $E_{OXC}(n)$ consumed by an OXC at node n depends on the node degree $d(n)$, the add/drop degree β, and some overhead power. It can be approximated as

$$E_{OXC}(n) = 85 \cdot d(n) + \beta \cdot 100 + 150 \tag{5.10}$$

Hence, the total OXC consumption when accommodating a new Υ with S available slots on each e is given by

$$E_{OXC}^{\Upsilon} = \sum_{n \in V_\Upsilon^n} \frac{S^{(e,n)}}{S} \cdot E_{OXC}(n), \tag{5.11}$$

where $S^{(e,n)}$ is the number of occupied slots on link e connecting node n and the next node of lightpath Υ and V_Υ^n is the set of nodes on Υ.

The power consumed by EDFAs on a link e can be estimated as

$$E_{EDFA}^{(e)} = \left(\frac{\ell^e}{L_s} + 1 \right) \cdot 100, \tag{5.12}$$

assuming the power consumed by an amplifier is approximately 100 W [102]. Hence, the total power consumed by the EDFAs along lightpath Υ is given as

$$E_{EDFA} = \sum_{e \in N_\Upsilon} \frac{S^{(e)}}{S} \cdot E_{EDFA}^{(e)} \tag{5.13}$$

where $S^{(e)}$ is the total number occupied slots on link e. The sum of these E_{BVT}, E_{OXC}, and E_{EDFA} is the total power consumed by a request on path Υ. And the total network power consumption (E_{NET}) calculated as the power consumed

by all BVTs, OXCs, and EDFAs use these expressions but sum up all active requests.

5.4 Multi-Attribute Decision Making Methods

Multi-criteria decision-making is a popular branch of decision-making that falls under the discipline of Operations Research. It is categorized into multi-attribute decision-making (MADM) and multi-objective decision making (MODM), depending on the domain of the alternatives. MODM methods are preferred when the problem is a decision problem and the decision variables have values in the continuous or integer domain. These methods generally have infinite or many alternatives. However, the MADM methods are applied when faced with the problem of selecting the best viable option (or sorting and ranking) from a given finite set of alternatives, as is the case for the considered RMSCA problem.

Optimization algorithms use an objective criterion to determine the optimal solution. Often in complex problems, simple objective functions cannot be phrased or solved. Heuristic algorithms are then used to weight multiple factors and decide on a viable solution. It is then essential to use scientific methods to structure the problem correctly and arrive at a well-informed decision. In this section, the proposed heuristic yet structured MADM approach to routing and core selection is described.

MADM methods need alternatives and attributes, and the values of the alternatives are calculated w.r.t. different attributes considered. The attributes influence the alternatives; hence, weights are assigned to them that determine the importance/influence they can have in the decision-making process to achieve a specific goal. What weights to assign to the attributes is the decision maker's choice. Example MADM methods include: simple additive weighting (SAW), analytic hierarchy process (AHP), preference ranking organization method for enrichment evaluations (PROMETHEE), technique for order preference by similarity to ideal solution (TOPSIS), compromise ranking method (VIKOR), etc. [103, 104].

Of the MADM methods, the PROMETHEE method is simple to apply, involves less computation, and can handle qualitative and quantitative attributes easily. Hence, in this work PROMETHEE combined with the AHP method is utilized [105]. The PROMETHEE method belongs to a category of outranking methods that were introduced by [106] and has been applied in various areas such

as banking, workforce planning, water resources, investments, medicine, chemistry, health care, dynamic management, etc, mainly due to its ease of application [106]. PROMETHEE handles the alternatives and attributes in a detailed manner but lacks a systematic way to compute the attribute weights [106]. AHP provides a systematic and practical approach to finding attribute weights and ranking the alternatives [107]. Therefore, to determine the attributes' weights, the present work uses the AHP method, and the same weights are used in the PROMETHEE method. The steps of the method are outlined below, and a detailed demonstration of the route-core selection process using the proposed AHP-enabled PROMETHEE method is given in Section 5.5.

Step 1: Identify the 'proper' attributes (or criteria) for the problem
The first step is to create a short-list of the alternatives based on the attributes identified. The attribute values can be the already-available data or data estimated by the decision-maker. Table 5.2 shows the general form of the decision table used in MADM methods based on these alternatives-attributes.

Table 5.2: General Form of Decision Table in MADM

Alternatives	Attributes			
	a_1	a_2	$\cdots$	a_Y
Alt_1	v_{11}	v_{12}	$\cdots$	v_{1Y}
Alt_2	v_{21}	v_{22}	$\cdots$	v_{2Y}
Alt_3	v_{31}	v_{32}	$\cdots$	v_{3Y}
$\vdots$	$\cdots$	$\cdots$	$\ddots$	$\cdots$
Alt_X	v_{X1}	v_{X2}	$\cdots$	v_{XY}

Alt_x (for $x = 1, 2, \cdots, X$) denotes alternative x, a_y (for $y = 1, 2, \cdots, Y$) denotes attribute y, and v_{xy} denote the performance measure used, i.e., the value corresponding to alternative x with respect to attribute y.

Step 2: Decide the attributes' weights using AHP
In this work, the steps of the AHP are adopted from [104]. Calculating weights involves an important step of forming a relative importance (RI) matrix that denotes the relative importance of the attributes considered and is determined by the decision maker depending on the goal of the task. AHP provides a relative importance relations table to quantitatively fill the RI matrix, showing the importance of a particular attribute over another using a standard scale of 1-9,

as shown in Table 5.3, rather than using random intuition. The generic structure of a RI matrix for Y attributes is given as

$$\text{RI} = \begin{array}{c} \text{Attribute} \\ a_1 \\ a_2 \\ \vdots \\ a_Y \end{array} \begin{array}{c} \begin{array}{cccc} a_1 & a_2 & \cdots & a_Y \end{array} \\ \begin{bmatrix} 1 & r_{12} & \cdots & r_{1Y} \\ r_{21} & 1 & \cdots & r_{2Y} \\ \vdots & \vdots & \ddots & \vdots \\ r_{Y1} & r_{Y2} & \cdots & 1 \end{bmatrix} \end{array} \tag{5.14}$$

where r_{ij} denotes the relative importance of attribute i over attribute j with r_{ij}=$1/r_{ji}$; r_{ij}=1 for $i = j$. Using the degree of importance in Table 5.3 as either r_{ij} or $1/r_{ij}$, the RI matrix is filled, and the weights are computed. The geometric means for each attribute are computed row-wise in the RI matrix (5.14) and then normalized by their sum to get the weights, w_y.

Table 5.3: Relative Importance scale

Degree of importance	Definition
1	Two attributes have equal importance
3	One attribute is slightly more important than the other
5	One attribute is strongly more important than the other
7	One attribute is very strongly more important than the other
9	One attribute is absolutely more important than the other
2, 4, 6, and 8	Intermediate values

To verify the correctness of the weights found, a consistency ratio (CR) is computed that should be less than 0.1, i.e., $< 10\%$ judgment error [105]. The additional steps to verify the weight computations are given as:

Step A: Compute the vector $M = (RI * W) \oslash W$, where $W = [w_1, w_2, ..., w_y]^T$ and the weights are from Step 2 above, and $\oslash$ represents a Hadamard division.

Step B: Find the average of M as (λ_{max}) to compute the consistency index (CI) as

$$CI = (\lambda_{max} - Y)/(Y - 1) \tag{5.15}$$

Step C: Compute the CR as $CR = CI/r_{index}$ where the r_{index}, known as the

random index, is a standard value computed using a table provided for AHP for a specific value of Y [105, 107]. The random index value for $Y = 6$ attributes, as considered in this work, is 1.25. A CR value less than 0.1, indicates good consistency in the relative importance relations assigned, and the weights can be used with confidence.

Step 3: Preference function calculation (Pref_y)
The preference functions Pref_y represents the evaluation difference between two alternatives (e.g., Alt_1 and Alt_2) w.r.t. a particular attribute y. They are calculated for each of the Y attributes and they assess the relative contribution of a given alternative concerning a given attribute. Pref_y outputs a preference degree ranging from 0 to 1. The PROMETHEE method offers six different types of preference functions. The "usual" preference function is the simplest one and is used in this work: it is the difference between the values $\text{v}_{x,y}$ and $\text{v}_{x',y}$ of alternatives Alt_x and $\text{Alt}_{x'}$, (for $x, x' \in X$) w.r.t. an attribute value a_y. Since this is for each of the Y attributes, we get Y separate preference tables. Then, a multiple attribute preference index table is formed using the weighted average of the preference function tables Pref_y, using the weights from Step 2.

Step 4: Calculation of leaving, entering flow, and net flow
Using the multiple attribute preference index table found in Step 3, we compute the leaving, entering, and net flow. The leaving flow value ϕ^+ is a measure of how much the particular alternative dominates the rest of the alternatives, and the entering flow value ϕ^- denotes how much the rest of the alternatives dominate the alternative. The leaving flow is calculated as the row-wise summation and the entering flow as the column-wise summation of the multiple-attribute preference index table described in Step 3. The net flow $(\phi^+ - \phi^-)$ is a measure of how attractive a particular alternative is. Therefore, the alternatives are ranked by net flow, giving the best rank to the one that has the highest net flow value.

5.5 Crosstalk and Fragmentation Aware RMSCA Algorithm

The proposed RMSCA algorithm is given in Algorithm 5.1. The algorithm begins by computing K ranked paths/cores using Algorithm 5.2, which takes as input

the K shortest paths. For each $k \in K$ and all cores, alternatives are formed and scored using AHP-enabled PROMETHEE. This set of ranked alternatives is used in the outer loop of Algorithm 5.1 (Line 2). The spectrum assignment algorithm is performed inside the loop and relies on a score function based on spectrum blocks on respective cores as described in Algorithm 5.3. The subsections below detail these two functions.

Algorithm 5.1 Proposed RMSCA algorithm

1: **procedure** RMSCA(Source, destination, requested bandwidth)
2: Run MADM_route procedure (Algorithm 5.2) to get ranked route-core alternatives
3: **while** viable spectrum block not found on ranked route-core alternatives and all alternatives not explored **do**
4: Calculate spectrally efficient modulation format
5: Create list of candidate spectrum blocks satisfying the continuity and contiguity constraints on that route-core combination
6: Obtain scores for the candidate blocks using Algorithm 5.3 and sort them in ascending order
7: **while** candidate block in sorted list does not satisfy QoT constraints **do**
8: Compute the impairments and the QoT using Eqs. (3.5), (5.1), (5.2), and (5.4)
9: **if** QoT is satisfied (Eq. (5.5)) and existing lightpaths not degraded **then**
10: selected spectrum block = candidate block
11: **else** check next spectrum block
12: **end if**
13: **end while**
14: **end while**
15: **return** current route, core, and selected spectrum block to provision the request
16: **end procedure**

5.5.1 Implementation Example: Route and Core

In this work, AHP-enabled PROMETHEE is used to find the best path and core combination among the available choices as detailed in Algorithm 5.2. Following the steps explained before, the alternatives here are the path and core combinations. The alternatives for K paths and with $|C|$ cores are denoted as (p_k, c_j) for $k = 1, \cdots, K$ and $j = 1, \cdots, |C|$. The total number of alternatives is $K \times |C|$. In this chapter, $K = 3$ routes and $|C| = 7$ or $|C| = 12$ cores are used.

Algorithm 5.2 MADM path and core selection

procedure MADM_ROUTE(Network topology, source, destination, set of cores C, network state)
    Find K shortest paths from source to destination
    Obtain core utilization, core fragmentation, number of amplifiers needed, available route bandwidth, power cost, and the QoT factor information for each path-core alternatives.
    Apply AHP-enabled PROMETHEE steps to obtain the ranking
    return Ranked $K \times |C|$ path-core alternatives
end procedure

Algorithm 5.3 Score function

procedure SCORE_FUNCTION(Route-core alternative, network status, candidate spectral block)
    for each link e of route Υ **do**
        $S_{occ}^{(e)}$ = number of occupied frequency slots on adjacent cores overlapping the spectral block
        S_{req} = number of frequency slots required to provision the current request
        $X^{(e)} = [S_{occ}^{(e)} - (S_{req}/2)]^2$
        $N_F^{(e)}$ = number of fragments created with a size less than the required slots
        E_{Tot} = power consumed due to using the particular link using Eqs. (5.8), (5.11), and (5.13)
        Compute weighted multi-objective function $Z^{(e)} = \alpha_1 X^{(e)} + \alpha_2 N_F^{(e)} + \alpha_3 E_{\text{Tot}}$
    end for
    Score(candidate block) = $\sum_{e \in N_\Upsilon} Z^{(e)}$
    return Score
end procedure

The relevant attributes identified are core utilization (C_U), core fragmentation (C_F), number of amplifiers needed (N_A), number of available frequency slots in the route (S_{Free}), power cost (E_{Tot}) and the QoT factor (QoT). C_U is included to take into account the uniform utilization of the cores present in a fiber. C_F affects the availability of *contiguous* spectrum resources and thus affects the blocking. N_A depends on the length of the paths and the S_{Free} affects the blocking directly. E_{Tot} captures the power cost of choosing a particular path and a core combination. The C_U, C_F, N_A, S_{Free}, E_{Tot} and QoT for a request using modulation m and a given candidate (path, core)= (N_Υ, c) are computed using the following

equations:

$$C_U = \sum_{e \in N_\Upsilon} \frac{S_m^e}{S}, \tag{5.16}$$

$$C_F = \sum_{e \in N_\Upsilon} F_c^e, \tag{5.17}$$

$$N_A = \sum_{e \in N_\Upsilon} N_s^e, \tag{5.18}$$

$$S_{Free} = \sum_{e \in N_\Upsilon} \frac{1}{|C|} \sum_{\zeta \in C} (S_m^{(e)})_\zeta, \tag{5.19}$$

$$E_{\text{Tot}} = E_{BVT} + E_{OXC} + E_{EDFA}, \tag{5.20}$$

$$QoT = \sum_{e \in N_\Upsilon} C_{XT}^{(c)} + (S - S_m^{(e)})_c + S_{req}, \tag{5.21}$$

$$C_{XT}^{(c)} = \sum_{ac \in N_{ac}} (S - S_m^{(e)})_{ac}, \tag{5.22}$$

where N_{ac} is the number of adjacent cores for the considered core c. All the above equations use notations having the same meanings as in Section 5.3 except that they are now defined for a specific core c, wherever used.

As an example, let us assume there are four (path, core) alternatives: (p_1, c_1), (p_2, c_3), (p_2, c_4) and (p_3, c_1). These alternatives are a subset of considered 21 and 36 alternatives (for 7 core and 12 core MCF, respectively, and three shortest paths) in this work and are only chosen to illustrate the algorithm's working. Table 5.4 shows the decision table containing the information about the alternatives, attributes and the corresponding data. Higher values of C_U and S_{Free} and lower values of C_F, N_A, E_{Tot} and QoT are desired. The relevant system and fiber parameters ([59]) are given in Table 3.1 in Chapter 3.

Table 5.4: Decision Table

Alternatives	C_U	C_F	N_A	S_{Free}	E_{Tot}	QoT
(p_1, c_1)	0.625	30	8	96	92	1740
(p_2, c_3)	0.9375	74	11	148	127	1405
(p_2, c_4)	0.828	132	11	148	127	1860
(p_3, c_1)	0.475	62	14	117	164	2587

Following this example, the attribute weights can be computed using the RI matrix, resulting in

$$\text{RI} = \begin{array}{c} \text{Attribute} \\ C_U \\ C_F \\ N_A \\ S_{Free} \\ E_{\text{Tot}} \\ QoT \end{array} \begin{array}{c} \begin{array}{cccccc} C_U & C_F & N_A & S_{Free} & E_{\text{Tot}} & QoT \end{array} \\ \left[\begin{array}{cccccc} 1 & 1/3 & 3 & 1 & 5 & 1/4 \\ 3 & 1 & 5 & 3 & 7 & 1/3 \\ 1/3 & 1/5 & 1 & 1/3 & 3 & 1/6 \\ 1 & 1/3 & 3 & 1 & 5 & 1/4 \\ 1/5 & 1/7 & 1/3 & 1/5 & 1 & 1/7 \\ 4 & 3 & 6 & 4 & 7 & 1 \end{array}\right] \end{array} \tag{5.23}$$

To obtain this, the C_U is considered slightly more important than the N_A required; hence, a value of 3 is assigned. Accordingly, the reciprocal 1/3 is given to N_A vs C_U matrix entry. Note that these assignments only illustrate the proposed AHP-enabled PROMETHEE method for path selection: in real practice, the decision-maker may assign values on a scale of 1-9 according to Table 5.3 based on their expertise toward solving the particular problem.

As explained in Section 5.4, the geometric means of the attributes are calculated as

For C_U: $(1 * 1/3 * 3 * 1 * 5 * 1/4)^{1/6} = 1.037$

For C_F: $(3 * 1 * 5 * 3 * 7 * 1/3)^{1/6} = 2.172$

For N_A: $(1/3 * 1/5 * 1 * 1/3 * 3 * 1/6)^{1/6} = 0.472$

For S_{Free}:$(1 * 1/3 * 3 * 1 * 5 * 1/4)^{1/6} = 1.037$

For E_{Tot}: $(1/5 * 1/7 * 1/3 * 1/5 * 1 * 1/7)^{1/6} = 0.254$

For QoT: $(4 * 3 * 6 * 4 * 7 * 1)^{1/6} = 3.554$

The sum of these geometric means is 8.526. The corresponding weights of the attributes are obtained by dividing their geometric means by the sum:

$w_{CU} = 1.037/8.526 = 0.1217$

$w_F = 2.172/8.526 = 0.2546$

$w_{N_A} = 0.472/8.526 = 0.0553$

$w_{S_{Free}} = 1.037/8.526 = 0.1217$

$w_{E_{\text{Tot}}} = 0.254/8.526 = 0.0298$

$w_{QoT} = 3.554/8.526 = 0.4167$

Putting these weights into a vector, we denote

$$W = [0.1217, 0.2546, 0.0553, 0.1217, 0.0298, 0.4167]^T$$

. The CR computations following the steps given in Section 5.4 are given as:

Step A: Derive the vector M:

$$M = \begin{bmatrix} 0.7478/0.1217 = 6.1454 \\ 1.6095/0.2546 = 6.3203 \\ 0.3464/0.0553 = 6.2550 \\ 0.7478/0.1217 = 6.1454 \\ 0.1928/0.0298 = 6.4629 \\ 2.6954/0.4167 = 6.4682 \end{bmatrix} \tag{5.24}$$

Step B: The value of λ_{max} is 6.2995. The CI value is computed as $CI = (6.2995 - 6)/(6 - 1) = 0.0599$.

Step C: The CR value is $0.0599/1.25 = 0.0479$. This is much less than 0.1, indicating good consistency in the relative importance relations assigned, and the weights can be accepted.

Next, the preference values (Pref_y) resulting from the pairwise comparisons of the alternatives with respect to each attribute are found. Table 5.5 shows these values for the C_U attribute; similar preference tables are formed for the remaining attributes. Pairwise comparison means that when an alternative Alt_i dominates another alternative Alt_j, a 1 is assigned to matrix element (i, j), and a 0 is assigned to element (j, i). However, if two alternatives are equal, no dominance exists and a 0 is assigned in both cases. Using the four preference tables for the $X = 4$ alternatives, a multiple attribute preference index table is formed, as shown in Table 5.6.

Table 5.5: Preference Values for C_U Attribute

CU (0.1217)	(p_1, c_1)	(p_2, c_3)	(p_2, c_4)	(p_3, c_1)
(p_1, c_1)	–	0	0	1
(p_2, c_3)	1	–	1	1
(p_2, c_4)	1	0	–	1
(p_3, c_1)	0	0	0	–

The leaving, entering, and net flows are calculated next. The leaving flow is computed as the row-wise summation and the entering flow as the column-wise summation of the preference values of Table 5.6. The net flow (ϕ) is calculated as

Table 5.6: Preference Relations and the Ranks of Alternatives

	(p_1, c_1)	(p_2, c_3)	(p_2, c_4)	(p_3, c_1)	ϕ^+
(p_1, c_1)	–	0.3485	0.7652	0.8869	2.0006
(p_2, c_3)	0.6601	–	0.793	0.754	2.2071
(p_2, c_4)	0.2434	0	–	0.754	0.9974
(p_3, c_1)	0.1217	0.2546	0.2546	–	0.6309
ϕ^-	1.0252	0.6031	1.8128	2.3949	

the difference between the leaving and entering flows i.e. $(\phi^+ - \phi^-)$, which come out to be 0.9754, 1.604, -0.8154 and -1.764 for the example shown. Based on these ϕ values, the alternatives are ranked in descending order and, the best alternative is the first one. Hence, the ranking of the alternatives becomes (p_2, c_3), (p_1, c_1), (p_2, c_4), (p_3, c_1), with (p_2, c_3) being the best choice.

5.5.2 Implementation Example: Spectrum Assignment

The next step is to find the spectral blocks satisfying the continuity and contiguity conditions for the particular route-core combination being considered. The score function algorithm, Algorithm 5.3, is called for the candidate blocks, and they are sorted in ascending order of their scores in Line 6. All spectrum blocks of the size required for the data rate and modulation format selected that obey the continuity and contiguity constraints of the EONs are considered candidate blocks. The QoT is checked starting with the first candidate block. If it does not satisfy the threshold criterion in Eq. (5.5) or unduly degrades other established lightpaths, the search proceeds toward the next spectrum block. However, if Eq. (5.5) is satisfied, then the current candidate block is selected. Hence, the loop at line 7 of Algorithm 5.1 continues until a QoT-satisfying block is found. Since the scores already incorporate the XT aspect as one term, it can be assured that the found block from the sorted set is one of the better choices w.r.t. XT satisfaction, and there is no need to continue the search for other spectrum blocks.

We define a weighted multi-objective function that computes a score for the feasible candidate spectrum block, returned by Algorithm 5.3. This score is calculated for the entire route-core alternative and considers the number of occupied slots surrounding the candidate block on adjacent cores and the amount of fragmentation incurred from selecting that block on that core and on that route. As seen from Algorithm 5.3, for each link, the first term, $X^{(e)}$, denotes the score value considering XT and the second term, $N_F^{(e)}$, denotes the score value relating to the

additional fragmentation caused by selecting that particular spectral block, and the third term E_{Tot} calculates the power consumption. Depending on the weights chosen, the algorithm can emphasize a lower expected XT, fragmentation-causing capability, or power cost when considering the whole route. This spectrum selection scheme using scores is named as score fit (SF) in this work.

To see how the $N_F^{(e)}$ term captures the spectral block's fragmentation-causing capability when compared to classical spectrum schemes [4], consider a link's spectrum status [ABCD111HIJKLM11PQRST11], where a '1' denotes an occupied slot, and the letters are position indicators denoting available slots. Assume 3 frequency slots are required to accommodate the current traffic request, i.e., $S_{req} = 3$. Then, the candidate blocks are [ABC], [BCD], [HIJ], [IJK], [JKL], [KLM], [PQR], [QRS], and [RST]. Assume that these candidates satisfy the continuity constraint. The classical spectrum allocation algorithms, FF , LF , EF , and Best Fit (BF) [108] would choose [ABC], [RST], [ABC], and [ABC], respectively. However, these blocks create fragments of sizes 1, 2, 1, and 1, respectively, which is wasteful w.r.t. future traffic. However, the $N_F^{(e)}$ term would encourage the selection of [HIJ] or [KLM] as they leave zero fragments with sizes less than S_{req}, thus leaving bigger blocks of contiguous available slots.

The complexity of the proposed algorithm is $O(KS|C||V|)$, where K is the number of routes considered, S is the number of frequency slots, $|C|$ is the number of cores, and $|V|$ is the number of network nodes.

5.6 Network Results

The proposed algorithm is tested on two network topologies, the 11-node and 52-link COST-239 and the 14-node and 21- link NSFNET, using a 7-core MCF on each link, as shown in Fig. 2.6. The NSFNET is additionally tested with 12-core links to check the robustness of the algorithms. Both these networks have a wide diversity of link distances (200 km - 2400 km), which is essential while considering the inclusion of PLI. This work assumes a 4 THz optical spectrum per core for both networks. Each frequency slot of a core supports 12.5 GHz transmission.

A Poisson traffic distribution model is used to generate 100,000 requests for varying loads with data rates uniformly distributed in [50, 300] Gbps. A request comprises a source node, a destination node, and requested data rate. Modulation selection is distance adaptive and the modulation formats considered are

binary phase shift keying, quadrature phase shift keying, 8-quadrature amplitude modulation (QAM), 16-QAM, and 32-QAM; the threshold SNRs are adopted from [109]. The algorithm's effectiveness is measured by calculating the blocking probability (BP), bandwidth blocking probability (BBP), network fragmentation (F_{NET}) computed using Eq. (3.10), and total power consumption (TEC). The BP and BBP are calculated using [Eqns. (2.1))-(2.2)].

The next sections show the simulation results where a 95% confidence interval is drawn as error bars around each mean value over 5 trials. In all the results, the conventional KSP routing with FF spectrum assignment algorithm is subjected to the QoT constraint for a fair comparison with the proposed approach. The results are also compared with a recently published impairment-aware RMSCA algorithm described in [92]. The authors proposed a dynamic impairment-aware (DI-aware) RMSCA algorithm. However, the SPM impairment was not considered in their work; hence, for a fair comparison, the proposed algorithms of this chapter are also simulated without the SPM effect whenever compared with the DI-aware algorithm.

5.6.1 Performance Analysis, 7-core MCF: Blocking Probability

This section analyzes the performance of the algorithms when operating in networks where all links use 7-core MCFs. The 7-core fiber has a core at the center and 6 cores surrounding it. Figs. 5.1 and 5.2 compare the blocking probability obtained using the benchmark KSP and the proposed MADM routing under FF spectrum allocation and the proposed SF approach for the two networks considered, respectively.

The results show that the MADM SF obtains the lowest blocking probability among the considered algorithms. For a given routing scheme (KSP or MADM), the SF performs better than the benchmark FF. And for a given spectrum allocation (FF or SF), the MADM routing aids in obtaining lower blocking. This behavior is because KSP only considers distance, whereas MADM-based routing uses a holistic approach, including blocking-affecting metrics. The performance of KSP SF is comparable with MADM FF but still performs better than the routing and spectrum benchmark (KSP using FF). Similar observations can be drawn from the blocking behavior in the NSFNET and COST239 networks.

Fig. 5.3 shows the blocking probability comparison between the proposed

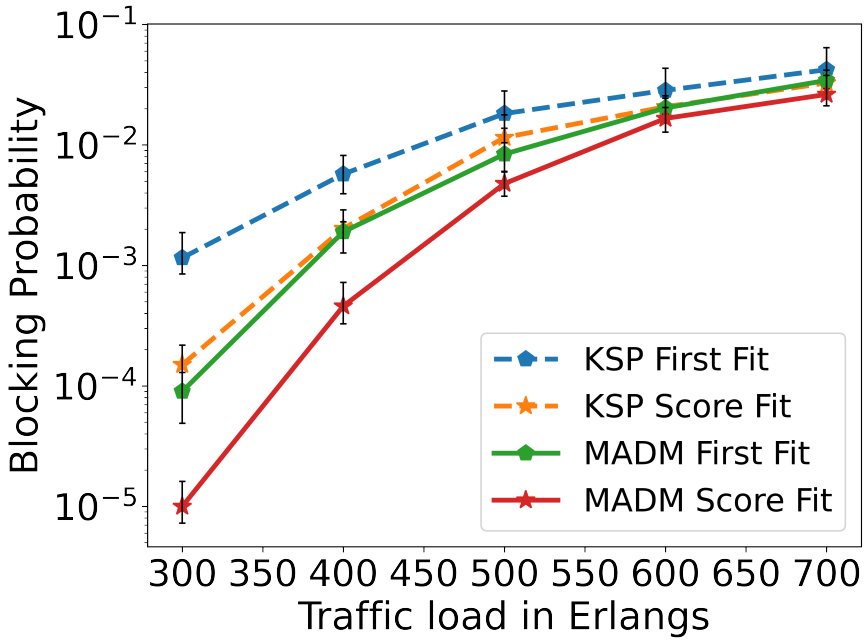

Figure 5.1: Blocking probabilities for the KSP FF, KSP SF, MADM FF and MADM SF in a 7-core NSFNET

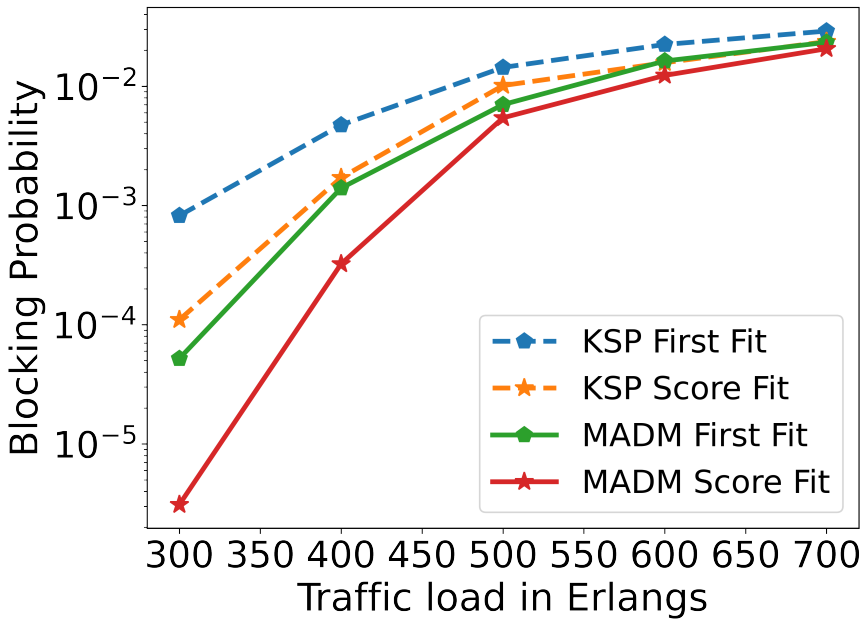

Figure 5.2: Blocking probabilities for the KSP FF, KSP SF, MADM FF and MADM SF in a 7-core COST239

algorithm and the DI-aware algorithm. The blocking probability is slightly lower than in Fig. 5.1 since the SPM effect is absent. The DI-aware algorithm uses KSP routing; hence, the KSP case is shown with the SF and the MADM routing

with SF. MADM SF offers significantly lower blocking, and even KSP SF offers slightly better performance than the DI-aware scheme. This is because the SF is more concerned with XT than with the other impairments considered in the MADM routing decision; hence, MADM SF performed better than the KSP SF when compared to the DI-aware scheme.

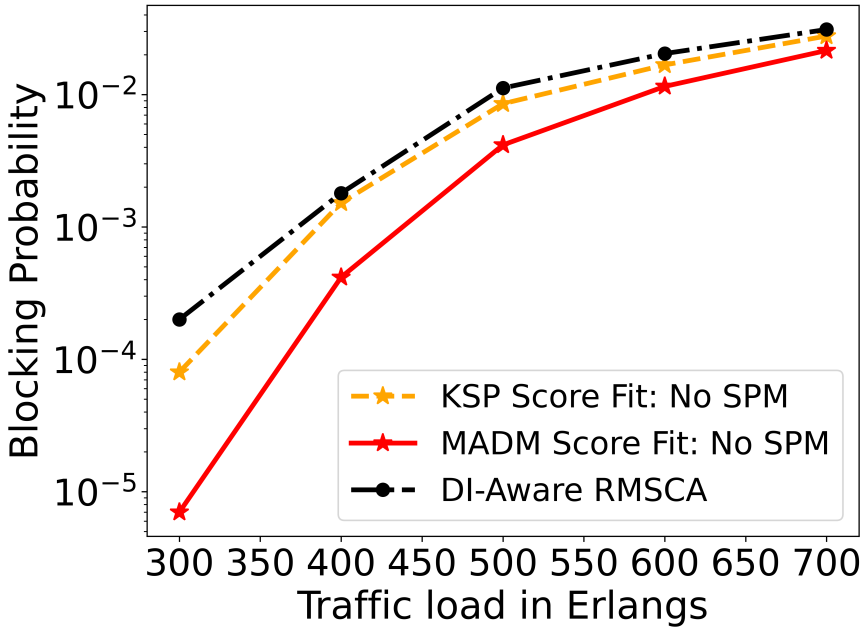

Figure 5.3: Blocking probabilities for the KSP SF, MADM SF, DI-aware RMSCA [92] in 7-core NSFNET

5.6.2 7-core MCF: Bandwidth Blocking Probability

Since SDM-EONs are expected to carry high amounts of data, analysis of BBP gives better insight into the network performance than the BP that treats all requests the same irrespective of their size [7]. Figs. 5.4 and 5.5 show the BBP for the benchmark KSP and the proposed MADM routing with FF and SF spectrum allocation for the two networks, respectively. Results show that MADM SF obtains the lowest BBP among the considered algorithms. This is because, at any given time, the SF tries to find a block that balances the XT and fragmentation-causing capabilities. As a result, the chance of successful allocation is higher in the proposed approach despite changes in the request sizes. Furthermore, with any given candidate spectral block, the algorithm considers how much fragmentation it could cause that can lead to the possibility of rejection of future bigger-sized requests. Similar performance conclusions as those of blocking probability can be

drawn regarding the relative performance of other approaches in NSFNET and COST239 networks.

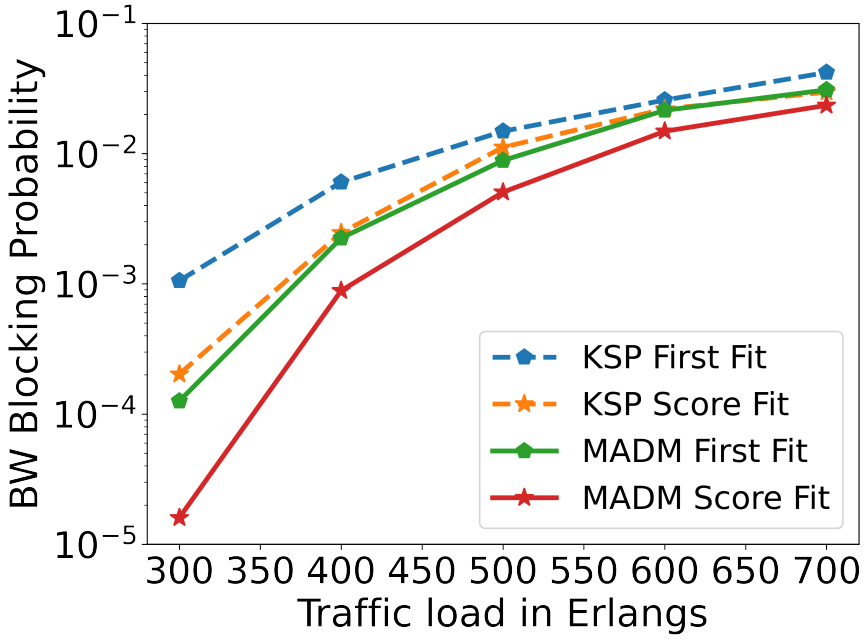

Figure 5.4: Bandwidth blocking probabilities for the KSP FF, KSP SF, MADM FF, and MADM SF in 7-core NSFNET

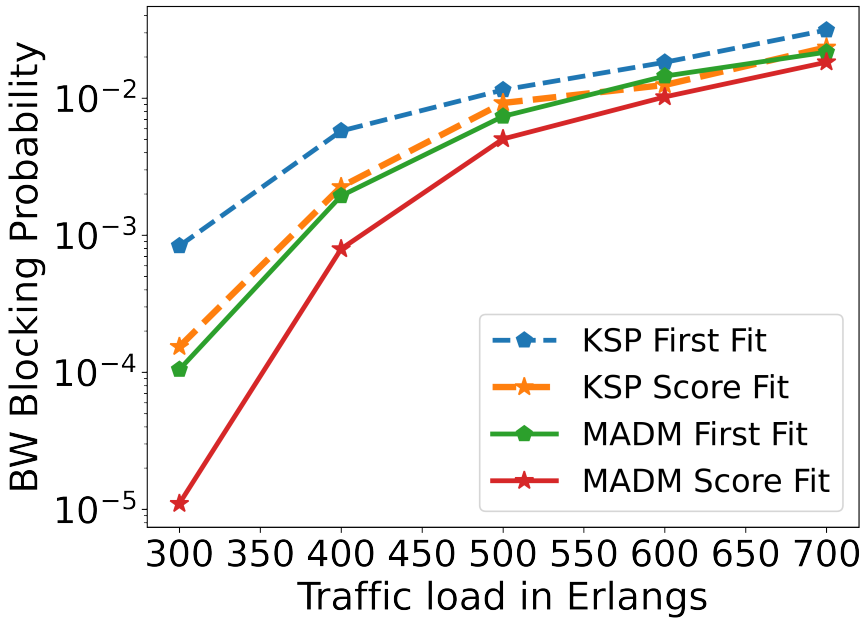

Figure 5.5: BW blocking probabilities for the KSP FF, KSP SF, MADM FF, and MADM SF in a 7-core COST239

5.6.3 7-core MCF: Power Consumption

Fig. 5.6 shows the power consumption (kW) in the NSFNET network as a function of traffic load when using the benchmark KSP and the proposed MADM routing under FF and SF spectrum allocation methods. As expected, the consumption increases with increasing load. Despite similar BP and BBP performances for KSP SF and MADM FF, they vary in power consumption. MADM-based RMSCA solutions are more power efficient than KSP-based ones. Including power cost via an attribute while applying the PROMETHEE method in the MADM routing decision stage has been more beneficial than in the spectrum allocation stage for the considered C-band operation. MADM FF shows lower power consumption than MADM SF and is due to its higher blocking. Similar reasoning goes for the performance differences between KSP FF and KSP SF.

The DI-aware approach of [92] did not consider power consumption. Hence, the consumption here is plotted by subjecting the algorithm to the formulas [Eqs. (5.8)-(5.13)], as used for the proposed methods. Results show that the DI-aware approach causes more power consumption than the proposed approaches – an algorithm being impairment-aware is unrelated to how power efficient it is.

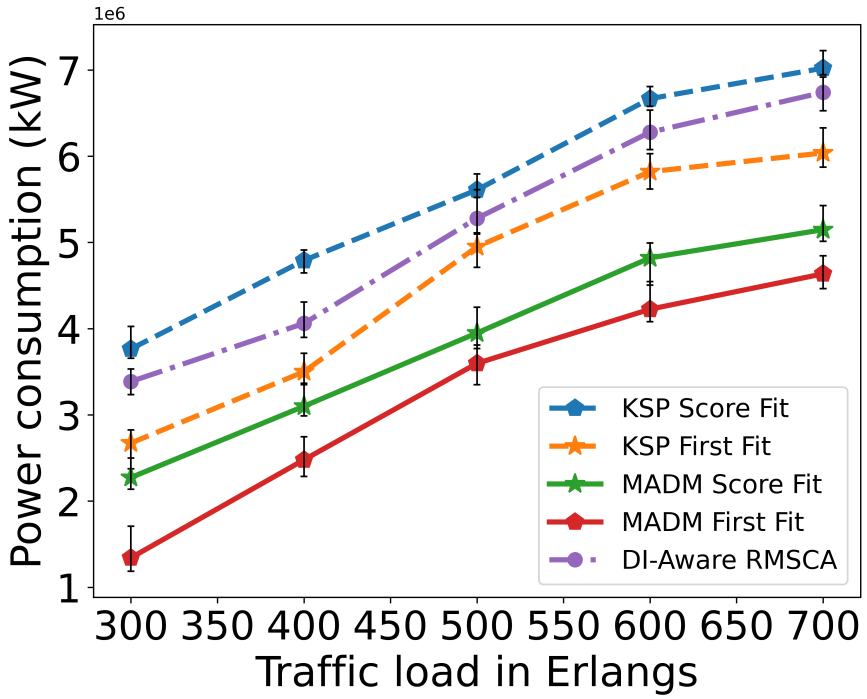

Figure 5.6: Total power consumption for KSP FF, KSP SF, MADM FF, MADM SF, and DI-aware RMSCA algorithm [92] in 7-core NSFNET

5.6.4 7-core MCF: Network Fragmentation

Fig. 5.7 shows the network fragmentation that occurs over different traffic loads for KSP and MADM routing under FF and SF spectrum allocation for the NSFNET network. In addition, the fragmentation resulting upon using the DI-aware published benchmark is also analyzed. The fragmentation metric can take values ranging from 0 to ∞ [33].

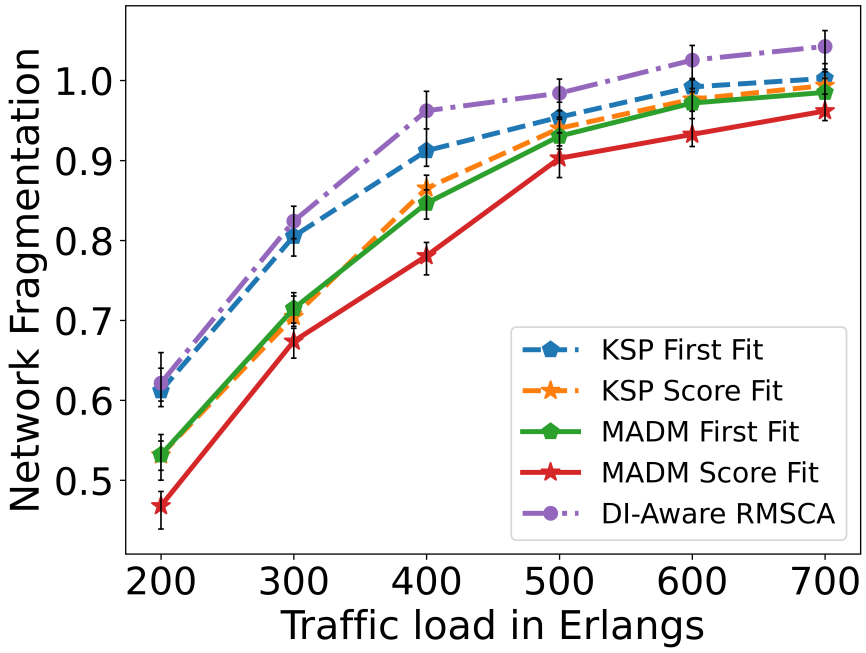

Figure 5.7: Network fragmentation for the KSP FF, KSP SF, MADM FF, MADM SF, and DI-aware RMSCA algorithm [92] in 7-core NSFNET

The MADM SF maintains lower fragmentation levels than the other algorithms for all traffic loads tested. The KSP FF compactly allocates the spectrum at any given time, but as seen in Section 5.5, the SF better quantifies and allocates the spectrum. This causes the proposed SF to perform better. In addition, the use of fragmentation as an attribute in the MADM route selection process helps to improve the performance further. The DI-aware approach did not consider fragmentation. Hence, the algorithm is subjected to the same formula Eq. (3.10) used for the proposed methods and plotted here. The algorithm results in higher fragmentation than the KSP FF. This is because the DI-aware approach minimizes the impairments' impact and does not include fragmentation in the spectrum allocation design process. Instead, it uses the KSP routing; hence, considering the spectrum part alone, the FF is naturally better at reducing frag-

mentation than the DI-aware allocation.

5.6.5 12-core MCF

Figs. 5.8-5.11 show the blocking probability, Bandwidth (BW) blocking probability, network fragmentation, and power consumption, respectively, in a 12-core based NSFNET. A ring-structured 12-core fiber is assumed for all simulations [110].

Fig. 5.8 shows that MADM SF obtains the lowest blocking probability among the algorithms tested for similar reasons as in the case of 7-core MCF. Similarly, the KSP SF and MADM FF give close results. However, the performance difference between the algorithms is smaller than in the 7-core case. The reason is that the number of neighbors in the ring-structured 12-core MCF link is less than in the 7-core type; hence, the XT experienced by a signal is lower. Since the algorithms are XT-aware, they might show a higher performance advantage when the XT is stronger. However, the algorithms still perform better than the KSP FF benchmark due to including holistic network features in routing and spectrum allocation decisions.

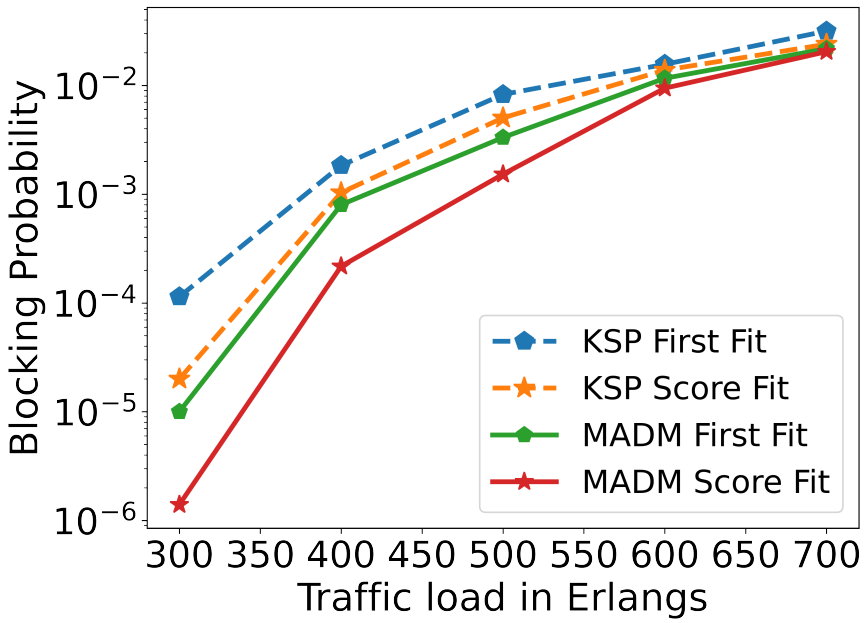

Figure 5.8: Blocking probabilities for the KSP FF, KSP SF, MADM FF and MADM SF in 12-core NSFNET

Conclusions drawn from the results in Fig. 5.9 are similar to those for the 7-core MCF network shown in Fig 5.4. The proposed methods maintained lower

BW blocking than the KSP FF with MADM SF being the best. Fig. 5.10 shows the obtained 12-core MCF network fragmentation for the proposed algorithms. Similar to the 7-core case, the SF aids in a better quantification of the network fragments before deciding the RMSCA solution and hence provides lower fragmentation when combined with MADM routing. Fig. 5.11 shows the power consumption in a 12-core MCF network; the MADM approaches maintain lower power consumption than the other approaches as the traffic loads increase.

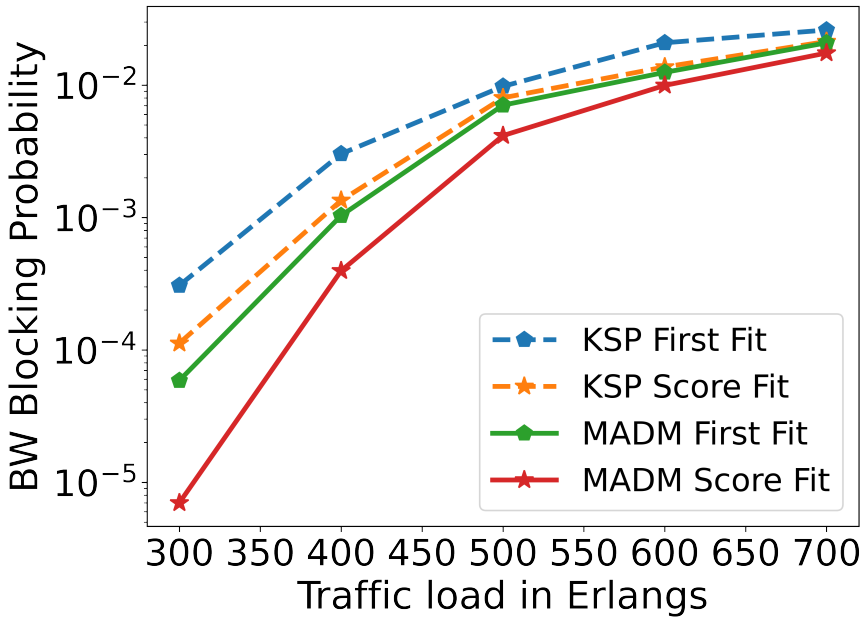

Figure 5.9: BW blocking probabilities for the KSP FF, KSP SF, MADM FF, and MADM SF in 12-core NSFNET

5.7 Chapter Summary

An impairment-aware, fragmentation-aware, and power-efficient RMSCA algorithm for C-band SDM-EONs is proposed in this chapter. The present work considers the XT, Kerr nonlinear impairments such as SPM and XPM, and also the ASE noise encountered by the signal along the chosen network path. Novelty is introduced in the form of new routing and new spectrum allocation processes. A MADM-based routing that considers relevant network aspects is used to rank the candidate routes and cores for traffic requests. In the spectrum allocation part, a score-based approach uses a weighted function that qualitatively incorporates the effects of the expected XT and the expected fragmentation on existing

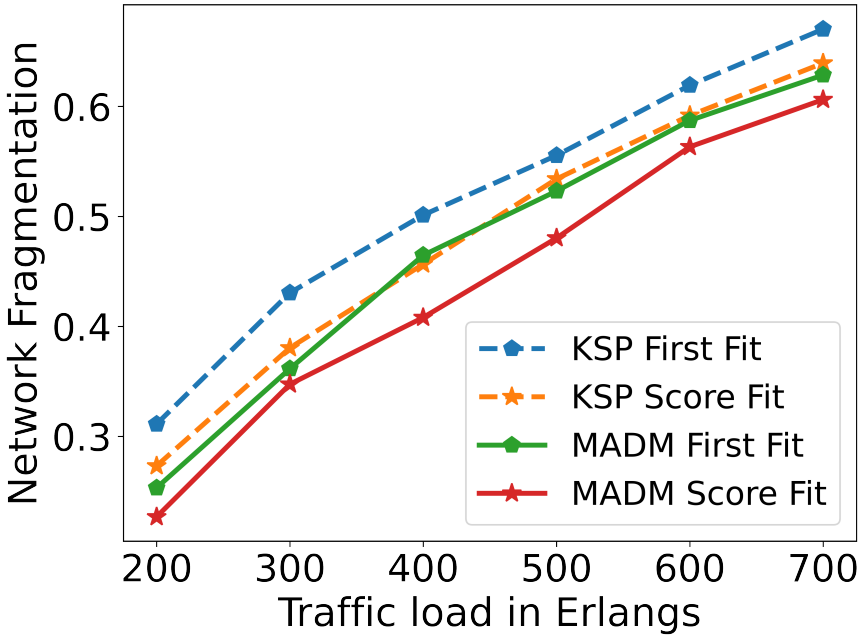

Figure 5.10: Network fragmentation for the KSP FF, KSP SF, MADM FF, and MADM SF in 12-core NSFNET

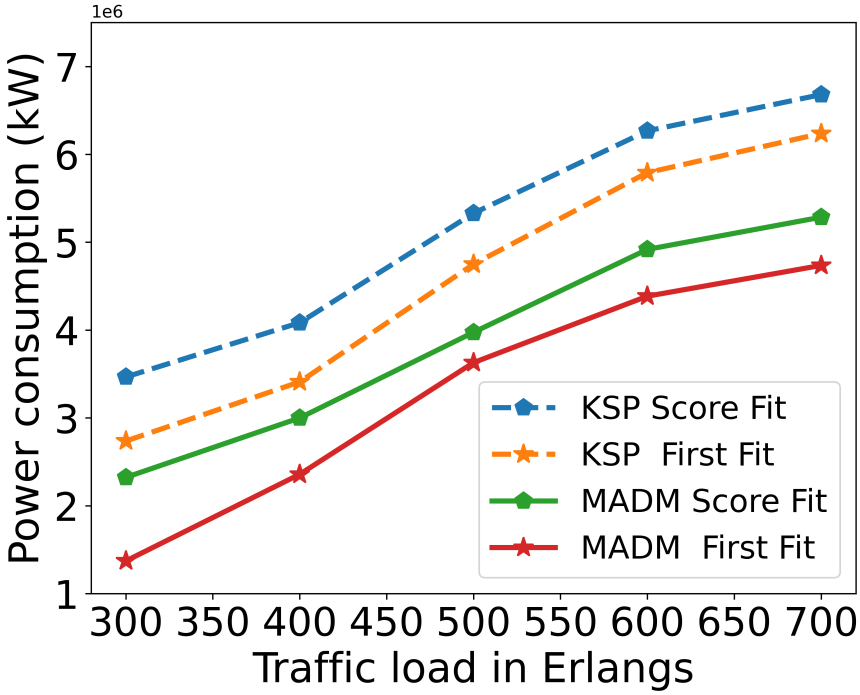

Figure 5.11: Total power consumption for KSP FF, KSP SF, MADM FF, and MADM SF in 12-core NSFNET

and upcoming traffic while maintaining lower power consumption levels. To the best of the knowledge when the work was published, this is the first work that considered all impairments in SDM-EONs while also being fragmentation and power aware.

The simulations are performed on two diverse network topologies, NSFNET and COST-239 with 7 and 12 core MCF links, and the results of blocking probability, bandwidth blocking probability, network fragmentation, and power consumption are analyzed. The novel combination of MADM routing and score function spectrum assignment performs significantly better than the conventional and published benchmarks for all cases tested.

Chapter 6

Multicore Resource Allocation: Machine Learning Approach

This chapter presents an RMSCA algorithm for SDM-EONs comprising multi-core links. A network state-dependent route and core selection method is proposed using a DNN classifier. The DNN is trained using an advanced optimization algorithm to predict lightpath suitability, considering the quality of transmission and resource availability. Physical layer impairments, including inter-core crosstalk, amplified spontaneous emission, and Kerr fiber nonlinearities, are considered, and a Random Forest (RF) based link noise estimator is proposed. A feature importance selection analysis is provided for all the features considered for the DNN classifier and the RF link noise estimator. The proposed machine learning enabled RMSCA approach is evaluated on three network topologies, US-NET, NSFNET, and COST-239 with 7-core and 12-core fiber links. It is shown to be superior in terms of blocking probability, bandwidth blocking probability, and computational time compared to the standard and published benchmarks at different traffic loads. This work was submitted for publication in February 2024 and is under editorial review in the *IEEE/Optica Journal of Optical Communications and Networking*.

6.1 Introduction

As emphasized in the previous chapters, a RMSCA solution needs to account for the PLIs present. Closed-form models and ML approaches have been used to estimate the dynamic PLI levels, the latter mainly for single-core fibers and rarely integrated into RMSCA schemes [25, 111, 112, 113]. In addition, the lightpath

acceptability is constrained by resource availability, spectrum continuity, and contiguity. The work in this chapter moves closer to integrating ML with multi-core optical networking by proposing an ML-enabled dynamic RMSCA algorithm that considers holistic factors affecting the lightpath suitability and incorporates a ML-enabled noise estimation to help check QoT conditions. The QoT model used in this chapter is the same as in Chapter 5.

ML intends to capture unknown optical network relationships for intelligent decision-making to improve network performance and faster computations. In recent years, there has been an increase in research works incorporating ML into traditional resource allocation at various stages, notably QoT estimation [114], traffic prediction [115], and network monitoring and survivability [116, 117]. Among the various applications, ML-based QoT estimation has received considerable attention [11, 118, 119, 120, 121, 112, 122]. In ML-based QoT estimation, regression and classification approaches usually decide the QoT suitability for a given lightpath. A regression method approximates the BER, whereas a binary classifier outputs a yes/no denoting the lightpath suitability w.r.t the defined tolerable BER, and this outcome can be used for resource allocation [121, 112]. The ML applications in the literature estimate or classify the lightpath solely on the QoT compared to a QoT metric threshold; they ignore the question of lightpath unavailability due to spectral resource shortages.

The ML optical networking community has focussed on improving ML models by enriching the training dataset quality and applying different ML tools, but not, as observed in the literature, on improving the inner workings of the ML models. Advanced training algorithms, as used in this work, can aid the current ML efforts to improve the model prediction capabilities. In addition, the previously proposed ML models have been well-analyzed for a given traffic load, but no works have considered all impairments under different traffic load scenarios for model robustness.

Keeping these aspects in mind, this chapter proposes an ML-enabled dynamic RMSCA method, a step toward ML integration into multi-core optical networking. It extends the previous work reported in [123], which introduced and described an ML classifier for route and core selection, by applying it to resource allocation and incorporating a random forest-based multi-core link noise estimator. The proposed approach uses ML at two stages: for multi-core link noise estimation and for the route and core selection process. The former uses a random forest (RF) model, and the latter uses a deep neural network (DNN)

trained by an advanced optimization algorithm called the Jaya algorithm [124]. The proposed scheme finds the best resources to reduce the probability of a connection request being blocked while reducing the computation time needed to find viable resource allocation candidates satisfying the QoT. A feature importance analysis is also performed on the proposed model for explainability.

The rest of this chapter is organized as follows. Section 6.2 summarizes the current literature in this area and highlights the chapter's novel contributions. Section 6.3 provides a description of the performance metrics employed. The proposed RF noise estimator and the DNN classifier are presented in Section 6.4. This section also describes the Jaya algorithm and the model tuning procedure. The proposed RMSCA algorithm is detailed in Section 6.5. The results and a chapter summary are provided in Sections 6.6 and 6.7, respectively.

6.2 Related Literature Review

This section describes the literature on applications of ML in single and multi-core optical networking. The mention of single-core here is important to notice the shift in research trends towards multi-core, to emphasize the comparatively smaller quantity of research performed in the latter under the umbrella of ML, and to also present to the readers the possibility of extensions of single-core solutions to multi-core networks.

ML has been widely used in the literature for QoT estimation for single-core fiber networks. In [118], an ML classifier for BER estimation was proposed based on lightpath characteristics, traffic volume, and modulation format. However, more features could be investigated to model the real network scenario better. Few works have extended the use of ML-QoT estimators for network planning. In [121], an integration of ML-based transmission reach estimator with RSA was presented. This work was one of the first attempts to show the application of ML outputs to resource allocation, albeit for a static RSA problem. The proposed framework was reported to achieve spectrum savings compared to conservative reach models. The work was extended in [112] by proposing a dual-stage framework to apply the ML predictions to RSA. However, these have not been extended to a dynamic resource allocation scenario. In [125], ML was used to model the fiber nonlinearities by calibrating the deviations resulting from nonlinear models in single-core fibers. Different fiber types and link configurations were used; hence, this model could be developed further for QoT-aware resource allocation,

including the XT effect for MCF links. In [126], a gradient-boosted ML model was presented that estimated the NLIs for multi-period network planning. The model was reported to have lower computation times than the GN-based network planning solutions. In [58], a ML model was used to estimate the optical SNR of in-service lightpaths in C+L bands before initiating defragmentation; they reported capacity increments in small and large-scale networks. In [127], a DNN-assisted QoT estimator was proposed for multi-band EON resource provisioning. The computational time, traffic admissibility, and number of contiguous blocks were improved compared to the benchmark schemes. The model could be adapted for QoT modeling in MCF networks.

In addition to supervised ML approaches, RL based solutions have been proposed in the optical networking literature, not just limited to QoT estimation. In [24], a DRL-based RMSA scheme was presented that selects a routing path and a spectral block. This was one of the initial works to pave the way for RL based optical networking to lower network blocking. However, only a few candidate spectral blocks were considered to enable successful policy learning by the RL agent, and a transmission reach model was used. Real-time nonlinear impairments were not considered, and the algorithm was limited to single-core networks. In [29], a Q-learning-based routing algorithm was proposed for RMSA in C+L band EON. Impairments and fragmentation were used to design the reward functions that helped lower blocking and fragmentation. In [23], a DRL based RMSA problem was studied, emphasizing the custom reward function design using path fragmentation levels. The method outperformed a heuristic and a simple reward-based DRL approach w.r.t. fragmentation. However, no PLIs were considered that would affect the resources chosen. In [22], a DRL-based RMSA scheme was proposed for inter-domain requests in a multi-domain EON. The method obtained lower blocking than KSP and a published benchmark for a multi-domain architecture. The PLIs, however, were ignored, so DRL agent actions were not sensitive to signal degradation when crossing multiple domains in real-time. In [128], a RL approach was proposed to find near-optimal parameters maximizing the overall bitrate of a 51-channel WDM link. Unlike most RL works, this approach considered linear and nonlinear impairments. The method was also reported to have lower computational time than optimization approaches.

Some works in the literature also reported the use of ML for SDM-EON network planning. In [116], a transfer learning (TL)-based optimization scheme was presented to predict the spectrum defragmentation time for improving re-

source utilization. However, the QoT aspect was simplified by categorizing the requests into four levels of BER. In [115], an Elman NN for traffic prediction and a fragmentation-reducing rectangular packing spectrum model were proposed. A spectrum partitioning method was used to reduce the XT effect; other impairments were not considered. In [129], an modulation format (MF) selection scheme using ML predictions was proposed. The ML was used to capture the relation between spectral efficiency, transmission reach, and XT to predict the optimal MF to obtain lower bandwidth blocking. Capturing the relation over more impairments would lead to a more realistic MF selection. In [122], a DNN was presented to predict an optimal set of XT thresholds to determine the MF selection that ensures XT compliance for a given traffic request in SDM-EONs. Other impairments were not included that would have yielded a more realistic effect on the thresholds chosen by the ML model. In [117], two defragmentation algorithms were proposed based on unsupervised ML. The lightpaths were clustered using link characteristics, and new lightpaths were assigned to the closest cluster as predicted by the ML model. This work is one of the few works that used the unsupervised approach for optical networking.

Few works also utilized ML to aid QoT calculations for SDM-EONs. In [114], deep graph convolutional neural networks (DGCNN) were applied for MCF QoT estimation. The DGCNN was used to find the feasibility of a lightpath in terms of QoT satisfaction and its effect on in-service traffic due to XT. In [130], a self-organizing feature mapping-based model was proposed to process multi-dimensional data of SDM-EONs. The model estimated the core transmission quality and was integrated into RCSA to locate higher transmission-quality cores for lower blocking. In [131], mode selection for a few-mode MCF was performed using ML-assisted XT prediction. Improved connection setup times and spectrum utilization were reported. However, in both these works, only the XT effect was considered for the estimation.

Table 6.1 shows the state-of-the-art related to the application of ML in single and multi-core optical networking, respectively. It is concluded from the literature that no ML-based works have covered all impairments in multi-core fiber networks. In addition, there is a lack of literature on applying ML methods to dynamic resource allocation in multi-core networks, and the work in this chapter addresses this gap. Furthermore, the literature on lightpath classification/regression solves the prediction problem from the QoT perspective and does not consider other factors affecting the network. Therefore, keeping all the above

Table 6.1: Literature on ML-Assisted Optical Networking in Single- and Multi-Core Networks

Related works	**Single core**	**Multi-core**	**Impairments**		**Focus of Application**
			ASE & NLIs	**XT**	
[121]	✓	-	✓	-	static resource allocation
[126]	✓	-	✓	-	multi- period planning
[118]	✓	-	✓	-	QoT prediction (no resource allocation)
[22]	✓	-	✓	-	multidomain EON
[120]	✓	-	✓	-	QoT estimation (no resource allocation)
[112]	✓	-	✓	-	static resource allocation
[128]	✓	-	✓	-	parameter optimization (no resource allocation)
[24]	✓	-	✓	-	resource allocation
[127]	✓	-	✓	-	multi-band
[29]	✓	-	✓	-	multi-band
[114]	-	✓	-	✓	QoT estimation (no resource allocation)
[115]	-	✓	-	✓	resource allocation
[116]	-	✓	-	✓	defragmentation time prediction
[117]	-	✓	-	-	lightpath clustering for defragmentation
[122]	-	✓	-	✓	MF selection
[129]	-	✓	-	✓	MF selection (no resource allocation)
Current work	-	✓	✓	✓	resource allocation via noise estimation and lightpath suitability

aspects in mind, the following contributions are made in this chapter:

- A DNN-based binary classifier and a RF-based link noise estimator are proposed to find viable resources and to aid QoT checking for impairment-affected SDM-EONs.
- The classifier is then used to perform a PLI-aware dynamic RMSCA using the results of the noise estimator. All physical layer impairments (ASE, XPM, SPM, and XT) are considered for realistic results.

- ML is used to predict the acceptability of a lightpath, including the acceptability of the QoT and the availability of end-to-end spectral resources.
- An advanced optimization algorithm called the Jaya algorithm [124] is adopted and presented for DNN training in the optical networking domain for the first time.
- Varying traffic loads are considered for improving prediction capability and robustness, and a feature selection analysis is provided.

The results of the proposed algorithm are compared with standard and published benchmarks on 7 and 12 core-based USNET, NSFNET, and COST-239 networks. The algorithm in [81], called the ICXT-aware algorithm, was chosen for comparison over the works described above because, while it is not an ML-based work, it is the closest to the work in this chapter as it considers a PLI-aware RMSCA for SDM-EONs. It is designed to reduce the impact of XT by utilizing core prioritization and spectrum partitioning. The cores are grouped together, and the spectrum is divided in each of these cores in a different manner, thus reducing signal overlapping that leads to XT.

6.3 Evaluation Metrics

The performance metrics of the DNN and RF, and the proposed RMSCA algorithm are described in this section.

6.3.1 DNN and RF Performance Metrics

The classification problem considered is imbalanced since the proportion of accepted and unaccepted lightpaths for any traffic load is not equal while considering all the RMSCA candidates. This is expected since rejections are rare at low loads and increase with traffic. Hence, the commonly used *classifier accuracy* metric fails here: the accuracy of a classifier predicting a 1 will be misleadingly high if the dataset has a significant proportion of class 1 samples. Therefore, the proposed classifier is evaluated using the area under the curve of the receiver operating characteristic (AUC ROC) metric whose range is $[0, 1]$ [132]. In general, any classifier with an AUC ROC ≥ 0.8 is considered very good, and ≥ 0.9 is deemed excellent for imbalanced problems [132, 133]. An ideal classifier has an AUC ROC $= 1.0$.

A binary classifier needs a threshold, denoted as V_{th}, to convert the prediction into a binary 0 or 1 decision. The best V_{th} for each DNN is found using the geometric mean (GM) technique [134]. The GM for an imbalanced classifier seeks a balance between sensitivity and specificity and is a point on the AUC ROC curve that maximizes the 0/1 distinguishing capability. The maximum GM is computed as

$$\max_{a}(\sqrt{TPR_a * (1 - FPR_a)}) \tag{6.1}$$

where TPR_a and FPR_a are the true positive rate and false positive rate for each point $a \in [0, 1]$, i.e., the range of values the FPR can take.

The performance of the RF regression model is assessed using the root mean square error (RMSE).

6.3.2 Network Performance Metrics

The proposed RMSCA algorithm's effectiveness is measured by calculating the BP, BBP, and average setup time (AST). The BP and BBP are given by [Eqns. (2.1)-(2.2)] in Chapter 2. The setup time for a successfully provisioned traffic request demand r is measured as the CPU time difference between when the search for resources starts and when a successful allocation is found. The AST for a set of R requests is the average setup time for all requests $r \in R$.

6.4 Proposed ML Models

The general three-step process to designing a ML-enabled RMSCA algorithm is (1) dataset generation using appropriate features, (2) model architecture selection, training, tuning, and testing, and (3) application of the trained ML model to the RMSCA problem to assist in successfully provisioning new resource requests. This section explains the first two steps, and the third step for the proposed algorithm is explained in Section 6.5.

6.4.1 Data Generation and Feature Selection

The dataset of a supervised ML model is composed of independent samples of the form (features, target). In regression, the target value is continuous, whereas in binary classification, the target class is a 1 or 0, denoting the lightpath success or

failure. This chapter proposes a DNN binary classifier and a RF-based link noise regression to predict the suitability of a lightpath and the noise levels on a link given the optical network features. The public datasets for optical networks from Abilene, GEANT, Mendeley, etc., do not include the desired features considered in this work and do not pertain to SDM-EONs [135]. An optical simulator such as GNPy does not consider MCF-enabled links to generate lightpath conditions. Hence, synthetic data generation is used, the most common methodology in similar studies [100, 130, 126]. It is generated using a custom RMSCA code by applying the KSP for routing, GN model based QoT aware modulation selection [76], FC for core selection, and FF for spectrum allocation. The GN and XT models described in Section 6.3 are used as the true value of impairments needed to set the target for each data sample. The training datasets are generated for each load of interest and for all K routes over the entire set of cores C ($K \times |C|$ combinations) for each request r with different modulations m.

The features in a dataset are representative of the problem being solved. Although using an exhaustive list of features may help the machine effectively learn the mapping from feature space to target space, it does not guarantee the best performing ML model and increases the training time. Choosing too small a set of features may not capture the problem well enough, leading to poor approximations. The feature selection problem in the context of EONs is well-explained in [136]. To this end, a technique called recursive feature elimination (RFE) is utilized in this work to identify the most influential features for improving the accuracy of the predictions made by the RF noise estimator [137]. RFE iteratively removes less essential features to create a subset that minimizes some loss function, the RMSE in the case of the RF model. For the DNN model, the set of features resulting in the highest testing AUC ROC is chosen.

RF link noise estimator

The output variable of the link noise estimator is an estimate of the combined PLIs over the link of interest. In this work, noise is selected for the estimation rather than the SNR directly, as is typically done, for two reasons. First, during the QoT checking phase, the possible degradation of in-service lightpaths due to the current request is checked. This checking requires the individual link noise values so that the overlapping lightpaths on each link of the candidate route can be analyzed for disturbance. Secondly, it allows us to estimate the SNRs for any input channel power.

The twelve lightpath features considered for the estimator for a given link e belonging to the candidate lightpath Υ, core $c \in C$, and a candidate spectrum block are:

1. S_{req}, the number of frequency slots required for the request based on the data rate requested
2. Modulation format selected for the new request, $m \in M$, where $M = \{$32-QAM, 16-QAM, 8-QAM, QPSK, BPSK$\}$
3. Link length $\ell^{(e)}$, which affects the XT and ASE
4. Spectrum usage of the core on link e, as a higher usage makes the provisioning difficult and also presents more interference to the candidate request
5. Number of active blocks on core c of link e, which affects the XPM
6. Number of occupied slots overlapping the candidate spectral blocks in adjacent cores of c.
7. Center frequency of the candidate spectral block, f
8. Modulation format of the neighbor occupying the frequency slots immediately to the left of f
9. Center frequency of the neighbor occupying the frequency slots immediately to the left of f
10. Center frequency of the neighbor occupying the frequency slots immediately to the right of f
11. Number of occupied spectrum slots to the left of the candidate spectral block, which captures spectral occupancy.
12. Number of spans in link e, $N_s^{(e)}$

DNN classifier

The output of the DNN classifier is a 1 or 0 and the eight features considered for the classifier are given by features number 1 and 2 of the estimator above, and the rest are:

1. Lightpath length
2. Number of spectrum blocks on c that satisfy the continuity and contiguity constraint; this feature directly relates to the spectrum provisioning capability.
3. Same as feature no. 4 of estimator but over the entire lightpath Υ
4. Same as feature no. 5 of estimator but over Υ
5. Number of occupied slots in adjacent cores on link e, as this relates to the crosstalk impairment
6. Core fragmentation from [33]. The fragmentation feature affects the availability of *contiguous* spectrum resources and thus affects the blocking probability.

6.4.2 ML Model Tuning and Training

A supervised ML model performance is dependent on how well it is 'tuned' and trained. This section describes the tuning and training processes for both the DNN classifier and the RF noise estimator.

Hyperparameter Tuning

A DNN is a collection of neurons arranged as an input layer, more than two hidden layers, and an output layer; each neuron requires a set of weights and biases. During training, the DNN classifier learns the optimal set of weights and biases that minimizes the loss function, thus best approximating the function mapping the feature space and the target class space. But the training performance of a DNN is affected by various hyperparameters that must be predefined, such as the number of hidden layers, the number of neurons per layer, the activation functions used, the training algorithm itself, learning rate, decay rate, number of epochs, batch size, etc. Tuning these parameters is tedious and requires trial and error, even when starting with educated guesses from the literature. In this work, various combinations of these parameters were tested on the DNN, and the maximum AUC ROC-producing combinations were narrowed down to serve as a starting point. These were further fine-tuned to improve the performance. The ranges of values tested and the final chosen values for the classifier are given in Table 6.2.

Table 6.2: DNN Hyperparameters and Their Tested Ranges

Hyperparameter	**Tested Values**	**Chosen Value**
Learning rate	10^{-1} to 10^{-5}	10^{-4}
Number of hidden layers	$1, 2, 3, 4$	3
Number of neurons per hidden layer	$16, 32, 64$	32
Number of neurons in last hidden layer	$2, 4, 8, 16, 32, 64$	16
Activation functions [134]	Sigmoid, ReLU, Tanh	ReLU, Sigmoid
Batch size	$32, 64, 128, 256, 1024$	256
Regularizer [134]	l_1, l_2	l_2
Initializer [134]	Glorot, He normal	He normal

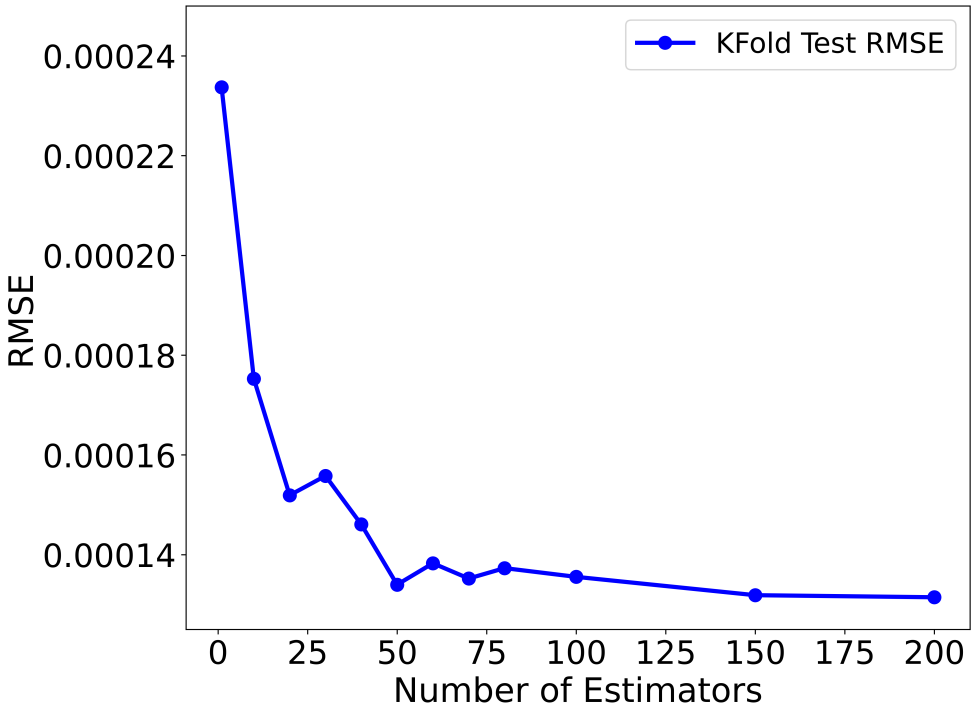

Figure 6.1: Test RMSE obtained for different numbers of trees in the RF model at a load of 400 Erlangs for the 7-core USNET

For the RF estimator, the hyperparameters are the number of decision trees in the forest, the maximum depth of the decision trees, the minimum number of

samples required to split a node, the minimum number of samples required to be at a leaf node, and the number of features to consider when looking for the best split. The final chosen values are (50, until all leaves contain less than two samples, 2, 1, 1), respectively. The RF tuning in this work needed trials only to determine the number of decision trees; the default Scikit-learn library values were used for the other parameters [134]. Fig. 6.1 shows the obtained test RMSE for different numbers of trees, i.e., estimators in the RF model. The plotted test RMSE values are a result of the RF model trained using the K-fold cross-validation technique (5 folds) to assess and ensure the model's generalizability [134]. The results show that 50 tree estimators resulted in the lowest RMSE with 150 and 200 estimators also performing at par. However, the computational time increases with the number of trees; hence, the 50 tree model was chosen for this work.

Jaya Algorithm for DNN training

Training algorithms differ in scalability, the computational effort needed in training, interpretability, and sensitivity to outliers. The commonly used training algorithms are gradient-based, such as Adam, stochastic gradient descent, RMSProp, and Adagrad [138]. Some metaheuristic algorithms can also be used for training, especially when the optimization problem is complex, non-convex, or high-dimensional and when traditional gradient-based optimization algorithms cannot find a good solution. Examples include particle swarm optimization (PSO), genetic algorithms (GA), ant colony optimization (ACO), differential evolution (DE), etc. [138].

In this work, one such advanced metaheuristic algorithm called the Jaya algorithm [124] is used for DNN training and to compare its performance with Adam. The Jaya algorithm has been shown to perform better than the commonly used optimizers in various problem domains [139, 140, 141, 142]. Algorithms such as PSO, GA, DE, ACO, etc., have their algorithm-specific parameters that must be tuned before applying them to the optimization problem [139]. In contrast, the simplicity of the Jaya algorithm lies in the absence of such parameters; only common control parameters, such as population size and termination criteria, need to be defined. Fig. 6.2 shows a flowchart of the Jaya algorithm. Only relevant details to understand the current work are provided; the detailed working of the algorithm can be found in [124].

The objective function to optimize during a binary classifier training is the

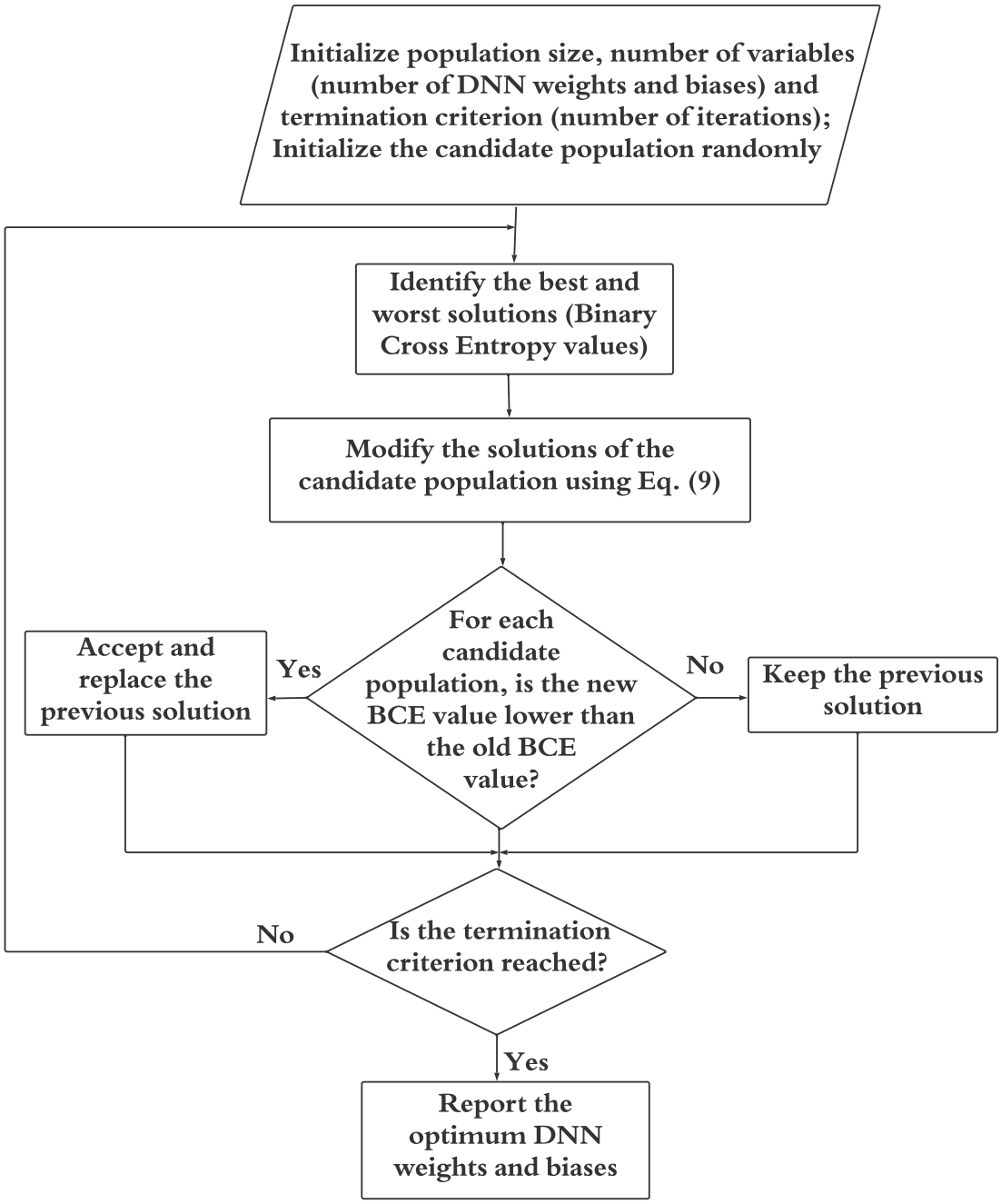

Figure 6.2: Flowchart of Jaya algorithm adapted for DNN training

loss function, the binary cross entropy (BCE) in this case. The Jaya algorithm begins by initializing the candidate population size U, the number of variables V, and the termination criterion, which in this work is taken as I, the number of iterations. The population is the set of candidate solutions (set of variable values); these are randomly initialized at the beginning of the algorithm, denoted as $X^1_{u,v}$, for all candidates $u = 1, \cdots, U$ and variables $v = 1, \cdots, V$. For a DNN,

the variables are the DNN weights and biases whose values are to be found.

At each iteration i, the values are updated using

$$X_{u,v}^{i+1} = X_{u,v}^{i} + r_{1,u}^{i}(X_{u,\text{best}}^{i} - |X_{u,v}^{i}|) + r_{2,u}^{i}(X_{u,\text{worst}}^{i} - |X_{u,v}^{i}|) \tag{6.2}$$

for all $u = 1, \cdots, U$, $v = 1, \cdots, V$, $i = 1, \cdots, I$. The new solution $X_{u,v}^{i+1}$ is computed as a function of the value $X_{u,v}^{i}$ from the previous iteration, the best and worst values of that variable, denoted as $X_{u,\text{best}}^{i}$ and $X_{u,\text{worst}}^{i}$, respectively, and two random numbers, $r_{1,u}^{i}$ and $r_{2,u}^{i}$, in the range $(0, 1)$. The best and worst solutions are the values of the variable yielding minimum and maximum BCE values at the previous iteration. The candidate values in the population, i.e., the DNN weights and biases, are updated at each iteration using Eq. (6.2). The corresponding objective function, i.e., BCE values, are computed. The new solutions are compared with those in the previous iteration and either accepted if the new solution is better or rejected if not. The procedure continues until the termination criterion is fulfilled and the optimum solution is reported, i.e., the set of weights and biases.

Two Approaches to the Proposed DNN Classifier

In this work, the trained DNN is applied to different traffic loads, and hence, it is natural to question whether a single DNN trained on the entire data for all loads would suffice or whether a separate DNN is required at each load. In the former case, the single DNN is trained with the dataset formed by merging 80% of the datasets of each load, and for the latter, separate approach, each DNN uses the corresponding load 80% dataset for training. For a fair AUC ROC comparison, both approaches are tested using the remaining 20% unseen test samples of the individual load datasets. Table 6.3 shows the corresponding results, which show that the separate DNN method obtains higher AUC ROCs for all loads tested. Hence, in the next sections, a custom-trained DNN is used for ML integration into RMSCA at each load.

6.5 DNN and RF-enabled RMSCA Algorithm

The proposed RMSCA algorithm is given in Algorithm 6.1. The algorithm begins by computing the K shortest paths for the given source and destination. The modulation formats are chosen starting from the most spectrally efficient one from

Table 6.3: Comparison of AUC ROC Obtained with Single DNN vs. Separate DNNs for Two Dataset Sizes Using the Adam Optimizer

	$R = 10,000$		$R = 100,000$	
Load	**Single DNN**	**Separate DNNs**	**Single DNN**	**Separate DNNs**
200	0.981	**0.987**	0.979	**0.982**
300	0.975	**0.981**	0.966	**0.974**
400	0.964	**0.973**	0.958	**0.963**
500	0.956	**0.965**	0.947	**0.953**
600	0.943	**0.952**	0.932	**0.941**

the set M (defined in Section 6.4). Using the K shortest paths and the set of cores C of the links, Algorithm 6.2 is invoked to find the $K \times |C|$ ranked path-core combinations. These are used in the second loop of Algorithm 6.1 (Line 6) for subsequent spectrum assignment. All spectrum blocks of the size required for the data rate and modulation format selected that obey the continuity and contiguity constraints of the EONs are considered candidate blocks in the innermost loop.

In Algorithm 6.2, for each of the $K \times |C|$ candidates, the input feature vector is formed from the dynamic network state as described in Section 6.4. The trained DNN model is used to predict the suitability and outputs a real value between 0 and 1. These predictions are stored if they satisfy the threshold V_{th} (obtained for the trained DNN at that network load), resulting in a classifier decision of "1". They are then sorted in ascending order to sort the candidates from the most viable route-core pair to the least viable one for use in the remainder of Algorithm 6.1.

The spectrum assignment loop (Step 8 of Algorithm 6.1) finds a spectral block that satisfies the QoT conditions on the particular route-core-modulation combination being considered. The RF link noise estimator of Algorithm 6.3 is invoked at this point to estimate the denominator of Eq. (5.5) and to perform the QoT check on the candidate route, core, and spectrum block found using Algorithm 6.2 and a first fit spectrum selection approach. The network topology information, the associated parameters, and the spectrum block are provided as the input to form a feature vector as described in Section 6.4. The algorithm returns a positive response ("QoT satisfied") if the threshold in Eq. (5.5) is met and the proposed demand provisioning causes no unduly degradation to in-service lightpaths. Hence, the loop at line 8 of Algorithm 6.1 continues until a QoT-satisfying block is found.

The DNN enables the RMSCA scheme to capture the hidden nonlinear re-

Algorithm 6.1 Proposed DNN enabled RMSCA algorithm

procedure RMSCA(Source, destination, requested bandwidth)
    Find K shortest paths from source to destination
    while viable resource allocation not found **do**
        Choose the next most spectral-efficient modulation format $m \in M$
        Run DNN_route_core procedure (Algorithm 6.2) to get ranked route-core candidates
        while viable spectrum block not found on ranked route-core candidate **do**
            Create a list of candidate spectrum blocks satisfying the continuity and contiguity constraints on that route-core combination
            while candidate block in the list does not satisfy QoT constraints **do**
                Check the QoT constraint using Algorithm 6.3
                if Algorithm 6.3 returns satisfied **then**
                    selected spectrum block = candidate block
                else check next spectrum block
                end if
            end while
        end while
    end while
    return current route, core, and selected spectrum block to provision the request
end procedure

Algorithm 6.2 Path and core selection using DNN classifier

procedure DNN_ROUTE_CORE(Network topology, K shortest paths, set of cores C, network state)
    for each candidate in set of $K \times |C|$ candidates **do**
        Form the feature vector using values stated in Section 6.4
        Predict the candidate's suitability using the trained DNN model of the corresponding traffic load
        if prediction $\leq V_{\text{th}}$ **then**
            Store the prediction
        end if
    end for
    Sort the predictions in ascending order and rearrange the corresponding $K \times |C|$ candidates
    return ranked $K \times |C|$ candidates
end procedure

lations using the selected features, which a straightforward scoring scheme may not be able to learn. By considering all the possible candidates, the DNN scheme

Algorithm 6.3 QoT checking using RF link noise estimator

```
1: procedure RF_NOISE_ESTIMATOR(Candidate spectrum block, Network topology, Link parameters)
2:     for each link e of the candidate path do
3:         Form the feature vector as described in Section 6.4
4:         Estimate the link noise using the trained RF model, which results in an estimate of [Eqns. (3.2) + (3.5) + (5.2)]
5:     end for
6:     Compute Eq. (5.4) using the estimated link noises.
7:     if QoT is satisfied (Eq. (5.5)) and existing lightpaths not degraded then
8:         return QoT satisfied
9:     else return QoT not satisfied
10:    end if
11: end procedure
```

helps to select the best candidate. Note that the selection of a candidate is kept limited to the route and core but not the spectrum. This is because there is a large number of spectral candidate blocks compared to the $K \times |C|$ route-core candidates.

6.6 Results and Analysis

This section analyzes the performance of the DNN training algorithm, feature selection procedure, and the RMSCA algorithm.

6.6.1 DNN Classifier Model Results

The performance of the trained DNNs is tested using 20% unseen test data reserved for testing. Fig. 6.3 shows the difference between the actual AUC ROC observed from simulations and the ideal AUC ROC = 1.0 for each DNN trained at different loads using the Adam or Jaya algorithms. The Jaya-trained DNNs are closer to an ideal classifier at all loads than the Adam-trained DNNs. Hence, the Jaya-trained classifiers would perform better in practice when unseen EON data is input to the DNN. This performance is because the Jaya algorithm can minimize the binary cross entropy loss better than Adam, and the resulting weights and biases provide comparatively better classification capability at each load.

Fig. 6.3 presumes that the operational network load is one of the loads the DNN was trained for. It is thus worthwhile to investigate its robustness when

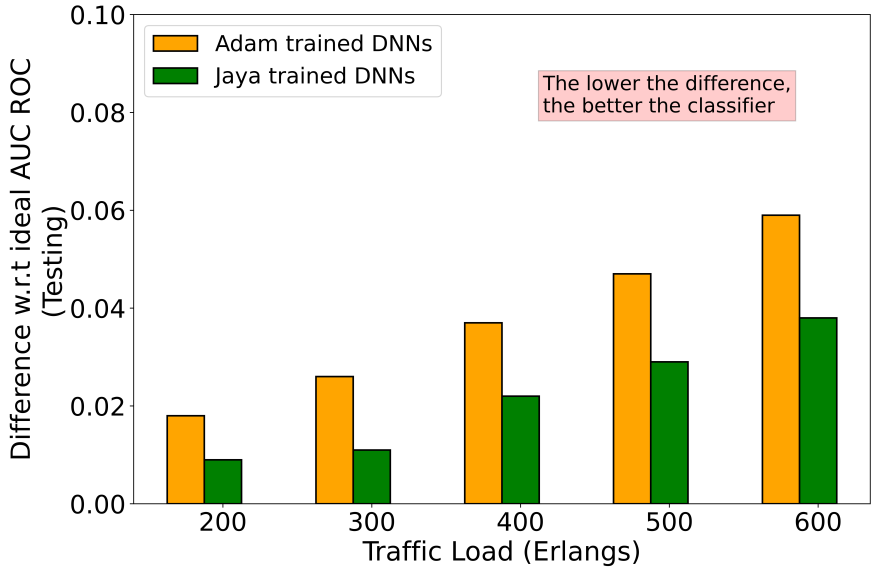

Figure 6.3: Difference between simulated AUC ROC and the ideal AUC ROC = 1.0 using Adam vs. Jaya-trained DNNs in a 7-core NSFNET

Table 6.4: Test AUC ROC for Untrained Loads Using Adam vs. Jaya-trained DNNs in a 7-core NSFNET

Actual Load	**Trained Load**	**AUC ROC for Adam**	**AUC ROC for Jaya**
350	300	0.910	0.910
	400	0.924	**0.936**
525	500	0.888	0.902
	600	0.892	**0.911**

this assumption is violated. Table 6.4 shows the AUC ROCs when the actual network load is 350 and 525 Erlangs. For both loads, DNNs trained on a higher load, i.e., 400 and 600, respectively, performed better than the DNN trained at 300 and 500 Erlangs. The lower AUC ROC values at the lower assumed loads can be attributed to an underprediction of QoT failures for loads 350 and 525 Erlangs. Similar reasoning follows for the Jaya-trained DNNs; these (shown in boldface in the table) again perform better than the Adam-trained ones at 400 and 600 Erlangs.

Considering the prediction quality enhancement obtained by using the Jaya-trained DNNs, these DNNs are chosen to test the RMSCA performance in all remaining results in this chapter.

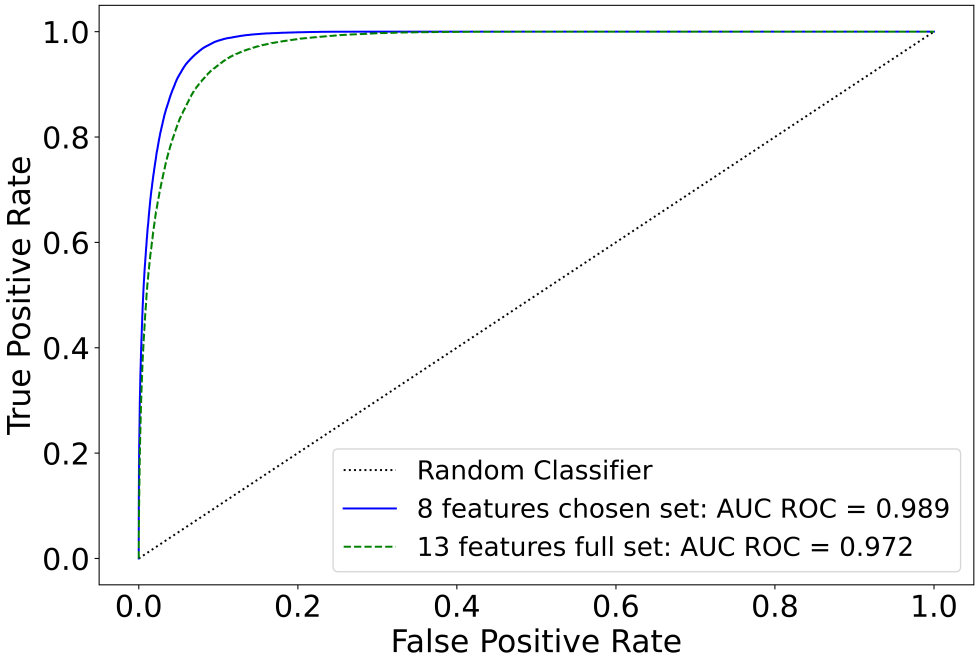

Figure 6.4: DNN classifier performance when using the full 13 features vs. the chosen 8 features at a load of 300 Erlangs for the 7-core NSFNET

6.6.2 Feature Selection Analysis

The RF noise estimator and the DNN classifier use the features stated in Section 6.4. These were determined as the best features by cross-validation using RFE to determine the best subset of features automatically to ensure model generalizability instead of manual selection.

For the RF, the entire set of possible features included the features stated in Section 6.4 alongside traffic load, the source, the destination of the request, data rate requirement, core fragmentation, link number, modulation format of the immediate right spectral neighbor, and spectral occupancy on right side of the candidate block. The twelve features listed in Section 6.4 resulted in the lowest RMSE for the RF estimator compared with using any other subset of possible features tested. For the DNN classifier, the additional features considered other than those listed in Section 6.4 are traffic load, the source, the destination of the request, data rate requirement, maximum link length, and the number of traversed links. For the DNN, the final set of features gives the highest AUC ROC; Fig. 6.4 shows how the prediction capability of the classifier is reduced when considering the additional features.

6.6.3 ML-enabled RMSCA Results

The proposed RMSCA algorithm described in Section 6.5 is tested on three network topologies (Chapter 2): the (11 node, 52 link) COST-239, the (24 node, 43 link) USNET, both using a 7-core MCF on each link, and the (14 node, 21 link) NSFNET using 12-core links to check the robustness of the algorithms. This work assumes a 4 THz optical spectrum per core for all networks. Each frequency slot in each core supports 12.5 GHz transmission.

For the simulation, 100,000 traffic demands are generated at 200 to 600 Erlangs loads and with data rates uniformly distributed in [50, 400] Gbps. Spectrally efficient modulation formats subjected to QoT constraint are selected from $M = \{$32-QAM, 16-QAM, 8-QAM, QPSK, BPSK$\}$; the threshold SNRs are adopted from [109]. The algorithm's effectiveness is measured by calculating the BP, BBP, and request AST, as described in Section 6.3.

The performance of the proposed algorithm is compared with the standard KSP with FC core selection and FF spectrum selection and a published algorithm described in [81]. In this section, KSP_All_PLI refers to the conventional KSP run on a network subjected to all impairments, (XT, ASE and NLI), for a fair comparison with the proposed algorithm. KSP_XT refers to the KSP considering the network is only affected by XT [81]. ICXT_Aware_XT refers to the ICXT-aware algorithm from [81] applied to a network only affected by XT. ICXT_Aware_All_PLI refers to the ICXT-aware algorithm from [81] but assuming the network is subjected to the additional ASE and NLI impairments. Both ICXT_Aware_XT and ICXT_Aware_All_PLI algorithms utilize core priorities and spectrum partitioning strategies as used in [81]. In all results, the DNN approach refers to the use of a load-specific trained DNN model for path-core selection, resulting in $K \times |C|$ sorted candidates to start the spectrum search from the best candidate, as described in Algorithm 6.2. The KSP_All_PLI and DNN approaches are subjected to two methods of estimating the QoT: the GN QoT model described in Section 6.5 and an ML-noise estimator based on a trained RF model to approximate the link noise in Eq. (5.5) described in Section 6.4.

In analyzing the XT effects on in-service requests, as described in Chapter 5, a dynamic neighbor and precise request-by-request SNR threshold comparison is used, which differs from the approach in [81]. In [81], an XT awareness model is adopted with complexity greater than that of passive avoidance and yet less than a dynamic neighbor and precise checking approach, which leads to higher blocking [77]. Hence, high levels of blocking in [81] are observed at very high load

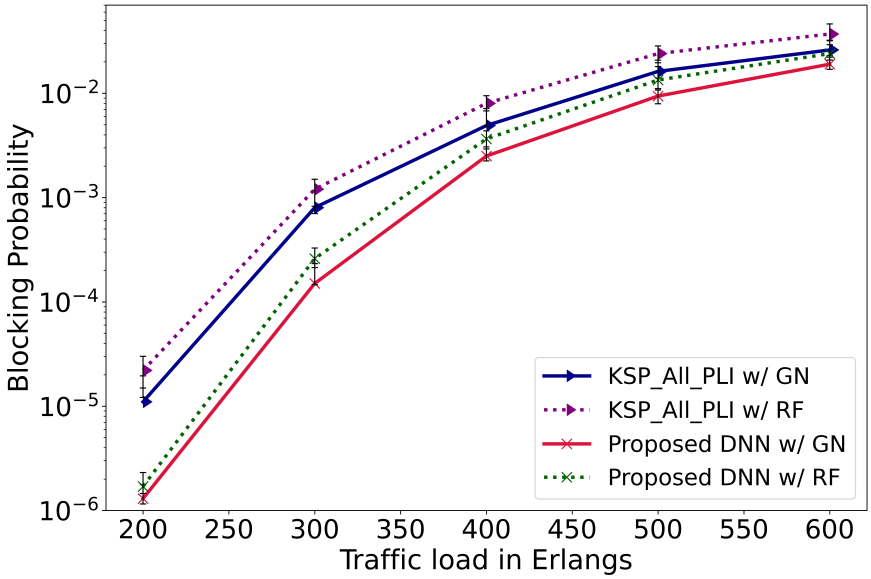

Figure 6.5: Blocking probabilities for the KSP and DNN approaches with GN-based vs. RF-based noise estimation for the 7-core USNET

levels.

Performance Analysis, 7 and 12-core MCF: Blocking Probability

The RMSCA algorithm is first analyzed by applying it to EONs using 7-core MCFs. Figs. 6.5 and 6.6 compare the BP obtained using the benchmark KSP and DNN-enabled path-core selection, both under FF spectrum allocation, on the USNET and COST-239 topologies, respectively. In Fig. 6.5, a 95% confidence interval is drawn as error bars around each mean value over 5 trials – these are similar for other figures but omitted for clarity.

The results in Fig. 6.5 show that the DNN approach obtained a lower BP than the conventional KSP, an average of 57% lower, indicating that the proposed DNN model's ability to accurately predict the lightpath suitability helps in selecting the best path-core candidates. In both KSP and DNN schemes, the blocking obtained using the RF QoT estimator is slightly higher than when using the GN QoT estimator. This is expected since the trained RF model can approximate the link noise with lower accuracy compared with the analytical GN model. However, the tradeoff is in the computational time, as explained below in Section 6.6.3.

Similar observations can be drawn from the blocking behavior in the COST-239 network shown in Fig. 6.6. However, a closer glance reveals that the performance difference between the RF and GN based allocation is slightly less than

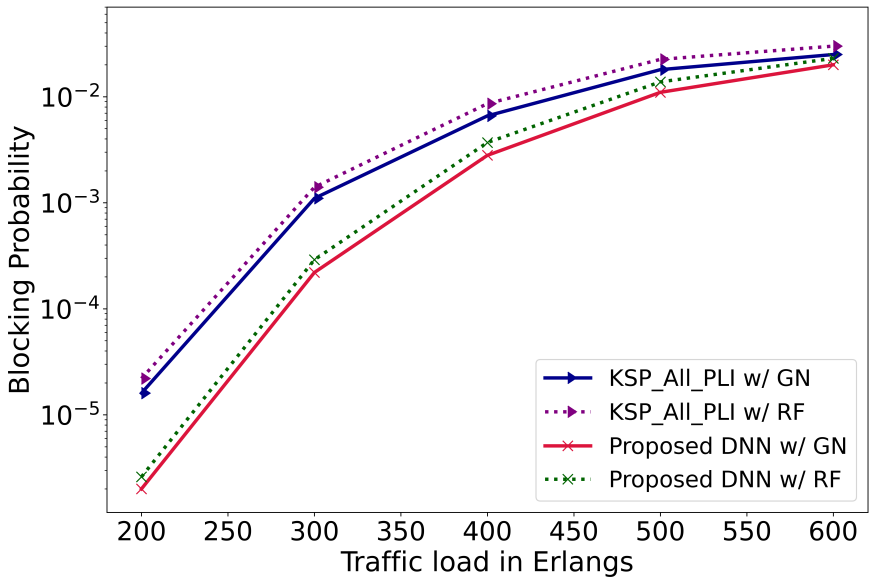

Figure 6.6: Blocking probabilities for the KSP and DNN approaches with GN-based vs. RF-based noise estimation for the 7-core COST-239

in Fig. 6.5. This behavior indicates that the optical network dimensions impact the RF model performance, especially at higher loads.

Fig. 6.7 compares the BP among KSP_All_PLI, KSP_XT, ICXT_Aware_All_PLI, ICXT_Aware_XT, and the DNN approach. The all-impairment versions obtain higher blocking than their XT only counterparts, almost 65% on average. This indicates that the effect of ASE and NLI noises on the blocking performance of a MCF network over the XT impairment is significant and highlights how important it is to consider all impairments in MCF networking algorithms. Between the KSP_All_PLI and ICXT_Aware_All_PLI algorithms, the latter maintained lower blocking only at low loads, with the BP approaching the former at higher loads. This is because the core grouping and spectrum divisions of the ICXT_Aware algorithm are only effective in the initial provisioning stages; when the traffic level increases, all the non-crosstalk groups are fully loaded, and the performance is limited. This behavior is observed in the case of KSP_XT and ICXT_Aware_XT as well [81]. However, the larger gap between their blocking performance in comparison to the KSP_All_PLI and ICXT_Aware_All_PLI is due to the careful design of the ICXT_Aware_XT algorithm to minimize the effects of XT. In the all-impairment versions, the other PLIs dominate, making it difficult to benefit from the improvement offered by the ICXT design.

Fig. 6.7 also shows that the proposed DNN w/ GN approach lowers the BP

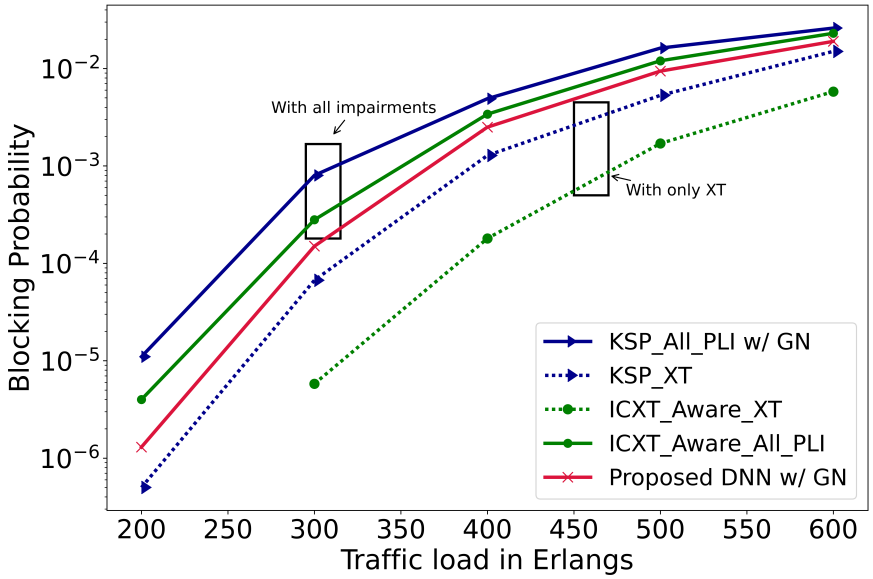

Figure 6.7: Blocking probabilities for the KSP_All_PLI, KSP_XT [81], ICXT_Aware_All_PLI, ICXT_Aware_XT [81], and DNN approaches for the 7-core USNET

by 57% and 35.8% on average compared with the KSP_All_PLI w/ GN and ICXT_Aware_All_PLI, respectively. A direct comparison cannot be made between the ICXT_Aware_XT approach and the DNN w/ classifier since the former is designed to focus on XT alone.

To check the applicability and performance of the proposed model for networks using a larger number of cores, Fig. 6.8 compares the BP using the KSP and DNN approaches with RF vs. GN QoT models in the 14-node NSFNET topology with 12-core MCF links. The same conclusions can be drawn regarding the relative performance of the approaches as for the 7-core MCF. However, the BP in the 12-core case is lower than in the 7-core case due to increased core availability and lower XT from a smaller number of adjacent neighbors. The DNN approach with the GN model outperforms all others due to its ability to find better-scored route-core candidates in the interest of the provisioned request and because it uses the benchmark QoT model. Also, despite the RF QoT estimator providing a slightly higher blocking than the GN model in general (35% on average), its combination with the DNN approach still performs well, and the blocking does not exceed that of the KSP based on GN QoT estimation.

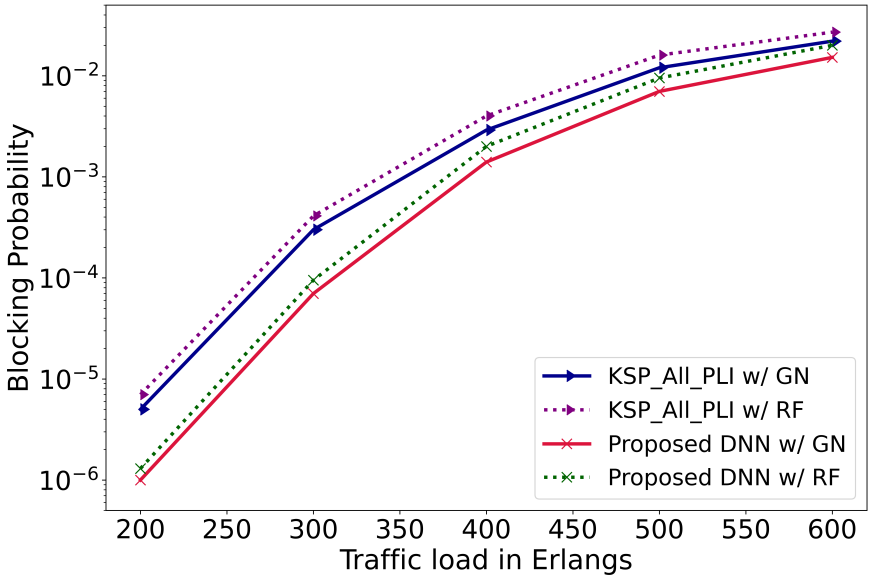

Figure 6.8: Blocking probabilities for the KSP and DNN approaches with GN-based vs. RF-based noise estimation for the 12-core NSFNET

Performance Analysis, 7 and 12-core MCF: Bandwidth Blocking Probability

Since SDM-EONs are expected to carry highly heterogeneous data, an analysis of the BBP gives better insight into the network performance than the BP metric that treats all requests equally irrespective of their size [7]. Fig. 6.9 shows the BBP for the benchmark KSP_All_PLI, the proposed DNN approach, and their QoT estimation variants. Results show that the DNN w/ GN approach obtains the lowest BBP among the four algorithms, with an average of 53.8% decrease and one order of magnitude at lower loads, in comparison to the KSP_All_PLI scheme. The DNN method considers features such as the required slots and the number of blocks that satisfy the continuity and contiguity constraints, which help it predict well the lightpath suitability even for higher data rate requests. Similar to the BP analysis, the DNN and KSP that use the RF QoT estimator results in lightly higher BBP at higher loads than their GN counterparts. Similar results are observed for the COST-239 network topology, as shown in Fig. 6.10.

Fig. 6.11 shows the BBP performance of the DNN w/ GN alongside the KSP_All_PLI, KSP_XT [81], ICXT_Aware_All_PLI, and ICXT_Aware_XT [81]. Similar to the performance of BP, the all-impairment variants obtain a higher BBP than their XT only counterparts. The NLI and ASE effects have pushed the blocking up compared to a network affected by XT alone. The lack of available

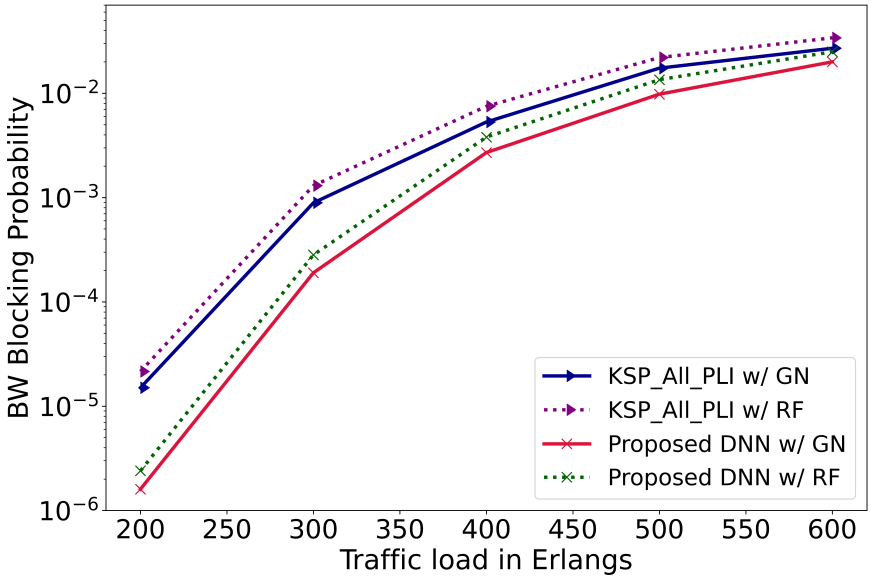

Figure 6.9: Bandwidth blocking probabilities for the KSP and DNN approaches with GN-based vs. RF-based noise estimation for the 7-core USNET

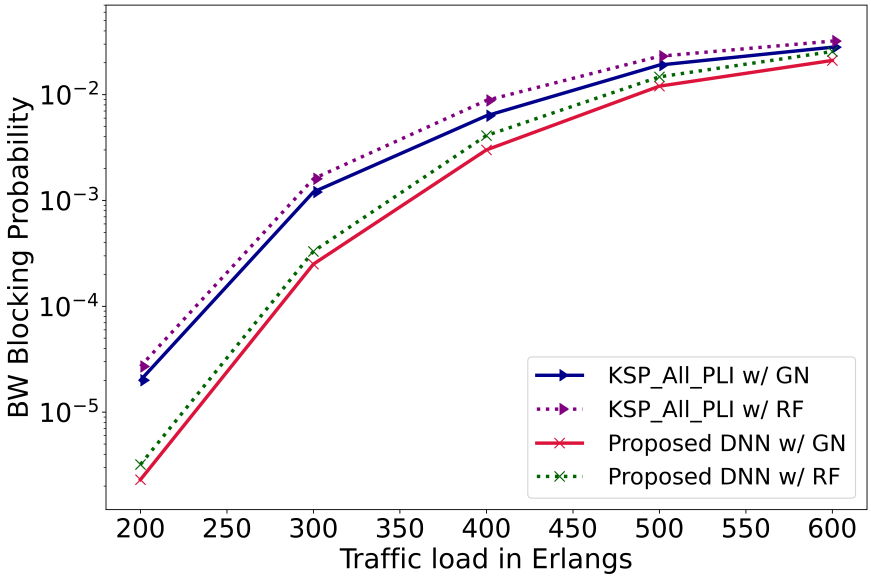

Figure 6.10: Bandwidth blocking probabilities for the KSP and DNN approaches with GN-based vs. RF-based noise estimation for the 7-core COST-239

continuous and contiguous spectrum can contribute to request blocking. However, comparing the KSP_All_PLI with KSP_XT and ICXT_Aware_All_PLI with ICXT_Aware_XT, on average seven times more failures are caused by the PLI in the former combination, as spectrum failures will be same in among the pairs.

Fig. 6.11 also shows that the ICXT_Aware_All_PLI maintained its superior

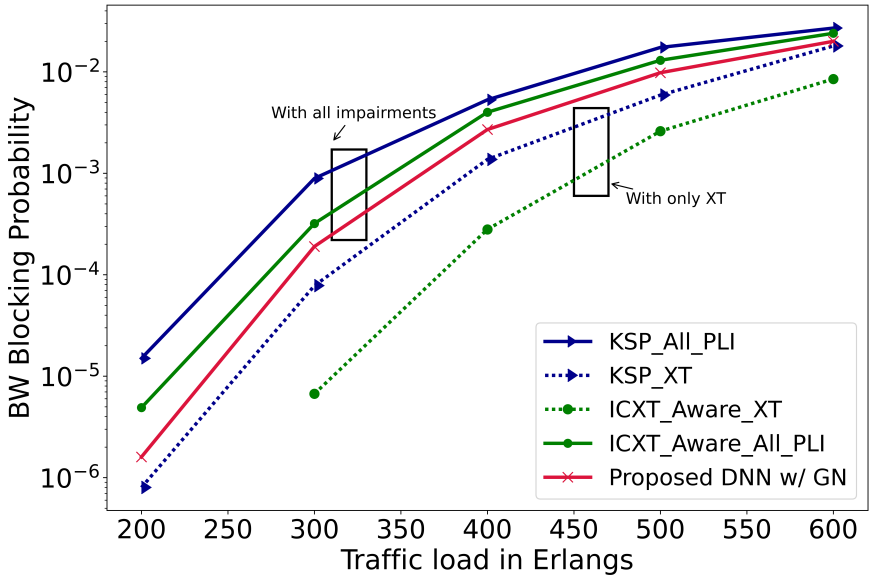

Figure 6.11: Bandwidth blocking probabilities for the KSP_All_PLI, KSP_XT [81], ICXT_Aware_XT [48], ICXT_Aware_All_PLI, and DNN approaches for the 7-core USNET

performance over KSP_All_PLI at low loads; the core grouping and spectrum divisioning approach was insufficient for it to avoid high bandwidth blocking at higher loads. This BBP behavior is observed in the case of KSP_XT and ICXT_Aware_XT as well [81]. The proposed DNN approach lowers the BBP by an average $\sim$ 1.5 times that of the KSP_All_PLI and ICXT_Aware_All_PLI.

Performance Analysis, 7 and 12-core MCF: Request Setup Time

Table 6.5 shows the AST for the KSP and DNN approaches under a FF spectrum assignment at different loads using GN and RF QoT models.[1] The simulation assumes all impairments are included.

The DNN takes a longer time to provision a request than the KSP scheme at all loads tested. This is because the former needs to collect the features of all the $K \times |C|$ candidate paths. It is not shown in the table but it was observed that, since the computations can be performed in parallel, the AST does not scale linearly with K and $|C|$. There is a tradeoff between achieving better network performance and taking longer to do so that depends on K and $|C|$. Between the GN and RF QoT estimation schemes, the former takes $\sim$1.7 and $\sim$1.75 times more computation time than the latter in the DNN and KSP

[1]The computations were performed on a Intel(R) Xeon(R) CPU E5-2630 v3 @ 2.40GHz machine.

Table 6.5: Average Request CPU Setup Time (ms) for KSP and DNN Approaches at Different Loads Using a GN or RF QoT Estimator

	GN QoT		**RF QoT**	
Load	**DNN**	**KSP**	**DNN**	**KSP**
200	15.5	10.5	7.3	5.7
300	21.8	20.3	13.5	11.4
400	32.8	24.1	20.6	13.2
500	45.6	33.6	28.3	20.3
600	52.5	46.3	32.7	28.7

schemes, respectively. The RF QoT model is able to reduce the AST significantly, which is a promising aspect considering how QoT computations are needed for every spectral candidate block. The reduction is slightly less at higher loads owing to increased active spectral and adjacent core neighbors that add to the feature computation.

6.7 Chapter Summary

An impairment-aware ML-enabled RMSCA algorithm for C-band SDM-EONs is proposed in this chapter. A RF based link noise estimator is presented to reduce the computation time during the QoT checking phase. The present work considers the XT, Kerr nonlinear impairments such as SPM and XPM, and also the ASE noise encountered by the signal along the chosen network path. Novelty is introduced by using a new training algorithm, the Jaya algorithm, to obtain better predictive performance of the DNN compared to the widely used Adam algorithm. The trained DNN is applied to an RMSCA algorithm for the first time, over varying loads. From literature, it is concluded that, this is the first work that considers all impairments in SDM-EONs while applying ML methods to perform RMSCA. The simulations are performed on three network topologies, USNET, NSFNET, and COST-239, with 7 and 12 core MCF links, and the results of BP, bandwidth BP, and request setup time are analyzed. The novel use of scored DNN predictions to find the best route-core candidates performs significantly better than the conventional KSP benchmark for all loads tested, and the ML based noise estimation lowers the computation time to find a successful solution.

Chapter 7

Conclusions and Future Work

This chapter describes the contributions of this dissertation, summarizes the main conclusions, and presents some avenues of possible future work.

7.1 Summary and Conclusions

Elastic optical networks (EONs) have emerged as a promising backbone technology to combat the challenges posed by the exponential growth of communication demands. Using heuristic and machine learning techniques, this dissertation examines the resource provisioning issue for multi-band and multicore fiber EONs.

The enhancement of the optical capacity within contemporary single-core EON can be achieved through advancements in both spectral and spatial dimensions. Regarding spectral expansion, the utilization of supplementary frequency bands presents a logical progression beyond the existing C-band extension. However, the incremental capacity gains in this aspect are relatively modest compared to the spatial expansion achievable through space division multiplexed (SDM) EON. The selection between multi-band and multicore approaches is contingent upon the projected network traffic volumes and the associated capital and operational expenditures. Nevertheless, there is a discernible trend towards adopting SDM capability via multicore fibers. Either multi-band or multicore, efficient optical network resource allocation for any request subjected to certain constraints has been the subject of extensive research. Different algorithms are used for routing, modulation, spectrum, and core (if multicore) allocation to improve traffic acceptance. Consequently, the dissertation work's contributions are mainly divided into four parts:

1. In light of the dynamic network status, a Q-learning (reinforcement learning) based routing selection for C+L band multi-band networks is proposed. Considerations include the L-band specific ISRS effect, Kerr nonlinear impairments like SPM and XPM, and the ASE noise the signal encountered along the selected network path. It is observed that utilizing state-dependent routing decisions helps improve traffic acceptance, and the proposed method obtains lower blocking than the conventionally used K-shortest paths approach. The algorithm is motivated to find routes with higher acceptability due to Q-learning's reward-based interactions. Utilizing custom rewards as a function of network characteristics such as fragmentation and PLI helps to find paths that would have been dismissed under K-shortest path routing. To the best of our knowledge, this is the first time that the Q-learning method has been used for online RMSA for C+L band EONs. Since Q-learning routing outperformed the K-shortest path method under different spectrum allocation methods, network operators can readily employ the straightforward Q-learning for routing in software-defined EON scenarios.

2. The resource allocation in the next higher capacity increase solution, MCF enabled EONs, is explored after the multi-band method. A gap in addressing impairments and the preferential treatment to XT alone in the PLI-aware networking literature of MCF EONs, especially with dynamic traffic, is noted. Hence, the effects of various impairments in a dynamic multicore fiber provisioning system for C-band are briefly investigated. Our results show that NLI and ASE contribute to failures by around $\sim 58\%$ compared to XT contributing $\sim 21\%$ and a noticeable contribution by a combination of these three (but insufficient to cause a failure on their own). It is observed that at multiple time instants over the operational lifetime of USNET and COST-239 network, a large majority of the links are more affected by ASE than XT. At low loads (at two different launch powers), XT is stronger than NLI on only $\sim 1/3\%$ of the links but showing presence in $\sim 1/2\%$ of the links as the load increases. Over two networks and two power levels, it is observed that the impact of XPM, SPM, and ASE noises averagely accounts for $\sim 30\%$ to $\sim 60\%$ of QoT failures compared to $\sim 20\%$ XT-induced failures. These can cause signal degradation that can go unnoticed if the dynamic resource allocation schemes only consider XT.

3. Incorporating all the MCF impairments, a novel RMSCA scheme is proposed via a new spectrum assignment and a multi-attribute decision-making MADM-based route and core selection mechanisms. The PROMETHEE and AHP approaches are combined to create the MADM method to rank the candidate routes and cores based on pertinent optical network characteristics. Energy consumption and fragmentation-reducing capability are incorporated into the spectrum selection phase. The results of the simulations are analyzed in terms of blocking probability, bandwidth blocking probability, network fragmentation, and energy usage. For every evaluated situation in NSFNET and COST-239, the innovative combination of scoring function spectrum assignment and MADM routing outperformed the traditional, published benchmarks by a wide margin over reasonable ranges of traffic loads. To the best of our knowledge, at the time of publication, this is the first study to take into account all impairments in SDM-EONs while also taking fragmentation and energy awareness into account.

4. An impairment aware RMSCA scheme utilizing deep neural networks is proposed to assess candidate resources' suitability for allocation. In addition, a random forest algorithm (ML algorithm) is used to estimate link noises, which expedites the process of verifying the QoT constraint when compared to the analytic Gaussian Noise (GN) model. Novelty is also introduced by employing a training method, the Jaya algorithm, to achieve improved predictive performance of the DNNs compared to the widely used Adam algorithm. The blocking and bandwidth blocking performance are analyzed with USNET and COST-239 networks with 7 and 12-core links over varying loads. Our results show that the blocking performance is improved by around $\sim 53\%$ when using scored DNN predictions to identify the best route-core candidates over the traditional KSP with the first core allocation policy. The GN QoT assisted allocation results in a slightly lower blocking than the RF-estimated QoT counterparts but also takes around ~ 1.75 times more computational time (measured in CPU time) indicating that the ML-based noise estimates reduce the computation time required to find a successful solution.

The proposed algorithms are evaluated, and their performance is compared with standard and published algorithms. The research work in this dissertation uses heuristic and machine learning techniques to conduct a thorough analysis

of resource provisioning algorithms for multi-band and multicore fiber networks. The proposed methods are straightforward, useful, and simple for network operators.

7.2 Future Work

As part of future work, additional link information may be incorporated in the state representation of reinforcement learning to make the routing more adaptive while crafting better reward functions. Comparing the proposed Q-learning with other routing approaches and extending it to spectrum allocation is also a fascinating subject of research.

For future work, more network metrics may be incorporated into the MADM attributes. Accordingly, the alternatives can be made diverse to make the final selection relevant to the network goal to be optimized. Reducing the number of alternatives may also be tried, but in a way that can still positively affect the network status upon being selected by the MADM method.

Autonomic EON operation may be tried using a software-defined network controller. Deep reinforcement learning may be used, and the whole resource allocation may be involved in the learning process. Various network objectives may be fulfilled by using multi-agent RL, where each agent can cater to a specific aim, such as reducing blocking probability, reducing fragmentation, minimizing power cost, etc. A DNN may be used to implement the DRL models.

List of Publications

1. Ravipudi, J. L., & Brandt-Pearce, M. (2023). Impairment-and fragmentation-aware dynamic routing, modulation and spectrum allocation in C+ L band elastic optical networks using Q-learning. Optical Switching and Networking, 47, 100717.

2. Ravipudi, J. L., & Brandt-Pearce, M. (2022, October). A Score Function Heuristic for Crosstalk-and Fragmentation-Aware Dynamic Routing, Modulation, Core, and Spectrum Allocation in SDM-EONs. In 2022 IEEE Future Networks World Forum (FNWF) (pp. 83-87). IEEE.

3. Ravipudi, J. L., & Brandt-Pearce, M. (2023). Impairment-and fragmentation-aware, energy-efficient dynamic RMSCA for SDM-EONs. Journal of Optical Communications and Networking, 15(9), D10-D22.

4. Ravipudi, J. L., & Brandt-Pearce, M. (2023, November). Machine Learning Based Lightpath Classifier for Impairment Aware Resource Allocation in SDM-EONs. In 2023 IEEE Future Networks World Forum (FNWF). IEEE.

5. Ravipudi, J. L., & Brandt-Pearce, M..Does Considering Only Crosstalk Suffice for QoT-Aware Provisioning in Multicore Fiber Networks?. In 2024 IEEE Optical Network Design and Modeling (ONDM). IEEE.

Papers under editorial review

6. Ravipudi, J. L., & Brandt-Pearce, M. .Machine Learning Based Impairment-Aware Dynamic RMSCA in Multi-core Elastic Optical Networks. Journal of Optical Communications and Networking.

Bibliography

[1] Cisco, "Cisco Annual Internet Report (2018–2023) White paper," *Online (accessed March 26, 2021) https://www. cisco. com/c/en/us/solutions/collateral/executive-perspectives/annual-internet-report/whitepaper-c11-741490. html*, 2020.

[2] "Mobile data traffic outlook," https://www.ericsson.com/en/reports-and-papers/mobility-report/dataforecasts/mobile-traffic-forecast, accessed: 2024-01-18.

[3] M. Jinno, "Elastic optical networking: roles and benefits in beyond 100-gb/s era," *Journal of Lightwave Technology*, vol. 35, no. 5, pp. 1116–1124, 2016.

[4] B. Chatterjee and E. Oki, *Elastic optical networks: fundamentals, design, control, and management*. CRC Press, 2020.

[5] O. Gerstel, M. Jinno, A. Lord, and S. B. Yoo, "Elastic optical networking: A new dawn for the optical layer?" *IEEE communications Magazine*, vol. 50, no. 2, pp. s12–s20, 2012.

[6] D. Adhikari, D. Datta, and R. Datta, "Impact of BER in fragmentation-aware routing and spectrum assignment in elastic optical networks," *Computer Networks*, vol. 172, p. 107167, 2020.

[7] Í. Brasileiro, L. Costa, and A. Drummond, "A survey on challenges of spatial division multiplexing enabled elastic optical networks," *Optical Switching and Networking*, vol. 38, p. 100584, 2020.

[8] B. C. Chatterjee, N. Sarma, and E. Oki, "Routing and spectrum allocation in elastic optical networks: A tutorial," *IEEE Communications Surveys & Tutorials*, vol. 17, no. 3, pp. 1776–1800, 2015.

[9] Y. Zhang, J. Xin, X. Li, and S. Huang, "Overview on routing and resource allocation based machine learning in optical networks," *Optical Fiber Technology*, vol. 60, p. 102355, 2020.

[10] P. Poggiolini, "The GN model of non-linear propagation in uncompensated coherent optical systems," *Journal of Lightwave Technology*, vol. 30, no. 24, pp. 3857–3879, 2012.

[11] S. Allogba, S. Aladin, and C. Tremblay, "Machine-learning-based lightpath QoT estimation and forecasting," *Journal of Lightwave Technology*, vol. 40, no. 10, pp. 3115–3127, 2022.

[12] F. S. Abkenar and A. G. Rahbar, "Study and analysis of routing and spectrum allocation (RSA) and routing, modulation and spectrum allocation (RMSA) algorithms in elastic optical networks (EONs)," *Optical Switching and Networking*, vol. 23, pp. 5–39, 2017.

[13] R. Ramaswami and K. N. Sivarajan, "Routing and wavelength assignment in all-optical networks," *IEEE/ACM Transactions on networking*, vol. 3, no. 5, pp. 489–500, 1995.

[14] X. Yang and B. Ramamurthy, "Sparse regeneration in translucent wavelength-routed optical networks: architecture, network design and wavelength routing," *Photonic network communications*, vol. 10, no. 1, pp. 39–53, 2005.

[15] K. Christodoulopoulos and E. Varvarigos, "Routing and spectrum allocation policies for time-varying traffic in flexible optical networks," in *2012 16th International Conference on Optical Network Design and Modelling (ONDM)*. IEEE, 2012, pp. 1–6.

[16] P. Johannisson and E. Agrell, "Modeling of nonlinear signal distortion in fiber-optic networks," *Journal of Lightwave Technology*, vol. 32, no. 23, pp. 4544–4552, 2014.

[17] P. Poggiolini, G. Bosco, A. Carena, V. Curri, Y. Jiang, and F. Forghieri, "A simple and effective closed-form GN model correction formula accounting for signal non-gaussian distribution," *Journal of Lightwave Technology*, vol. 33, no. 2, pp. 459–473, 2015.

[18] A. Carena, G. Bosco, V. Curri, Y. Jiang, P. Poggiolini, and F. Forghieri, "EGN model of non-linear fiber propagation," *Optics express*, vol. 22, no. 13, pp. 16 335–16 362, 2014.

[19] D. Semrau, R. I. Killey, and P. Bayvel, "The Gaussian noise model in the presence of inter-channel stimulated raman scattering," *Journal of Lightwave Technology*, vol. 36, no. 14, pp. 3046–3055, 2018.

[20] X. Wang, M. Brandt-Pearce, and S. Subramaniam, "Impact of wavelength and modulation conversion on translucent elastic optical networks using MILP," *Journal of Optical Communications and Networking*, vol. 7, no. 7, pp. 644–655, 2015.

[21] M. Mehrabi, H. Beyranvand, and M. J. Emadi, "Multi-band elastic optical networks: inter-channel stimulated Raman scattering-aware routing, modulation level and spectrum assignment," *Journal of Lightwave Technology*, vol. 39, no. 11, pp. 3360–3370, 2021.

[22] L. Xu, Y.-C. Huang, Y. Xue, and X. Hu, "Hierarchical reinforcement learning in multi-domain elastic optical networks to realize joint RMSA," *Journal of Lightwave Technology*, 2023.

[23] F. Tang, G. Shen, and G. N. Rouskas, "Crosstalk-aware shared backup path protection in multi-core fiber elastic optical networks," *Journal of Lightwave Technology*, vol. 39, no. 10, pp. 3025–3036, 2021.

[24] X. Chen, B. Li, R. Proietti, H. Lu, Z. Zhu, and S. B. Yoo, "DeepRMSA: A deep reinforcement learning framework for routing, modulation and spectrum assignment in elastic optical networks," *Journal of Lightwave Technology*, vol. 37, no. 16, pp. 4155–4163, 2019.

[25] M. A. Amirabadi, M. H. Kahaei, S. A. Nezamalhosseini, F. Arpanaei, and A. Carena, "Deep neural network-based QoT estimation for SMF and FMF links," *Journal of Lightwave Technology*, vol. 41, no. 6, pp. 1684–1695, 2022.

[26] J. Yu, B. Cheng, C. Hang, Y. Hu, S. Liu, Y. Wang, and J. Shen, "A deep learning based RSA strategy for elastic optical networks," in *2019 18th International Conference on Optical Communications and Networks (ICOCN)*. IEEE, 2019, pp. 1–3.

[27] A. Mitra, D. Semrau, N. Gahlawat, A. Srivastava, P. Bayvel, and A. Lord, "Effect of channel launch power on fill margin in C+L band elastic optical networks," *Journal of Lightwave Technology*, vol. 38, no. 5, pp. 1032–1040, 2019.

[28] Sadeghi, Rasoul and Correia, Bruno and Souza, André and Costa, Nelson and Pedro, João and Napoli, Antonio and Curri, Vittorio, "Transparent vs translucent multi-band optical networking: capacity and energy analyses," *Journal of Lightwave Technology*, vol. 40, no. 11, pp. 3486–3498, 2022.

[29] J. L. Ravipudi and M. Brandt-Pearce, "Impairment-and fragmentation-aware dynamic routing, modulation and spectrum allocation in C+L band elastic optical networks using Q-learning," *Optical Switching and Networking*, vol. 47, p. 100717, 2023.

[30] J. L. Ravipudi and Brandt-Pearce, "Impairment-and fragmentation-aware, energy-efficient dynamic RMSCA for SDM-EONs," *Journal of Optical Communications and Networking*, vol. 15, no. 9, pp. D10–D22, 2023.

[31] F. A. Al-Zahrani, "Estimating the survivability impact of multi-fiber wavelength-division multiplexing networks," *IEEE Access*, vol. 8, pp. 202 387–202 400, 2020.

[32] Y. Xu, H. Xing, B. Chen, and M. Brandt-Pearce, "Throughput optimization in hybrid C-C+ L-band elastic optical networks enabled by hybrid modulation and wavelength/modulation conversion," *Journal of Optical Communications and Networking*, vol. 15, no. 11, pp. 900–912, 2023.

[33] P. Lechowicz, M. Tornatore, A. Włodarczyk, and K. Walkowiak, "Fragmentation metrics and fragmentation-aware algorithm for spectrally/spatially flexible optical networks," *Journal of Optical Communications and Networking*, vol. 12, no. 5, pp. 133–145, 2020.

[34] F.-J. Moreno-Muro, R. Rumipamba-Zambrano, P. Pavón-Marino, J. Perelló, J. M. Gené, and S. Spadaro, "Evaluation of core-continuity-constrained ROADMs for flex-grid/MCF optical networks," *Journal of Optical Communications and Networking*, vol. 9, no. 11, pp. 1041–1050, 2017.

[35] J. Wang, S. Chen, Q. Wu, Y. Tan, and M. Shigeno, "Solving the static resource-allocation problem in SDM-EONs via a node-type ILP model," *Sensors*, vol. 22, no. 24, p. 9710, 2022.

[36] J. Comellas, J. Perelló, J. Solé-Pareta, and G. Junyent, "Spatial partitioning for proactive spectrum fragmentation avoidance in flex-grid/SDM dynamic optical core networks," *Photonic Network Communications*, vol. 40, no. 2, pp. 59–67, 2020.

[37] M. Yang, Q. Wu, and Y. Zhang, "Joint assignment of spatial granularity, routing, modulation, and spectrum in SDM-EONs: minimizing the network CAPEX considering spectrum, WSS, and laser resources," *Journal of Lightwave Technology*, vol. 36, no. 18, pp. 4153–4166, 2018.

[38] M. Yang, Q. Wu, K. Guo, and Y. Zhang, "Evaluation of device cost, power consumption, and network performance in spatially and spectrally flexible sdm optical networks," *Journal of Lightwave Technology*, vol. 37, no. 20, pp. 5259–5272, 2019.

[39] G. Savva, K. Manousakis, J. Rak, I. Tomkos, and G. Ellinas, "High-power jamming attack mitigation techniques in spectrally-spatially flexible optical networks," *IEEE Access*, vol. 9, pp. 28 558–28 572, 2021.

[40] R. Goścień and K. Walkowiak, "On the efficiency of survivable flex-grid SDM networks," *Journal of Lightwave Technology*, vol. 36, no. 10, pp. 1815–1823, 2018.

[41] F. Tang, Y. Li, G. Shen, and G. N. Rouskas, "Minimizing inter-core crosstalk jointly in spatial, frequency, and time domains for scheduled lightpath demands in multi-core fiber-based elastic optical network," *Journal of Lightwave Technology*, vol. 38, no. 20, pp. 5595–5607, 2020.

[42] X. Yu, J. Wang, K. Zhang, J. Lv, Y. Zhao, K. Gao, X. Guo, and J. Zhang, "Brown-field migration aware routing and spectrum assignment in backbone optical networks," *Applied Sciences*, vol. 12, no. 1, p. 438, 2022.

[43] G. P. Agrawal, *Fiber-optic communication systems*. John Wiley & Sons, 2021, 5th ed.

[44] G. Saavedra, D. Semrau, M. Tan, A. Iqbal, D. J. Elson, L. Galdino, P. Harper, R. I. Killey, and P. Bayvel, "Inter-channel stimulated Raman

scattering and its impact in wideband transmission systems," in *2018 Optical Fiber Communications Conference and Exposition (OFC)*. IEEE, 2018, pp. 1–3.

[45] Y. Xu, E. Agrell, and M. Brandt-Pearce, "Cross-layer static resource provisioning for dynamic traffic in flexible grid optical networks," *Journal of Optical Communications and Networking*, vol. 13, no. 3, pp. 1–13, 2021.

[46] Y. Xu, L. Yan, E. Agrell, and M. Brandt-Pearce, "Iterative resource allocation algorithm for EONs based on a linearized GN model," *Journal of Optical Communications and Networking*, vol. 11, no. 3, pp. 39–51, 2019.

[47] L. Yan, Y. Xu, M. Brandt-Pearce, N. Dharmaweera, and E. Agrell, "Robust regenerator allocation in nonlinear flexible-grid optical networks with time-varying data rates," *IEEE/OSA Journal of Optical Communications and Networking*, vol. 10, no. 11, pp. 823–831, 2018.

[48] L. Li and H.-j. Li, "Performance analysis of novel routing and spectrum allocation algorithm in elastic optical networks," *Optik*, vol. 212, p. 164688, 2020.

[49] P. D. Choudhury, P. R. Reddy, B. C. Chatterjee, E. Oki, and T. De, "Performance of routing and spectrum allocation approaches for multicast traffic in elastic optical networks," *Optical Fiber Technology*, vol. 58, p. 102247, 2020.

[50] B. Dai, Y. Cao, Z. Wu, Z. Dai, R. Yao, and Y. Xu, "Routing optimization meets machine intelligence: A perspective for the future network," *Neurocomputing*, vol. 459, pp. 44–58, 2021.

[51] M. Amirabadi, "A survey on machine learning for optical communication [machine learning view]," *arXiv preprint arXiv:1909.05148*, 2019.

[52] R. Amin, E. Rojas, A. Aqdus, S. Ramzan, D. Casillas-Perez, and J. M. Arco, "A survey on machine learning techniques for routing optimization in SDN," *IEEE Access*, 2021.

[53] Z. Mammeri, "Reinforcement learning based routing in networks: review and classification of approaches," *IEEE Access*, vol. 7, pp. 55 916–55 950, 2019.

[54] T. Shimoda, "Routing and spectrum assignment using deep reinforcement learning in optical networks," *NTT Technical Review*, pp. 1–5, 2021.

[55] X. Chen, R. Proietti, and S. B. Yoo, "Building autonomic elastic optical networks with deep reinforcement learning," *IEEE Communications Magazine*, vol. 57, no. 10, pp. 20–26, 2019.

[56] X. Chen, R. Proietti, C.-Y. Liu, and S. B. Yoo, "A multi-task-learning-based transfer deep reinforcement learning design for autonomic optical networks," *IEEE Journal on Selected Areas in Communications*, vol. 39, no. 9, pp. 2878–2889, 2021.

[57] B. Li and Z. Zhu, "GNN-based hierarchical deep reinforcement learning for NFV-oriented online resource orchestration in elastic optical dcis," *Journal of Lightwave Technology*, vol. 40, no. 4, pp. 935–946, 2021.

[58] R. K. Jana, B. C. Chatterjee, A. P. Singh, A. Srivastava, B. Mukherjee, A. Lord, and A. Mitra, "Machine learning-assisted nonlinear-impairment-aware proactive defragmentation for C+L band elastic optical networks," *Journal of Optical Communications and Networking*, vol. 14, no. 3, pp. 56–68, 2022.

[59] D. Semrau, E. Sillekens, R. I. Killey, and P. Bayvel, "A modulation format correction formula for the Gaussian noise model in the presence of inter-channel stimulated Raman scattering," *Journal of Lightwave Technology*, vol. 37, no. 19, pp. 5122–5131, 2019.

[60] D. Semrau, R. I. Killey, and P. Bayvel, "A closed-form approximation of the Gaussian noise model in the presence of inter-channel stimulated Raman scattering," *Journal of Lightwave Technology*, vol. 37, no. 9, pp. 1924–1936, 2019.

[61] P. Poggiolini, "A generalized GN-model closed-form formula," *arXiv preprint arXiv:1810.06545*, 2018.

[62] B. C. Chatterjee, S. Ba, and E. Oki, "Fragmentation problems and management approaches in elastic optical networks: A survey," *IEEE Communications Surveys & Tutorials*, vol. 20, no. 1, pp. 183–210, 2017.

[63] R. S. Sutton and A. G. Barto, *Reinforcement learning: An introduction*. MIT press, 2018.

[64] Z. Zheng, A. K. Sangaiah, and T. Wang, "Adaptive communication protocols in flying ad hoc network," *IEEE Communications Magazine*, vol. 56, no. 1, pp. 136–142, 2018.

[65] X.-J. Shen, Q. Chang, L. Liu, J. Panneerselvam, and Z.-J. Zha, "CCLBR: Congestion control-based load balanced routing in unstructured P2P systems," *IEEE Systems Journal*, vol. 12, no. 1, pp. 802–813, 2016.

[66] C. Wu, T. Yoshinaga, Y. Ji, and Y. Zhang, "Computational intelligence inspired data delivery for vehicle-to-roadside communications," *IEEE Transactions on Vehicular Technology*, vol. 67, no. 12, pp. 12 038–12 048, 2018.

[67] M. Boushaba, A. Hafid, A. Belbekkouche, and M. Gendreau, "Reinforcement learning based routing in wireless mesh networks," *Wireless networks*, vol. 19, no. 8, pp. 2079–2091, 2013.

[68] B. C. Chatterjee, A. Wadud, and E. Oki, "Proactive fragmentation management scheme based on crosstalk-avoided batch processing for spectrally-spatially elastic optical networks," *IEEE Journal on Selected Areas in Communications*, vol. 39, no. 9, pp. 2719–2733, 2021.

[69] B. C. Chatterjee, A. Wadud, I. Ahmed, and E. Oki, "Priority-based inter-core and inter-mode crosstalk-avoided resource allocation for spectrally-spatially elastic optical networks," *IEEE/ACM Transactions on Networking*, vol. 29, no. 4, pp. 1634–1647, 2021.

[70] A. Mitra, D. Semrau, N. Gahlawat, A. Srivastava, P. Bayvel, and A. Lord, "Effect of reduced link margins on C+L band elastic optical networks," *Journal of Optical Communications and Networking*, vol. 11, no. 10, pp. C86–C93, 2019.

[71] B. C. Chatterjee, I. Ahmed, A. Wadud, M. Maity, and E. Oki, "BPRIA: crosstalk-avoided bi-partitioning-based counter-propagation resource identification and allocation for spectrally-spatially elastic optical networks," *IEEE Transactions on Network and Service Management*, vol. 19, no. 4, pp. 4369–4383, 2022.

[72] Y. Ma, X. Yang, Q. Sun, and Y. Zhao, "Dynamic resource allocation for multicast in SDM-EON: time-decoupled dynamic path crosstalk and joint

weight," *Journal of Optical Communications and Networking*, vol. 15, no. 9, pp. 687–699, 2023.

[73] M. Yang, Y. Zhang, and Q. Wu, "Routing, spectrum, and core assignment in SDM-EONS with MCF: node-arc ILP/MILP methods and an efficient XT-aware heuristic algorithm," *Journal of Optical Communications and Networking*, vol. 10, no. 3, pp. 195–208, 2018.

[74] B. Shariati, A. Mastropaolo, N.-P. Diamantopoulos, J. M. Rivas-Moscoso, D. Klonidis, and I. Tomkos, "Physical-layer-aware performance evaluation of SDM networks based on smf bundles,MCFs, and FMFs," *Journal of Optical Communications and Networking*, vol. 10, no. 9, pp. 712–722, 2018.

[75] S. Behera, G. Savva, K. Manousakis, and G. Ellinas, "Impairment-aware routing, modulation, spectrum, and core allocation with bit loading in spectrally–spatially flexible optical networks," *Journal of Optical Communications and Networking*, vol. 15, no. 6, pp. 318–332, 2023.

[76] L. Yan, E. Agrell, H. Wymeersch, and M. Brandt-Pearce, "Resource allocation for flexible-grid optical networks with nonlinear channel model," *Journal of Optical Communications and Networking*, vol. 7, no. 11, pp. B101–B108, 2015.

[77] M. Klinkowski and G. Zalewski, "Dynamic crosstalk-aware lightpath provisioning in spectrally–spatially flexible optical networks," *Journal of Optical Communications and Networking*, vol. 11, no. 5, pp. 213–225, 2019.

[78] Zhang, Shengyu and Yeung, Kwan L, "Revisiting the modulation format selection problem in crosstalk-aware SDM-EONs," *Computer Networks*, vol. 221, p. 109524, 2023.

[79] K. Takeda, T. Sato, B. C. Chatterjee, and E. Oki, "Joint inter-core crosstalk-and intra-core impairment-aware lightpath provisioning model in space-division multiplexing elastic optical networks," *IEEE Transactions on Network and Service Management*, vol. 19, no. 4, pp. 4323–4337, 2022.

[80] Y. Xiong, J. Shi, Y. Yang, Y. Lv, and G. N. Rouskas, "Lightpath management in SDN-based elastic optical networks with power consumption considerations," *Journal of Lightwave Technology*, vol. 36, no. 9, pp. 1650–1660, 2018.

[81] H. Liu, Q. Xiong, and Y. Chen, "Routing core and spectrum allocation algorithm for inter-core crosstalk and energy efficiency in space division multiplexing elastic optical networks," *IEEE Access*, vol. 8, pp. 70 453–70 464, 2020.

[82] S. Fujii, Y. Hirota, H. Tode, and T. Watanabe, "On-demand routing and spectrum allocation for energy-efficient AoD nodes in SDM-EONs," *Journal of Optical Communications and Networking*, vol. 9, no. 11, pp. 960–973, 2017.

[83] J. Halder, S. Paira, T. Acharya, and U. Bhattacharya, "Design of a novel XT-aware energy and spectrum efficient RSCA scheme in offline SDM-EON," *Optical Fiber Technology*, vol. 63, p. 102502, 2021.

[84] J. Halder, T. Acharya, and U. Bhattacharya, "On crosstalk aware energy and spectrum efficient survivable RSCA scheme in offline SDM-EON," *Journal of Network and Systems Management*, vol. 30, no. 1, pp. 1–35, 2022.

[85] H. Tode and Y. Hirota, "Routing, spectrum, and core and/or mode assignment on space-division multiplexing optical networks," *Journal of Optical Communications and Networking*, vol. 9, no. 1, pp. A99–A113, 2017.

[86] S. Zhang and K. L. Yeung, "Dynamic service provisioning in space-division multiplexing elastic optical networks," *Journal of Optical Communications and Networking*, vol. 12, no. 11, pp. 335–343, 2020.

[87] R. Zhu, A. Samuel, P. Wang, S. Li, L. Li, P. Lv, and M. Xu, "Survival multipath energy-aware resource allocation in SDM-EONs during fluctuating traffic," *Journal of Lightwave Technology*, vol. 39, no. 7, pp. 1900–1912, 2020.

[88] Zhang, Shengyu and Yeung, Kwan-Lawrence and Jin, Along, "LBFA: A load-balanced and fragmentation-aware resource allocation algorithm in space-division multiplexing elastic optical networks," in *Photonics*, vol. 8, no. 10. MDPI, 2021, p. 456.

[89] X. Li, J. Yuan, L. Yang, Q. Zhang, and Z. Yu, "A crosstalk-and fragmentation-aware RMSCA strategy in SDM-EONs based on aligned

prime-partition of spectrum resources," *Optical Fiber Technology*, vol. 72, p. 102978, 2022.

[90] A. Samuel, Y. Zhang, and R. Zhu, "Deadline-aware multicast resource allocation in SDM-EONs with fluctuating delay-sensitive traffic," *Journal of Lightwave Technology*, 2022.

[91] J. Ravipudi and M. Brandt-Pearce, "A score function heuristic for crosstalk- and fragmentation-aware dynamic routing, modulation, core, and spectrum allocation in SDM-EONs," *presented at the IEEE Future Networks World Forum, Montreal, Canada*, 2022.

[92] J. Su, J. Zhang, J. Wang, D. Ren, J. Hu, and J. Zhao, "Dynamic impairment-aware RMCSA in multi-core fiber-based elastic optical networks," *Optics Communications*, vol. 518, p. 128361, 2022.

[93] Pourkarimi, Elham and Rahbar, Akbar Ghaffarpour, "Novel fragmentation-aware algorithms in space division multiplexing elastic optical networks," *Optical Fiber Technology*, vol. 66, p. 102655, 2021.

[94] K. Walkowiak, A. Wlodarczyk, and M. Klinkowski, "Effective worst-case crosstalk estimation for dynamic translucent SDM elastic optical networks," in *ICC 2019-2019 IEEE International Conference on Communications (ICC)*. IEEE, 2019, pp. 1–7.

[95] Y. Zhao, L. Hu, R. Zhu, X. Yu, X. Wang, and J. Zhang, "Crosstalk-aware spectrum defragmentation based on spectrum compactness in space division multiplexing enabled elastic optical networks with multicore fiber," *IEEE Access*, vol. 6, pp. 15 346–15 355, 2018.

[96] D. Kumar and R. Ranjan, "Optimal design for crosstalk analysis in 12-core 5-lp mode homogeneous multicore fiber for different lattice structure," *Optical Fiber Technology*, vol. 41, pp. 95–103, 2018.

[97] E. E. Moghaddam, H. Beyranvand, and J. A. Salehi, "Crosstalk-aware resource allocation in survivable space-division-multiplexed elastic optical networks supporting hybrid dedicated and shared path protection," *Journal of Lightwave Technology*, vol. 38, no. 6, pp. 1095–1102, 2019.

[98] Zhu, Ruijie and Samuel, Aretor and Wang, Peisen and Li, Shihua and Oun, Bounsou Kham and Li, Lulu and Lv, Pei and Xu, Mingliang and

Yu, Shui, "Protected resource allocation in space division multiplexing-elastic optical networks with fluctuating traffic," *Journal of Network and Computer Applications*, vol. 174, p. 102887, 2021.

[99] Proietti, Roberto and Liu, Lei and Scott, Ryan P and Guan, Binbin and Qin, Chuan and Su, Tiehui and Giannone, Francesco and Yoo, SJ Ben, "3D elastic optical networking in the temporal, spectral, and spatial domains," *IEEE Communications Magazine*, vol. 53, no. 2, pp. 79–87, 2015.

[100] Oliveira, Ramon A and Rosário, Denis and Cerqueira, Eduardo and Oliveira, Helder, "Machine Learning Assisted Traffic-Aware Approach to Path Assignment in SDM-EONs," in *Anais do XL Simpósio Brasileiro de Redes de Computadores e Sistemas Distribuídos*. SBC, 2022, pp. 29–42.

[101] Pinto-Ríos, Juan and Calderón, Felipe and Leiva, Ariel and Hermosilla, Gabriel and Beghelli, Alejandra and Bórquez-Paredes, Danilo and Lozada, Astrid and Jara, Nicolás and Olivares, Ricardo and Saavedra, Gabriel, "Resource Allocation in Multicore Elastic Optical Networks: A Deep Reinforcement Learning Approach," *arXiv preprint arXiv:2207.02074*, 2022.

[102] M. Ju, F. Zhou, S. Xiao, and Z. Zhu, "Power-efficient protection with directed p-cycles for asymmetric traffic in elastic optical networks," *Journal of Lightwave Technology*, vol. 34, no. 17, pp. 4053–4065, 2016.

[103] G.-H. Tzeng and J.-J. Huang, *Multiple attribute decision making: methods and applications*. CRC press, 2011.

[104] R. Rao and B. K. Patel, "Decision making in the manufacturing environment using an improved PROMETHEE method," *International Journal of Production Research*, vol. 48, no. 16, pp. 4665–4682, 2010.

[105] R. V. Rao, "Multiple attribute decision making in the manufacturing environment," in *Decision Making in Manufacturing Environment Using Graph Theory and Fuzzy Multiple Attribute Decision Making Methods*. Springer, 2013, pp. 1–5.

[106] J.-P. Brans, P. Vincke, and B. Mareschal, "How to select and how to rank projects: The PROMETHEE method," *European Journal of Operational Research*, vol. 24, no. 2, pp. 228–238, 1986.

[107] R. L. Saaty, "The analytic hierarchy process—what it is and how it is used," *Mathematical modelling*, vol. 9, no. 3-5, pp. 161–176, 1987.

[108] F. S. Abkenar, A. G. Rahbar, and A. Ebrahimzadeh, "Best fit (BF): A new spectrum allocation mechanism in elastic optical networks (EONs)," in *2016 8th International Symposium on Telecommunications (IST)*. IEEE, 2016, pp. 24–29.

[109] J. Zhao, H. Wymeersch, and E. Agrell, "Nonlinear impairment-aware static resource allocation in elastic optical networks," *Journal of Lightwave Technology*, vol. 33, no. 22, pp. 4554–4564, 2015.

[110] Matsuo, Shoichiro and Sasaki, Yusuke and Akamatsu, Tsuyoshi and Ishida, Itaru and Takenaga, Katsuhiro and Okuyama, Kazuhiro and Saitoh, Kunimasa and Kosihba, Masanori, "12-core fiber with one ring structure for extremely large capacity transmission," *Optics express*, vol. 20, no. 27, pp. 28 398–28 408, 2012.

[111] R. Proietti, X. Chen, K. Zhang, G. Liu, M. Shamsabardeh, A. Castro, L. Velasco, Z. Zhu, and S. B. Yoo, "Experimental demonstration of machine-learning-aided QoT estimation in multi-domain elastic optical networks with alien wavelengths," *Journal of Optical Communications and Networking*, vol. 11, no. 1, pp. A1–A10, 2019.

[112] M. Salani, C. Rottondi, L. Ceré, and M. Tornatore, "Dual-stage planning for elastic optical networks integrating machine-learning-assisted QoT estimation," *IEEE/ACM Transactions on Networking*, 2022.

[113] D. F. Semrau, "Physical layer modelling of optical fibre communication systems in the nonlinear regime," Ph.D. dissertation, UCL (University College London), 2020.

[114] G. Savva, T. Panayiotou, I. Tomkos, and G. Ellinas, "Deep graph learning for QoT estimation of unseen optical sub-network states: Capturing the crosstalk impact on the in-service lightpaths," *Journal of Lightwave Technology*, vol. 40, no. 4, pp. 921–934, 2021.

[115] Y. Xiong, Y. Yang, Y. Ye, and G. N. Rouskas, "A machine learning approach to mitigating fragmentation and crosstalk in space division mul-

tiplexing elastic optical networks," *Optical Fiber Technology*, vol. 50, pp. 99–107, 2019.

[116] Q. Yao, H. Yang, A. Yu, and J. Zhang, "Transductive transfer learning-based spectrum optimization for resource reservation in seven-core elastic optical networks," *Journal of Lightwave Technology*, vol. 37, no. 16, pp. 4164–4172, 2019.

[117] S. Trindade and N. L. Da Fonseca, "Machine learning for spectrum defragmentation in space-division multiplexing elastic optical networks," *IEEE Network*, vol. 35, no. 1, pp. 326–332, 2020.

[118] C. Rottondi, L. Barletta, A. Giusti, and M. Tornatore, "Machine-learning method for quality of transmission prediction of unestablished lightpaths," *Journal of Optical Communications and Networking*, vol. 10, no. 2, pp. A286–A297, 2018.

[119] I. Khan, M. Bilal, M. U. Masood, A. D'Amico, and V. Curri, "Lightpath QoT computation in optical networks assisted by transfer learning," *Journal of Optical Communications and Networking*, vol. 13, no. 4, pp. B72–B82, 2021.

[120] J. Lu, Q. Fan, G. Zhou, L. Lu, C. Yu, A. P. T. Lau, and C. Lu, "Automated training dataset collection system design for machine learning application in optical networks: an example of quality of transmission estimation," *Journal of Optical Communications and Networking*, vol. 13, no. 11, pp. 289–300, 2021.

[121] M. Salani, C. Rottondi, and M. Tornatore, "Routing and spectrum assignment integrating machine-learning-based QoT estimation in elastic optical networks," in *IEEE INFOCOM 2019-IEEE Conference on Computer Communications*. IEEE, 2019, pp. 1738–1746.

[122] S. Petale and S. Subramaniam, "An ML approach for crosstalk-aware modulation format selection in SDM-EONs," in *2022 International Conference on Optical Network Design and Modeling (ONDM)*. IEEE, 2022, pp. 1–6.

[123] J. Ravipudi and M. Brandt-Pearce, "Machine learning based lightpath classifier for impairment-aware resource allocation in SDM-EONs," *presented at the IEEE Future Networks World Forum, Montreal, Canada*, 2023.

[124] R. V. Rao, *Jaya: an advanced optimization algorithm and its engineering applications*. Switzerland: Springer Cham, 2019.

[125] Q. Zhuge, X. Zeng, H. Lun, M. Cai, X. Liu, L. Yi, and W. Hu, "Application of machine learning in fiber nonlinearity modeling and monitoring for elastic optical networks," *Journal of Lightwave Technology*, vol. 37, no. 13, pp. 3055–3063, 2019.

[126] J. Müller, S. K. Patri, T. Fehenberger, H. Griesser, J.-P. Elbers, and C. Mas-Machuca, "QoT estimation using EGN-assisted machine learning for multi-period network planning," *Journal of Optical Communications and Networking*, vol. 14, no. 12, pp. 1010–1019, 2022.

[127] R. K. Jana, B. C. Chatterjee, A. P. Singh, A. Srivastava, B. Mukherjee, A. Lord, and A. Mitra, "Quality-aware resource provisioning for multiband elastic optical networks: a deep-learning-assisted approach," *Journal of Optical Communications and Networking*, vol. 14, no. 11, pp. 882–893, 2022.

[128] R. Koch, S. Kühl, R. M. Morais, B. Spinnler, W. Schairer, B. Sommernkorn-Krombholz, and S. Pachnicke, "Reinforcement learning for generalized parameter optimization in elastic optical networks," *Journal of Lightwave Technology*, vol. 40, no. 3, pp. 567–574, 2022.

[129] M. Klinkowski, P. Ksieniewicz, M. Jaworski, G. Zalewski, and K. Walkowiak, "Machine learning assisted optimization of dynamic crosstalk-aware spectrally-spatially flexible optical networks," *Journal of Lightwave Technology*, vol. 38, no. 7, pp. 1625–1635, 2020.

[130] H. Yang, Q. Yao, B. Bao, A. Yu, J. Zhang, and A. V. Vasilakos, "Multi-associated parameters aggregation-based routing and resources allocation in multi-core elastic optical networks," *IEEE/ACM Transactions on Networking*, vol. 30, no. 5, pp. 2145–2157, 2022.

[131] Q. Yao, H. Yang, R. Zhu, A. Yu, W. Bai, Y. Tan, J. Zhang, and H. Xiao, "Core, mode, and spectrum assignment based on machine learning in space division multiplexing elastic optical networks," *IEEE Access*, vol. 6, pp. 15 898–15 907, 2018.

[132] B. Krawczyk, "Learning from imbalanced data: open challenges and future directions," *Progress in Artificial Intelligence*, vol. 5, no. 4, pp. 221–232, 2016.

[133] D. W. Hosmer Jr, S. Lemeshow, and R. X. Sturdivant, *Applied logistic regression*. John Wiley & Sons, 2013, vol. 398.

[134] J. Brownlee, *Imbalanced classification with Python: better metrics, balance skewed classes, cost-sensitive learning*. Machine Learning Mastery, 2020.

[135] T. Panayiotou, M. Michalopoulou, and G. Ellinas, "Survey on machine learning for traffic-driven service provisioning in optical networks," *IEEE Communications Surveys & Tutorials*, 2023.

[136] O. Ayoub, S. Troia, D. Andreoletti, A. Bianco, M. Tornatore, S. Giordano, and C. Rottondi, "Towards explainable artificial intelligence in optical networks: the use case of lightpath QoT estimation," *Journal of Optical Communications and Networking*, vol. 15, no. 1, pp. A26–A38, 2023.

[137] J. Brownlee, *Data preparation for machine learning: data cleaning, feature selection, and data transforms in Python*. Machine Learning Mastery, 2020.

[138] M. Kaveh and M. S. Mesgari, "Application of meta-heuristic algorithms for training neural networks and deep learning architectures: A comprehensive review," *Neural Processing Letters*, vol. 55, no. 4, pp. 4519–4622, 2023.

[139] R. A. Zitar, M. A. Al-Betar, M. A. Awadallah, I. A. Doush, and K. Assaleh, "An intensive and comprehensive overview of JAYA algorithm, its versions and applications," *Archives of Computational Methods in Engineering*, vol. 29, no. 2, pp. 763–792, 2022.

[140] B. H. Abed-alguni and S. H. AL-Jarah, "IBJA: An improved binary DJaya algorithm for feature selection," *Journal of Computational Science*, vol. 75, p. 102201, 2024.

[141] F. Zhao, R. Ma, and L. Wang, "A self-learning discrete jaya algorithm for multiobjective energy-efficient distributed no-idle flow-shop scheduling problem in heterogeneous factory system," *IEEE Transactions on Cybernetics*, vol. 52, no. 12, pp. 12 675–12 686, 2021.

[142] M. Aslan, M. Gunduz, and M. S. Kiran, "Jayax: Jaya algorithm with xor operator for binary optimization," *Applied Soft Computing*, vol. 82, p. 105576, 2019.